2010

Development of metal-based luminescent probes for applications in biomolecular structure and dynamics

Ayesha Sharmin

Development of metal-based luminescent probes for applications in biomolecular structure and dynamics

By

AYESHA SHARMIN

M.Phil. Chemistry, Jahangirnagar University, Bangladesh, 2005

Dissertation

Presented in partial fulfillment of the requirements
For the degree of

Doctor of philosophy

The University of Montana
Missoula, MT

Spring 2010

Approved by:
Dr. Perry J. Brown, Associate Provost
Graduate Education

Dr. Edward Rosenberg, Committee Chairperson
Department of Chemistry & Biochemistry

Dr. J. B. Alexander Ross, Committee Member
Department of Chemistry & Biochemistry

Dr. Klara Briknarova, Committee Member
Department of Chemistry & Biochemistry

Dr. David Bolstad, Committee Member
Department of Chemistry & Biochemistry

Dr. Michelle McGuirl, Committee Member
Division of Biological Sciences

Sharmin, Ayesha, Ph.D., Spring 2010 Chemistry

Development of metal-based luminescent probes for applications in biomolecular structure and dynamics

Chairperson: Dr. Edward Rosenberg, Department of Chemistry & Biochemistry

Abstract

New transition-metal complexes containing luminescent properties have been designed and synthesized for application as structural probes for biomolecules. Potential DNA intercalators, 2-amino-anthracene substituted triosmium clusters, were synthesized by the reactions of 2-amino-anthracene with $[Os_3(CO)_{10}(CH_3CN)_2]$. The products $[Os_3(CO)_{10}(\mu\text{-}\eta^2\text{-}(N\text{-}C(1))\text{-}NH_2C_{14}H_8)(\mu\text{-}H)]$, $[Os_3(CO)_{10}(\mu\text{-}\eta^2\text{-}(N\text{-}C(3))\text{-}NHC_{14}H_9)(\mu\text{-}H)]$, $[Os_3(CO)_9(\mu\text{-}\eta^2\text{-}(N\text{-}C(3))\text{-}NHC_{14}H_8)(\mu\text{-}H)_2]$ and $[Os_3(CO)_9(\mu_3\text{-}\eta^2\text{-}(N\text{-}C(3))\text{-}NHC_{10}H_9)(\mu\text{-}H)]$ obtained from this reaction have been structurally characterized by spectroscopic, photophysical and electrochemical techniques. Solid state structures are also reported for the complexes $[Os_3(CO)_{10}(\mu\text{-}\eta^2\text{-}(N\text{-}C(3))\text{-}NHC_{14}H_9)(\mu\text{-}H)]$ and $[Os_3(CO)_9(\mu\text{-}\eta^2\text{-}(N\text{-}C(3))\text{-}NHC_{14}H_8)(\mu\text{-}H)_2]$. To investigate bio-macromolecular dynamics on the sub-microsecond-to-microsecond timescale, a series of ruthenium based mono-nuclear metal-ligand charge-transfer complexes (MLCs) of formula $[XRu(CO)(L\text{–}L)(L')_2][PF_6]$ (X = H, TFA, Cl; L–L = 2,2′-bipyridyl, 1,10-phenanthroline, 5-amino-1,10-phenanthroline and 4,4′-dicarboxylic-2,2′-bipyridyl; $L'_2 = 2PPh_3$, $Ph_2PC_2H_4PPh_2$, $Ph_2PCH{=}CHPPh_2$) have been synthesized from the starting complex $K[Ru(CO)_3(TFA)_3]$ (TFA = CF_3CO_2) by first reacting with the phosphine ligand, followed by reaction with the L–L and anion exchange with NH_4PF_6. In the case of L–L = phenanthroline and $L'_2 = 2PPh_3$, the neutral complex $Ru(Ph_3P)(CO)(1,10\text{-phenanthroline})(TFA)_2$ is also obtained and its solid state structure is reported. Solid state structures are also reported for the cationic complexes where L–L = phenanthroline, $L_2 = 2PPh_3$ and X = Cl and for L–L = 2,2′-bipyridyl, $L_2 = 2PPh_3$ and X = H. All the complexes were characterized in solution by a combination of ^1H and ^{31}P NMR, IR, mass spectrometry and elemental analyses. These complexes contain only one chelating heterocycle, which decreases the molecular symmetry and thereby increases the luminescence anisotropy. The photophysical and structural properties of these complexes indicated that these complexes can be used as potential probes to study bio-macromolecular dynamics in the presence of oxygen. The carboxy- and amine-substituted diimine ligands in $[HRu(CO)(4,4'\text{-dicarboxy-bipyridyl})(PPh_3)_2][PF_6]$ and $[(TFA)Ru(CO)(dppene)(5\text{-amino-1,10phen})][PF_6]$ have been covalently-conjugated with biomolecules by simple ligand modifications. Complex $[HRu(CO)(4,4'\text{-dicarboxy-bipyridyl})(PPh_3)_2][PF_6]$ has been conjugated to dipalmitoylphosphatidylethanolamine (DPPE) and complex $[(TFA)Ru(CO)(dppene)(5\text{-amino-1,10-phen})][PF_6]$ conjugated to DPPE and cholesterol. The lipid and cholesterol conjugates were characterized by spectroscopic and photophysical techniques. These conjugates were incorporated in 100 nm-diameter-unilamellar lipid-membrane vesicles to investigate the photophysical properties of the probes in a model membrane environment and to evaluate the utility of these probes for investigating the physical properties of lipid membranes. These studies revealed an unusual blue shift in their luminescence in the case of the lipid conjugates while the cholesterol conjugate did not. Anisotropy studies of the conjugates revealed details about the probe dynamics in the vesicle environment.

ACKNOWLEDGEMENTS

I am extremely delighted to express my deepest sense of gratitude and sincere thanks to my reverend thesis advisors, Professor Edward Rosenberg and Professor J. B. Alexander Ross, for their indispensable guidance, constant encouragement, and thoughtful suggestions throughout the progress of this research work. I would like to offer my thanks to the members of my advisory committee for their guidance and cooperation during the course of work. I wish to offer my pleasant thanks to Professor Shariff E. Kabir for his inspiration. My sincere thanks to Professor K. I. Hardcastle for solving the X-ray structures of my compounds. I would like to thank Professor Mauro Ravera for helping me in learning electrochemistry. I wish to offer my deepest sense of gratitude to the department of Chemistry & Biochemistry for the support I got during my graduate study here at the UM. I owe my warm thanks to Dr. Luca Salassa, Laurie Franklin, Reuben Darlington, Roslyn Pinson, Glenn Pinson, Raj Kailasam and all the members of Professor Rosenberg's and Professor Ross's groups. I wish to offer my heartiest compliments to my parents and my brother for their unconditional love and constant inspirations throughout my studies. Above all, my warm thanks to my husband Mainul for his support, patience and inspiration during my research.

Table of Contents

List of figures

Chapter One

Chapter Two

Chapter Three

Chapter Four

Chapter Five

List of Tables

List of Abbreviations

MLCs	Metal-ligand complexes
Ind	Indazole
Terpy	2,2':6',2"-terpyridine
cdta	1,2-cyclohexanediamine tetraacetate
Im	Imidazole
μs	Microsecond
ms	Millisecond
ns	Nanosecond
MLCT	Metal-ligand charge-transfer
Bpy	2,2 bipyridyl
dcbpy	4,4'-dicarboxy-2,2 bipyridyl
phen	1,10 phenanthroline
TFA	trifluoroacetate
dppe	diphenylphosphinoethane
dppene	diphenylphosphinoethylene
Py	Pyridyl
TCSPC	Time-correlated single-photon counting
5-amin-1,10-phen	5-amine-1,10-phenanthroline
aphen	5-amine-1,10-phenanthroline
chol	cholesterol
DPPE	1,2-dihexadecanoyl-*sn*-glycero-3-
DPPC	phosphoethanolamine
Egg-PC	1,2-dihexadecanoyl-*sn*-glycero-3-phosphocholine
	L-α-phosphatidylcholine from chicken egg

CHAPTER 1: GENERAL INTRODUCTION

1.1 Introduction

The rich intrinsic properties of metal complexes—redox activity, octahedral geometry, magnetic, spectroscopic and photophysical properties—give us the opportunity to use them to monitor and/or alter biological functions. Metal complexes can serve as useful research probes of biological function, as structural probes for biomolecules, as biological sensors and as potential diagnostic and therapeutic agents [1-3]. The success of cisplatin as an anti-tumor agent demonstrates that metal complexes can be developed as therapeutic agents [2]. The ability to synthesize sophisticated metal complexes has become well established. Advances have occurred in understanding and controlling the reactivity of metal complexes in vitro and in vivo. The actions of these compounds may provide insights that are different from those that can be achieved through other chemical, biochemical, or genetic manipulations. Therefore, investigations utilizing the power of the unique properties of transition metal complexes offer interesting research, diagnostic, and therapeutic opportunities [3]. The main focus of my dissertation is the synthesis of novel transition-metal luminescent complexes for labeling bio-macromolecules. The goals are as follows: **(I)** synthesis of luminescent metallo-intercalators as deoxyribonucleic acid (DNA) labeling agents; **(II)** synthesis of luminescent metal-ligand-charge-transfer (MLC) complexes suitable for studying slow dynamics (microsecond timescale) in bio-macromolecules; and **(III)** covalent conjugation of MLCs with lipids and cholesterol for studying photophysical properties of the conjugated probes in model membrane environments.

1.2 Synthesis of DNA intercalators

The study of the genetic material DNA would be enhanced by the development of new molecular tools as structural probes. Metal ions and metal coordination compounds are known to affect both normal (e.g. cell division and gene expression) and pathogenic (e.g. toxicity, carcinogenicity and anti-tumor activity) cellular processes [2]. Transition-metal complexes can act as efficient DNA binders or cleavers. A major current research interest in bioinorganic chemistry concerns binding and cleavage of DNA by metal complexes which relate to the utility of these complexes in the design and development of synthetic restriction enzymes, new drugs and DNA footprinting agents [3]

Transition-metal (Os, Ru, Rh, Re) complexes that have octahedral geometry so they are rigid, chiral and also include the availability of additional coordination sites in octahedral complexes. Therefore they can undergo alterations in ligand affinity and substitution kinetics and changes in oxidation state, which could be useful in photodynamic approaches to therapy. In the design of these new drugs, ruthenium complexes have attracted much interest [4]. Several ruthenium complexes such as *fac*[Ru(III)$Cl_3(NH_3)_3$], *trans*-[Ru(II)$Cl_2(DMSO)_4$], *trans*-[HIn][Ru(III)$Cl_4(Ind)_2$] (Ind = indazole), *mer*-[Ru(III)$Cl_3(terpy)_3$] (terpy = 2,2':6',2"-terpyridine), α-[Ru(2-(phenylazo)pyridine)$_2Cl_2$] and -[Ru(IV)Cl_2(cdta)] (cdta = 1,2-cyclohexane-diamine-tetraacetate) are found to be very active as anti-tumor agents [5]. The first ruthenium complex (*trans*-[Him] [Ru(III)Cl_4(DMSO)(Im)]) (Im = imidazole) used in clinical trials was relatively nontoxic, but active against tumor metastases [6]. Peter Sadler and coworkers [6] have shown that Ru(II) arene complexes have anticancer activity both in vivo and in vitro. Metallo-intercalators have been used as (1) luminescent probes of

DNA, (2) tools to examine local structural polymorphism of nucleic acids, (3) photoreactive and electrochemically active probes of DNA structure and protein binding, and (4) reagents targeted to recognize mismatches or to repair thymine dimers. All of these applications depend primarily upon the structural interactions of the metallo-intercalator with its nucleic acid binding site [7]. The intercalation is favored by the presence of extended, fused aromatic ligands. The use of trimetallic clusters as biomarkers holds the possibility for direct observation of the binding site by electron microscopy on the supramolecular level [7].

Recently E. Rosenberg *et al.* [8] reported the synthesis of water-soluble benzoheterocycle triosmium clusters with the general formula $[Os_3(CO)_9(\mu_3{-}\eta_2\text{-L-H})(\mu{-}H)(PR_3)]$ [8] (Figure 1.1**)** (L= (1) quinoline, (2) 3-amino quinoline, (3) quinoxaline, (4) phenanthridine) (R= (a) $C_6H_4SO_3Na$ and (b) $OCH_2CH_2N(CH_3)_3I$) and the interaction of these clusters with plasmid pUC19, single and double-stranded DNA and the telomerase enzyme. Our group has developed an effective method for synthesizing the electron-deficient cluster $[Os_3(CO)_9(\mu_3{-}\eta_2\text{-L-H})(\mu{-}H)]$ from $[Os_3(CO)_{10}(MeCN)_2]$ via the thermolysis reaction of the initially formed, electronically saturated cluster $[Os_3(CO)_{10}(\mu{-}\eta_2\text{-L-H})(\mu{-}H)(PR_3)]$ [8]. Two-electron donor ligands, for example phosphines, can be introduced to the electron deficient cluster simply by addition reaction at ambient conditions.

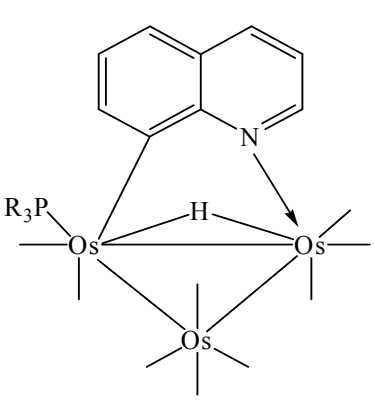

[1]

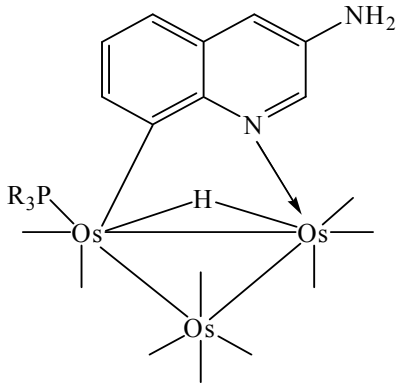

[2]

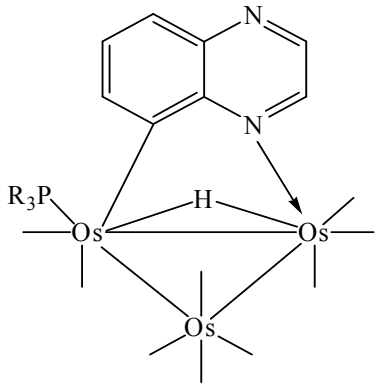

[3]

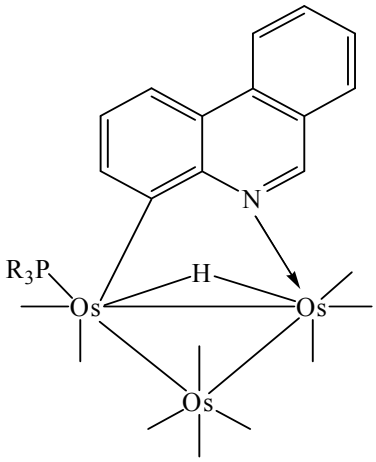

[4]

Solid line represents CO ligand in these complexes

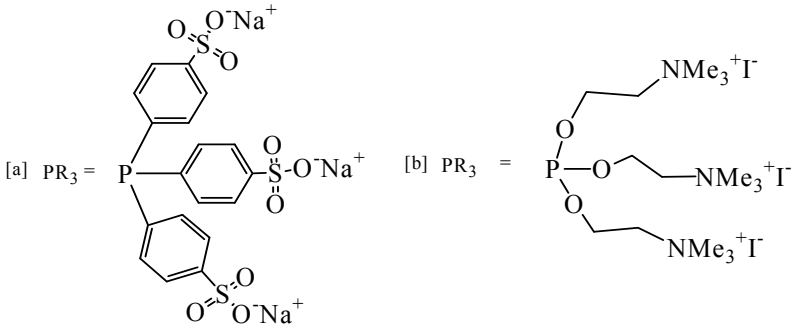

Figure 1.1: Benzoheterocycle triosmium clusters with the general formula

$[Os_3(CO)_9(\mu_3\text{–}\eta_2\text{-L-H})(\mu\text{–H})(PR_3)]$

Peter Sadler and coworkers [6] have also showed that ruthenium complexes containing extended π-systems are more efficient as DNA intercalators than single-ring aromatic systems by comparing Ru-DNA adduct formation with [(*η*6-arene)Ru(II)(en)(Cl)]$^{+}$ complexes [where arene biphenyl (BIP), dihydroanthracene (DHA), tetrahydroanthracene (THA), *p*-cymene(CYM), or benzene (BEN)]. The less effective intercalation with the less extended aromatic systems is the result of steric clash of the ancillary ligands with the phosphodiester backbone of DNA, as has been observed in the case of $[Ru(phen)_3]^{2+}$ [6].

Studies have shown that anthracene-metal complexes are effective intercalators into the major groove of DNA. The extended aromatic molecule, 2-amino-anthracene, is a fluorophore (emission maximum at 488nm). Therefore a metallo-intercalator containing 2-amino-anthracene ligand could be utilized to study the intercalation in DNA using the luminescent properties of the complex as a reporter. In light of our previous reports on the selective binding of triosmium complexes containing aromatic nitrogen hetrocycles to DNA [8], we thought it would be interesting to study interaction of 2-aminoanthracene-triosmium clusters with DNA. The synthesis of 2-aminoanthracene-substituted triosmium clusters from $[Os_3(CO)_{10}(MeCN)_2]$ and their structural characterization by spectroscopic methods and X-ray diffraction are discussed in Chapter 2. This chapter also contains the description of the photophysical and electrochemical properties of 2-aminoanthracene-substituted triosmium clusters [9].

1.3 Luminescent metal-ligand complexes

The excellent sensitivity, long lifetimes, polarized emission, quenching efficiency and radiative and nonradiative energy transfer have made fluorescence spectroscopy a very effective analytical tool in the life sciences [10]. Organic fluorophors show luminescent lifetimes ranging from 1 to 20 ns whereas lanthanide complexes have millisecond (ms) lifetimes. However, there are numerous dynamic processes that take place where intermediate decay times which are required in the 100-nanosecond (ns) to 10-microsecond (μs) range. The dynamics of proteins and protein assemblies that associate with membrane surfaces are in the 100 ns to 10 μs range. The rotational motions of membrane-associated proteins can have submicrosecond-to-microsecond correlation times, whereas proteins in solution have correlation times in the range of tens of nanoseconds. Study of these dynamics requires probes with excited-state lifetimes in the submicrosecond-to-microsecond range. Microsecond and millisecond timescale dynamics are often studied by using phosphorescent probes [11-13]. The Jablonski diagram of the absorption and emission processes is presented in Figure 1.2. Emission from a triplet-state is known as the phosphorescence. The triplet state (T_1) is populated via intersystem crossing (ISC) from the excited singlet state (S_1) [11].

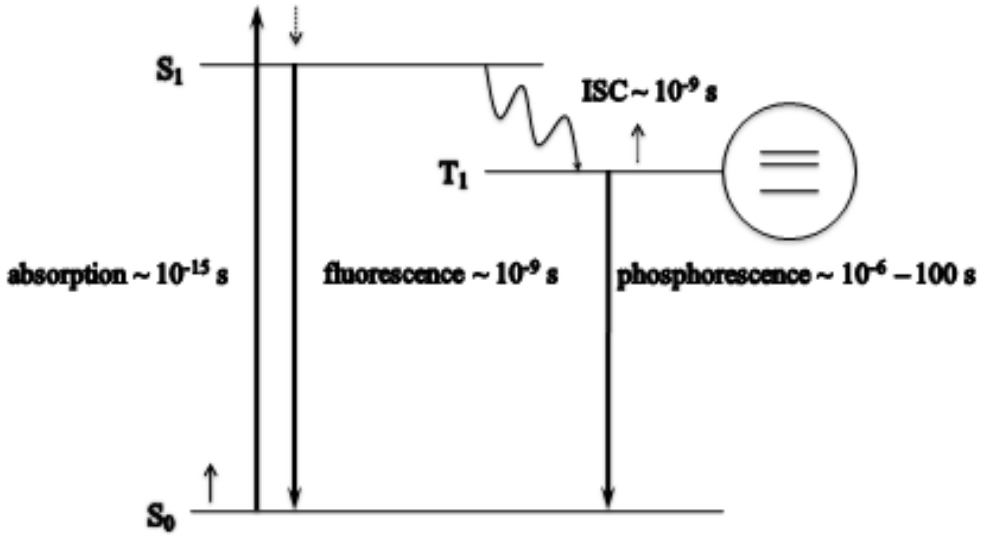

Figure 1.2: Jablonski diagram

Typically phosphorescence studies at room temperature require complete removal of oxygen. Lanthanide emissions are not sensitive to oxygen but are also not usually polarized. As a result, they are not useful for measurements of rotational diffusion in a large protein [10]. Transition-metal complexes containing one or more diimine ligands, referred as metal-ligand complexes (MLC), exhibit tunable, long luminescence lifetimes (100 ns to ~10 μs), polarized emission, high photostability, large Stokes shifts and sensitivity to the probe's environment [10, 14]. The luminescent behavior of transition metal complexes arises from the MLCT (metal-to-ligand charge-transfer) band. As the emission of the metal-ligand complex is dominated by the MLCT transition, the MLCs behave like a single chromophoric unit and they have high chemical and photochemical stabilities under physiological conditions. All the known octahedral luminescent complexes contain metal centers with d^6 electronic configurations. In the presence of strong ligands (good σ donor or π-acceptor) the *d*-orbital energy levels split into three

lower (*t*) and two higher (*e*) orbitals. The *d-d* transition is formally forbidden and hence is not observed [11]. However, the transition of the electron from the metal's *t* energy level to the ligand's π^* orbital is a spin-allowed process, and this transfer is known as the metal-to-ligand charge-transfer (MLCT). Typically the absorption band resulting from the MLCT transition appears in the near-visible region of the electromagnetic spectrum (350-600 nm), and this energy depends on the combination of metal and ligand. The presence of a heavy metal atom at the center of the complex has a significant effect on the excited states. The heavy metal facilitates the excited singlet (^{1}MLCT) to excited triplet (^{3}MLCT) intersystem crossing through spin-orbit coupling. Because the transition from triplet-excited state to singlet-ground state is spin forbidden, the lifetime of emission from the ^{3}MLCT is expected to be long compared to ^{1}MLCT relaxation, the latter which is spin allowed [10].

The energy gap law [13] determines the luminescent properties of these complexes (Figure 1.3). Therefore, several criteria must be satisfied in order to observe luminescence from their MLCT state. The ligand field must be strong enough to raise the *d-d* state above the MLCT state. This is the reason why $[Fe(L\text{-}L)_3]^{2+}$ is not luminescent but $[Ru(L\text{-}L)_3]^{2+}$ shows radiative decay and hence useful luminescence (L = 2,2 bipyridyl, 1,10 phenanthroline and their derivatives). However, as the energy of the excited state becomes closer to the ground state for the Os-MLCs, they typically show weak luminescence. The smaller energy gap facilitates more rapid radiationless decay [10].

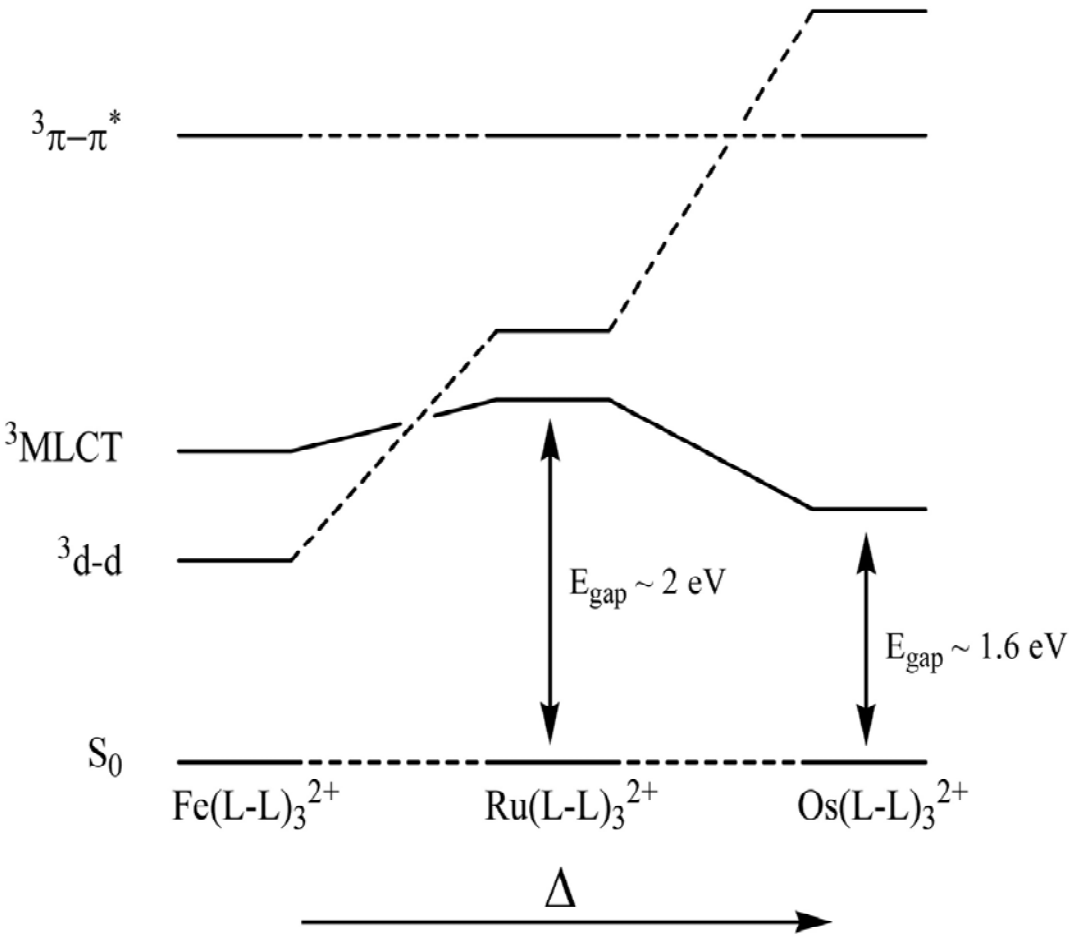

Figure 1.3: Lowest energy triplet states for metal-ligand complexes with increasing crystal field strength [10].

Upon excitation with polarized light the emission from MLC, containing nonidentical diimine ligands is also polarized, which makes these complexes useful for studying luminescence anisotropy. The first of such complexes reported was $[Ru(bpy)_2(dcbpy)]^{2+}$ (dcbpy = 4,4'-dicarboxy-2,2'-bipyridyl) (Figure 1.4). This dicarboxy derivative showed higher fundamental anisotropies than $[Ru(bpy)_3]^{2+}$ [10]. Introducing electron-withdrawing groups on the diimine ligand resulted in red-shifted emission and

an increase in anisotropy, which suggests that one ligand accepts the electron preferentially over the other diimine ligands in the MLCT excited states [16].

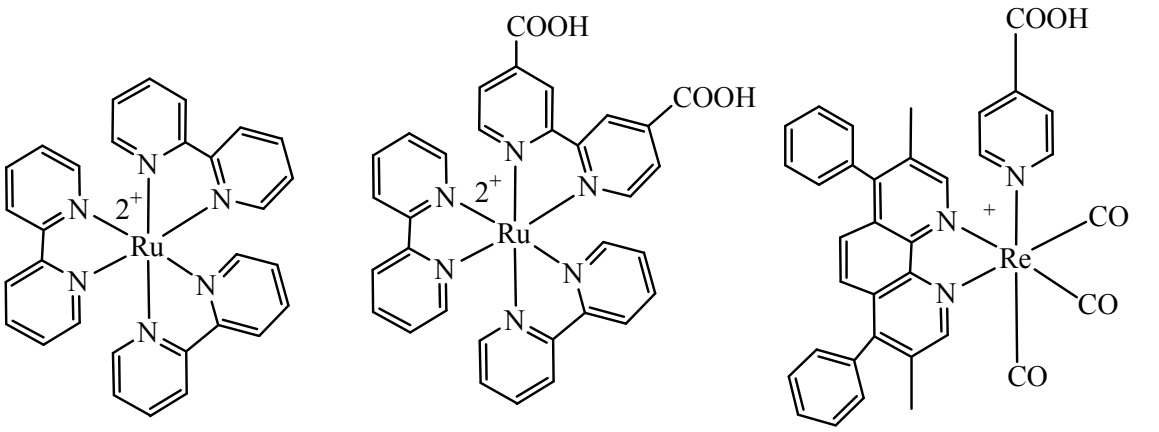

$[Ru(bpy)_3]^{2+}$ **$[Ru(bpy)_2(dcbpy)]^{2+}$** **$[Re(bcp)(CO)_3(4\text{-}COOHPy)]^{+}$**

Figure 1.4: Chemical structures of $[Ru(bpy)_3]^{2+}$, $[Ru(bpy)_2(dcbpy)]^{2+}$ and $[Re(bcp)(CO)_3(4\text{-}COOHPy)]^{+}$

The possibility of improving the fundamental anisotropy with a single chromophoric ligand in MLCs was observed for Re(I) complexes (e.g. $[Re(bcp)(CO)_3(4\text{-}COOHPy)(PF_6)]$ [10] (Figure 1.4). To overcome the limitation of low quantum yield of MLCs, the electronic effect of ligands on the energy gap can be utilized to increase quantum efficiency. Previous studies have shown that replacing diimines with chelating phosphine ligands can increase quantum yields for the $[Os(phen)(dppene)_2]^{2+}$ and $[Os(phen)_2(dppene)]^{2+}$ compared to $[Os(phen)_3]^{2+}$ (Q = 0.518, 0.138 and 0.016 respectively) **(**Figure 1.5**)**. Therefore, careful selection of the metal and the ligands can yield properties useful for the study of specific biological systems [10].

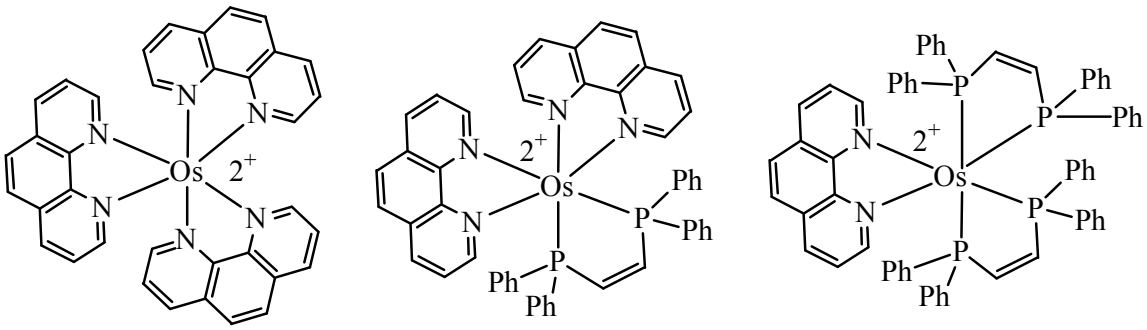

$[Os(phen)_3]^{2+}$ **$[Os(phen)_2(dppene)]^{2+}$** **$[Os(phen)(dppene)_2]^{2+}$**

Figure 1.5: Structure of osmium MLCs with different quantum yields.

The group of Joseph Lakowicz has reported the use of the long lifetime probe $[Re(4,7\text{-}Me_2phen)(CO)_3(4\text{-}COOHPy)(PF_6)]$ (Figure 1.3) to study overall rotational motion in lipid vesicles and microsecond dynamics of cell membranes [17]. In order to develop better probes for applications to specific biosystems a deeper understanding of their photophysical properties, generally governed by energy gap law, is required. The lifetimes can be tuned by varying the ligands attached to the metal center. Long excited-state lifetimes and polarized emission make them useful probes for studying dynamics on membranes. Our aim is to develop a series of complexes where the MLCT band is red-shifted and well-separated from the intra-ligand transitions and the excited-state lifetime is tunable so that we could tailor a particular probe to a particular dynamic process in a bio-macromolecule. We also wanted probes exhibiting high quantum yields (> 0.062) and fundamental anisotropy (≥ 0.1). Synthesis of MLCs having all of these favorable properties is challenging. Our strategy was to take advantage of the well-known fact that incorporation of π-acid ligands into complexes containing chelating nitrogen heterocycles has the effect of prolonging excited-state lifetimes of MLCs, thus providing a way to tune

the excited-state lifetime. Then, starting with the easily-substituted ruthenium complex $K[Ru(CO)_3(TFA)_3]$ (TFA = trifluoroacetate) [18], we developed synthetic pathways to complexes having most, if not all, of the desired photophysical properties. In Chapter 3, the syntheses and spectroscopic characterizations of a series of complexes having the chemical formula $[XRu(CO)(L–L)(L')_2][PF_6]$ (X = H, TFA, Cl; L–L = 2,2′-bipyridyl, 1,10-phenanthroline, 5-amino-1,10-phenanthroline and 4,4′-di-carboxylic-2,2′-bipyridyl; $(L')_2 = 2PPh_3$, $Ph_2PC_2H_4PPh_2$, $Ph_2PC_2H_2PPh_2$) are discussed [19]. The photophysical and structural properties of these complexes indicate that these complexes can be used as potential probes to study bio-macromolecular dynamics in the presence of oxygen.

1.4 Bioconjugation of the synthesized probes and study of conjugated probe dynamics in lipid bilayer vesicles

Model membrane systems are very helpful for understanding the lipid dynamics in complex biological membranes, membrane protein function and molecular recognition between membrane components (i.e. lipid, cholesterol, proteins and other small molecules). Unilamellar vesicles, which are also known as the liposomes constructed from single phospholipid membrane bilayers, are excellent model systems for studying the dynamics and structural features of many cellular processes [20]. Because of the importance of model membrane systems in (1) basic biological research, (2) gene transfer in medical therapy, (3) microcapsules for proteolytic enzymes in the food industry and (4) drug delivery vehicles, various methods to prepare vesicles of different sizes and membrane compositions have been developed [21-23]. A potentially useful luminescent

membrane probe should be sensitive to the changes in environment of the bilayer caused by interactions of different membranes components and also the changes in micro-viscosity and membrane-fluidity resulted from the changes in physical conditions (temperature and pressure).

For efficient probe incorporation into liposomes, the probe should be covalently attached to a membrane component. There are a few examples where the MLC (Ru and Re) complexes have been covalently attached to the polar head group of lipid molecules [12]. Although cholesterol is an important component of biological membrane, to our knowledge no cholesterol-MLC conjugate has yet been reported. Therefore, based on the photophysical studies presented in Chapter 3, Ru-MLCs have been covalently conjugated with the phospholipid polar head groups and to the polar end of the cholesterol. Diimine ligands with functional groups such as –COOH, and $–NH_2$ are suitable for covalent conjugation to phospholipids (e.g., phosphatidylethanolamine), cholesterol and also proteins (residues having $–NH_2$ and –SH) [14]. The changes in the photophysical properties upon the covalent conjugation were studied. We have incorporated conjugated-MLC probes in liposomes and studied the photophysical properties of the conjugates in model membrane environment (Chapter 4). These MLC-conjugates are highly lipophilic and easily incorporated in lipid vesicles. The luminescent studies reveal that these probes are sensitive to the local environment of the liposomes and can be used as probes for dynamics affected by changes in temperature, viscosity and molecular interactions.

References

1. (a) Y. L. Angelique and J. M. Thomas *Chem. Rev.* ***99***(1999)*,* p.2711 (b) F. Li, W. Chen, C. Tang and S. Zhang, *Talanta*, **77** (2008), p.1.
2. S. J. Lippard, *Science*, **261 (**1993), p.699.
3. (a) K. E. Erkkila, D. T. Odom and J. K. Barton, *Chem. Rev.,* **99 (**1992), p.777; (b) T. W. Johann and J. K. Barton, *Philos. Trans. R. Soc.* (*London*), **299** (1996), p.354; (c) C. J. Murphy and J. K. Barton, *Methods Enzymol*., **226 (**1993), p.576; (d) A. M. Pyle, and J. K. Barton, *In Progress in inorganic chemistry: Bioinorganic chemistry* (ed.) (New York: John Willey), **38 (**1990), p.413.
4. M. J. Clarke, F. Zhu and D.R. Frasca, *Chem. Rev*., ***99*** (1999), p.2511.
5. M. J. Clarke, *Met. Ions Biol. Syst*., **11** (1980), p.231.
6. H. Chen, J.A. Parkinson, S. Parsons, R.A. Coxall, R.O. Gould, and P.J. Sadler, *J. Am. Chem. Soc.,* **124** (2002), p.3064.
7. (a) L. S. Lerman, *J. Mol. Bio.* **3** (1961), p.18; (b) B. M. Zeglis, V. C. Pierrea and J. K. Bartona. *Chem Commun (Camb)*., **44** (2007), p.4565; (c) A. E. Friedman, J. C. Chambron, J. P. Sauvage, N. J. Turro, J. K. Barton, *J. Am. Chem. Soc.* **112** (1990), p. 4960; (d) C. Moucheron, A. Krischdemesmaeker, J. M. Kelly, *Photochem. Phobiol. B.* **40 (**1997), p.91; (e) J. G. Collins, A. D. Sleeman, J. R. Aldric-Wright, I. Greguric and T. W. Hambleyh, *Inorg. Chem*. **37** (1998), p.3133; (f) D. Ossipov, P. I. Pradeepkumar, M. Holmer and J. Chattopadhyaya, *J. Am. Chem. Soc.* **123** (2001), p.3551.
8. (a) D. Colangelo, A. Ghiglia, A. Ghezzi, M. Ravera, E. Rosenberg, F. Spada and D. Osella, *Journal of Inorganic Biochemistry*, **99** (2005), p.505; (b) E. Rosenberg,

F. Spada, K.Sugden, B. Martin, R.o Gobetto, L. Milone and A. Viale, *Journal of Organometallic Chemistry* **, 689** (2004), p.4729; (c) C. Nervi, R. Gobetto, L. Milone, A. Viale, E. Rosenberg, F. Spada, D. Rokhsana and J. Fiedler, *Journal of Organometallic Chemistry***, 689** (2004), p. 1796.

9. A. Sharmin, A. Minzaao, L. Salassa, E. Rosenberg, J.B.A. Ross, S. Kabir and K. Hardcastle, *Inorg. Chim. Acta*, **361** (2008), p.1624.
10. J. R. Lakowicz, (2006). Principles of Fluorescence Spectroscopy. Springer.
11. V. Dadak, J. M. Vanderkooi, and W. W. Wright, *Biochim Biophys Acta,* **1100** (1992), p.33.
12. M. Bartholdi, F. J. Barrantes, and T. M. Jovin, *Eur J Biochem,* **120** (1981), p.389.
13. A. Che, and R. J. Cherry, *Biophys J,* **68** (1995), p.1881.
14. G. Piszczek, *Arch. Biochem. Biophys.* **453**(2006), p.54.
15. (a) J. Casper and T. J. Meyer, *J Phys. Chem*, **87** (1983), p.952 (b) E. M. Kober, J. L. Marshall, W.J. Dressick, B. P. Sullivan, J. Casper and T. J. Meyer, *Inorg. Chem.*, **24** (1985), p.2755.
16. E. Terpetsching, H. Szmacinsky, H. Malak and J. R. Lakowicz, *Biophys J*, **68** (1995), p.342.
17. L. Li, H. Szmacinski and J. R. Lakowicz, *biospectroscopy*, **3** (1997), P.155.
18. Albertino, C. Garino, S. Ghiani, R. Gobetto, C. Nervi, L. Salassa, E. Rosenberg, G. Viscardi, R. Buscaino, G. Croce, M. Milanesio and A. Sharmin. *J. Organometal Chem*, **692** (2007). p.1377.
19. A. Sharmin, R. C. Darlington, K. I. Hardcastle, M. Ravera, E. Rosenberg and J. B.A. Ross, *Journal of Organometallic Chemistry,* **694** (2009), p.988.

20. B. R. Gennis, (1989), Biomembranes, Springer- Verlag.

21. M. J. Ostro and P. R., Cullis, *Am. J. Hosp. Pharm.*, **46** (1989), p. 1576.

22. G. J. Dimitriadis, *Nature*, **274**, (1978), p. 923.

23. D. D. Lasic, (1995), Liposomes: From Physics to Applications, Elsevier.

CHAPTER 2: SYNTHESIS, STRUCTURE, PHOTOPHYSICAL AND ELECTROCHEMICAL BEHAVIOR OF 2-AMINO-ANTHRACENE TRIOSMIUM CLUSTERS

2.1 Introduction

In recent years we have been studying the reactivity of bicyclic nitrogen-containing heteroaromatics with $[Os_3(CO)_{10}(CH_3CN)_2]$. The resulting complexes have proven to be interesting from several points of view. First of all, the formation of formally electron deficient 46e-complexes of the general formula $[Os_3(CO)_9(\mu_3\text{-}\eta^2\text{-}(L\text{-}H))(\mu\text{-}H)]$ (L = quinoline, phenanthridine, 5,6-benzoquinoline, quinoxaline, benzimidazole, benzoxazole, benzothiazole) results in a dramatic change in the reactivity of the coordinated heterocycle relative to the free ligand. Thus, nucleophilic attack on the coordinated ligand takes place on the carbocyclic ring while in the free ligand it is invariably on the heterocyclic ring. Moreover, the regio- and stereoselectivity can be controlled in a previously unprecedented way [1–3]. Subsequent density functional theory (DFT) computational studies revealed that it was not the actual electron deficiency in the carbocyclic ring that lead to the observed novel reaction chemistry but rather the ability of the metal core to stabilize the anionic intermediates that are formed after nucleophilic attack [4].

These same complexes also proved to be good electron acceptors and electrochemical or chemical reduction results in the formation of stable radical anions, even in aqueous solutions, which have been studied spectroscopically and modeled with DFT calculations [5−7]. Here again, the ability for the metal core to communicate with the organic ligand via the electron deficient μ_3-η^2-bonding mode proved to be an important factor in determining the overall stability of the radical anions produced by reduction. Recently, it has been shown that this type of bonding mode can result from the reaction of an aromatic carbocycle containing exocyclic amine substituents [8]. Also, there have been recent reports that metal complexes of anthracene are particularly good intercalators into the major groove of DNA [9]. In light of our previous reports regarding the selective binding of triosmium complexes containing aromatic nitrogen heterocycles to DNA we thought it would be interesting to study the reactions of 2-aminoanthracene with $[Os_3(CO)_{10}(CH_3CN)_2]$ [10, 11]. We report here the results of these studies including the electrochemical and photophysical properties of the complexes formed as well as their structural characterization by solid state and solution spectroscopic techniques.

2.2 Experimental

2.2.1 General methods and materials

Reactions were carried out under a nitrogen atmosphere but were worked up in air using preparative thin layer chromatography (10 × 20 cm plates coated with

1 mm silicagel PF 60_{254}-EM Science). Solvents were reagent grade. Tetrahydrofuran was distilled from benzophenone ketyl and methylene chloride and acetonitrile were distilled from calcium hydride. Osmium carbonyl purchased from Strem Chemicals and was used to prepare of $[Os_3(CO)_{10}(MeCN)_2]$ by oxidation with trimethylamine N-oxide(Aldrich) in acetonitrile according to the known literature procedures [12]. 2-Aminoanthracene 98% (Aldrich) was used as received.

General crystallization method: Sample was dissolved in minimum volume of CH_2Cl_2 in a clean test tube. n-Hexane was added slowly by dripping down the side of the test tube to form a discreet layer of hexane. The test tube was covered and placed in refrigerator at 4 ºC to obtain single crystals suitable for X-ray crystallography.

^{1}H NMR spectra were obtained on a Varian 400 MHz Unity Plus or a Varian NMR Systems 500 MHz spectrometer. Infrared spectra were obtained on a Thermo-Nicolet 633 FT-IR spectrometer. Elemental analyses were performed by Schwarzkopf Microanalytical Labs, Woodside, NY.

Electrochemical methods were performed on a BAS 100 electrochemical analyzer in CH_2Cl_2 using tetra-*n*-butyl ammonium hexafluorophosphate ($[NBu_4]PF_6$) as the carrier electrolyte and are reported referenced to the ferrocene/ferrocenium ion couple. A standard three-electrode cell was designed to allow the tip of the reference electrode (saturated calomel electrode, SCE) to closely approach the working (a glassy carbon disk, diameter 0.1 cm, sealed in epoxy resin), and the auxiliary (a Pt wire) electrodes. All measurements were carried out under nitrogen in CH_2Cl_2 solutions containing 0.1 M $[NBu_4]PF_6$ as supporting electrolyte and the metal complexes at 1.0×10^{-3} M.

UV–Vis absorption spectra and emission spectra were recorded on a Molecular devices Spectra Max M2 using acetonitrile as the solvent. Time-resolved luminescence decay measurements were performed by time-correlated single-photon counting (TCSPC), using the Quantum Northwest FLASC 1000 sample chamber (Spokane, WA). The fluorescence intensity decay was calculated by fitting the data to a single exponential decay model; here I(t) is the time dependent intensity and I_0 is the intensity at time 0 and τ is the excited-state lifetime.

$$I(t)=I_0\exp(-t/\tau) \qquad (1)$$

2.2.2 The reaction of $[Os_3(CO)_{10}(MeCN)_2]$ with 2-aminoanthracene at ambient temperature

The reaction of $[Os_3(CO)_{10}(MeCN)_2]$ (0.220 g, 0.21 mmol) with 2-aminoanthracene (0.08 g, 0.41 mmol) in CH_2Cl_2 (40 mL) at room temperature was carried out for 15hr. The solvent was removed on a rotary evaporator and the residue was purified using thin layer chromatography on silica. Elution with hexane/CH_2Cl_2 (4:1 v/v) gave four bands. The fastest moving band was the unreacted starting material (actually $[Os_3(CO)_{12}]$ because $[Os_3(CO)_{10}(MeCN)_2]$ converts to the parent carbonyl with decomposition on silicagel in the absence of acetonitrile). The second band afforded compound $[Os_3(CO)_{10}(\mu\text{-}\eta^2\text{-(N-C3)-}NHC_{14}H_9)(\mu\text{-H})]$ (**2**) as greenish yellow crystals from CH_2Cl_2/hexane at 4 °C in 14% (0.034 g) yield. Elemental *Anal*. Calc. for $C_{24}H_{11}N_1O_{10}Os_3$: C, 27.91; H, 1.03; N, 1.23%. Found: C, 27.61; H, 1.06; N, 1.34%. IR in CH_2Cl_2: 2100(s), 2060(vs), 2049(vs), 2017(s), 2000(s), 1988(sh), 1974(sh); ^{1}H NMR in

$CDCl_3$: δ 8.07(s, br, 1H); 7.99(s, 1H); 7.806(m, 1H), 7.66(m, 1H); 7.65(s, 1H); 7.42(m, 3H), 4.12(d, 1H); 3.85(d, 1H); −14.169(s, 1H).

The third band afforded $[Os_3(CO)_{10}(\mu\text{-}\eta^2\text{-}(N\text{-}C1)\text{-}NH_2C_{14}H_8)(\mu\text{-}H)]$ (**1**) as red crystals from CH_2Cl_2/hexane at 4 °C in 35% (0.088 g) yield. Elemental *Anal*. Calc. for $C_{24}H_{11}N_1O_{10}Os_3$: C, 28.15; H, 0.80; N, 1.19%. Found: C, 27.61; H, 1.06; N, 1.34%. IR in CH_2Cl_2: 2100(s), 2062(vs), 2050(vs), 2018(s), 1998(s), 1988(sh), 1974(sh); ^{1}H NMR in $CDCl_3$: δ 8.02(s, 1H); 7.97(d, 2H); 7.81(s, 1H); 7.54(m, 3H), 4.45(br, 2H); −14.06(br, 1H).

The fourth band yielded a small amount of compound $[Os_3(CO)_9(\mu\text{-}\eta^2\text{-}(N\text{-}C(3))\text{-}NHC_{14}H_8)(\mu\text{-}H)_2]$ (**3)** as yellow crystals from CH_2Cl_2/hexane at 4 °C. Elemental *Anal*. Calc. for $C_{23}H_{11}N_1O_9Os_3$: C, 26.75; H, 0.85; N, 1.21%. Found: C, 27.19; H, 1.09; N, 1.38%. IR in CH_2Cl_2: 2122(s), 2080(vs), 2049(vs), 2003(s), 1992(sh), 1972(sh); ^{1}HNMR in $CDCl_3$: δ 8.13(s, 1H), 8.06(d, 2H), 7.88(m, 2H), 7.35(m, 2H), 7.04(s, 1H), 5.85(br, 1H) and −14.59(s, 2H).

2.2.3 The reaction of $[Os_3(CO)_{10}(MeCN)_2]$ with 2-aminoanthracene at elevated temperature

A THF solution (60 mL) of $[Os_3(CO)_{10}(MeCN)_2]$ (0.400 g, 0.43 mmol) and 2-amino-anthracene (0.120 g, 0.62 mmol) was refluxed for 3 h during which time the color of the solution changed from yellow to greenish yellow. The solvent was removed on a rotary evaporator and the residue was purified by using thin layer chromatography on silica. Elution with hexane/CH_2Cl_2 (3:1 v/v) generated four bands. The faster moving

band was the unreacted starting material. The second band contained a trace amount of a green compound. The third band gave $[Os_3(CO)_{10}(\mu\text{-}\eta^2\text{-}C_{14}H_9NH)(\mu\text{-}H)]$ (**2**) as greenish yellow crystals from CH_2Cl_2/hexane at 4 °C in 24% (0.107 g) yield. The slowest moving band afforded $[Os_3(CO)_9(\mu_3\text{-}\eta^2\text{-}C_{14}H_8NH)(\mu\text{-}H)_2]$ (**3**) as yellow crystals from CH_2Cl_2/hexane at 4 °C in 28% (0.120 g) yield.

2.2.4 Synthesis of $[(\mu\text{-}H)Os_3(CO)_9(\mu_3\text{-}\eta^2\text{-}C_{14}H_8NH_2)]$ (4)

Thermolysis of $[Os_3(CO)_{10}(\mu\text{-}\eta^2\text{-}(N\text{-}C(3)C_{14}H_9NH)(\mu\text{-}H)]$ (**2**) (0.046 g, 0.044 mmol) in refluxing cyclohexane (40 mL) gave a deep green solution. The solvent was removed by rotary evaporator and the residue was purified by using thin layer chromatography on silica gel. Elution by hexane/CH_2Cl_2 (3:1 v/v) gave two bands. The faster moving band yielded compound $[Os_3(CO)_9(\mu_3\text{-}\eta^2\text{-}C_{14}H_9NH_2)(\mu\text{-}H)]$ (**4**) as green crystals from CH_2Cl_2/hexane at 4 °C in 68% (0.030 g) yield. Elemental *Anal*. Calc. for $C_{23}H_{11}N_1O_9Os_3$: C, 27.40; H, 0.53; N, 1.20. Found: C, 27.19; H, 1.09; N, 1.38%. IR in CH_2Cl_2: 2102(s), 2063(s), 2052(vs), 2021(s), 2003(s), 1970(w); ^{1}HNMR in $CDCl_3$: 10.67(s, 2H); 8.52(s, 1H); 8.01(s, 1H); 7.86(t, 2H); 7.6(m, 2H); 7.5(t, 1H); 5.33(s, 2H); −14.36(s, 1H).

2.2.5 Photolysis of 2

The photolysis of compound **2** was done by irradiating a methylene chloride (70 mL) solution of compound **2** (0.045 g, 0.044 mmol) by UV radiation for 2 h.

The resulting brown solution was then dried on an evaporator. The chromatographic separation of the residue gave two bands as eluted by hexane/CH_2Cl_2 (4:1 v/v). The faster moving band was the unreacted compound **2** and the slower moving band yielded compound **3.**

2.2.6 Reaction of $[Os_3(CO)_9(\mu_3\text{-}\eta^2\text{-}(N\text{-}C(3))\text{-}NHC_{10}H_9)(\mu\text{-}H)]$ 4 with $P(C_2H_5O)_3$

The green methylenechloride solution of cluster **4** turned yellow after the addition of $P(C_2H_5O)_3$, (in 1: 1 molar ratio) at room temperature under N_2, within 5 minutes. The solvent was removed on a rotary evaporator and the residue was purified by using thin layer chromatography on silica. Elution with hexane/CH_2Cl_2 (4:1 v/v) gave two bands with a heavy baseline. The fastest moving UV-band was the unreacted phosphine ligand. The slower moving yellow band was recovered and it yielded a small amount of yellow complex **5**, which was analyzed by infrared and NMR spectroscopy. IR in CH_2Cl_2: 2083(w), 2060(vs), 2042(vs), 2000(s), 1987(s), 1970(s), 1955 (sh), 1712 (s); ^{1}H NMR in $CDCl_3$: δ 8.5-6.8 (m), 3.8-3.4(m); 1.6(s, br); 1.25 (s, br); −14.1 (m); −14.4 (m); −14.7 (dd).

2.2.6 Crystal structure analysis

Suitable crystals of **2** and **3** were coated with Paratone N oil, suspended in a small fiber loop and placed in a cooled nitrogen gas stream at 173 K on a Bruker D8 SMART APEX CCD sealed tube diffractometer with graphite-monochromated Mo Kα

(0.71073 Å) radiation. Data were measured using a series of combinations of phi and omega scans with 10 s frame exposures and 0.3° frame widths. Data collection, indexing and initial cell refinements were all carried out using SMART [13] software. Frame integration and final cell refinements were done using SAINT [14] software. The final cell parameters were determined from least-squares refinement on 2481 and 5705 reflections, respectively. The SADABS [15] program was used to carry out absorption corrections. The structure was solved using the Patterson method and difference Fourier techniques (SHELXTL, V6.12) [16]. Hydrogen atoms were placed in their expected chemical positions using the HFIX command and were included in the final cycles of least squares with isotropic U_{ij}'s related to the atom's ridden upon. The bridging hydrides were positioned by using XHYDEX [17]. All non-hydrogen atoms were refined anisotropically. Scattering factors and anomalous dispersion corrections are taken from the International Tables for X-ray Crystallography [18]. Structure solution, refinement, graphics and generation of publication materials were performed by using SHELXTL, V6.12 software. Additional details of data collection and structure refinement are given in Table 2.1.

2.3 Results and discussion

2.3.1. Compound synthesis and reaction pathways

The reaction of $[Os_3(CO)_{10}(MeCN)_2]$ with 2-aminoanthracene in CH_2Cl_2 at room temperature yielded $[Os_3(CO)_{10}(\mu\text{-}\eta^2\text{-}(N\text{-}C(1))\text{-}NH_2C_{14}H_8)(\mu\text{-}H)]$ (**1**) and $[Os_3(CO)_{10}(\mu\text{-}\eta^2\text{-}(N\text{-}C(3))\text{-}NHC_{14}H_9)(\mu\text{-}H)]$ (**2**) in 35% and 14% yield, respectively, along with trace amounts of $[Os_3(CO)_9(\mu\text{-}\eta^2\text{-}(N\text{-}C(3))\text{-}NHC_{14}H_8)(\mu\text{-}H)_2]$ (**3**) (Scheme 2.1). When the same

reaction is performed in refluxing THF only **2** and **3** in 24% and 28% yield, respectively, are obtained along with a trace amount of a dark green compound which was subsequently identified as $[Os_3(CO)_9(\mu_3\text{-}\eta^2\text{-}C_{14}H_8NH)(\mu\text{-}H)]$ (**4**) (vide infra) (Scheme 2.1). In a separate experiment, red crystals of **1** were dissolved in $CDCl_3$ and monitored by ^1H NMR. The initially red solution gradually turns yellow and the proton resonances associated with **2** gradually appear. Thus it appears that C–H activation at the 1- and 3-positions of the anthracene ring is competitive at room temperature but that **2** is more thermodynamically stable than **1**. The structures of **2** and **3** based on the NMR, IR and elemental analysis were verified by solid state structure determinations. The thermal instability of **1** precluded obtaining good single crystals and is based on its ^1H NMR and the observed dynamic behavior of the hydride ligand (vide infra). It would appear that if activation of the C–H bond at the 3-position takes place this intermediate goes on to form **3** but if activation at the 1-position occurs than the initially formed **1** is unstable with respect to conversion to **2**.

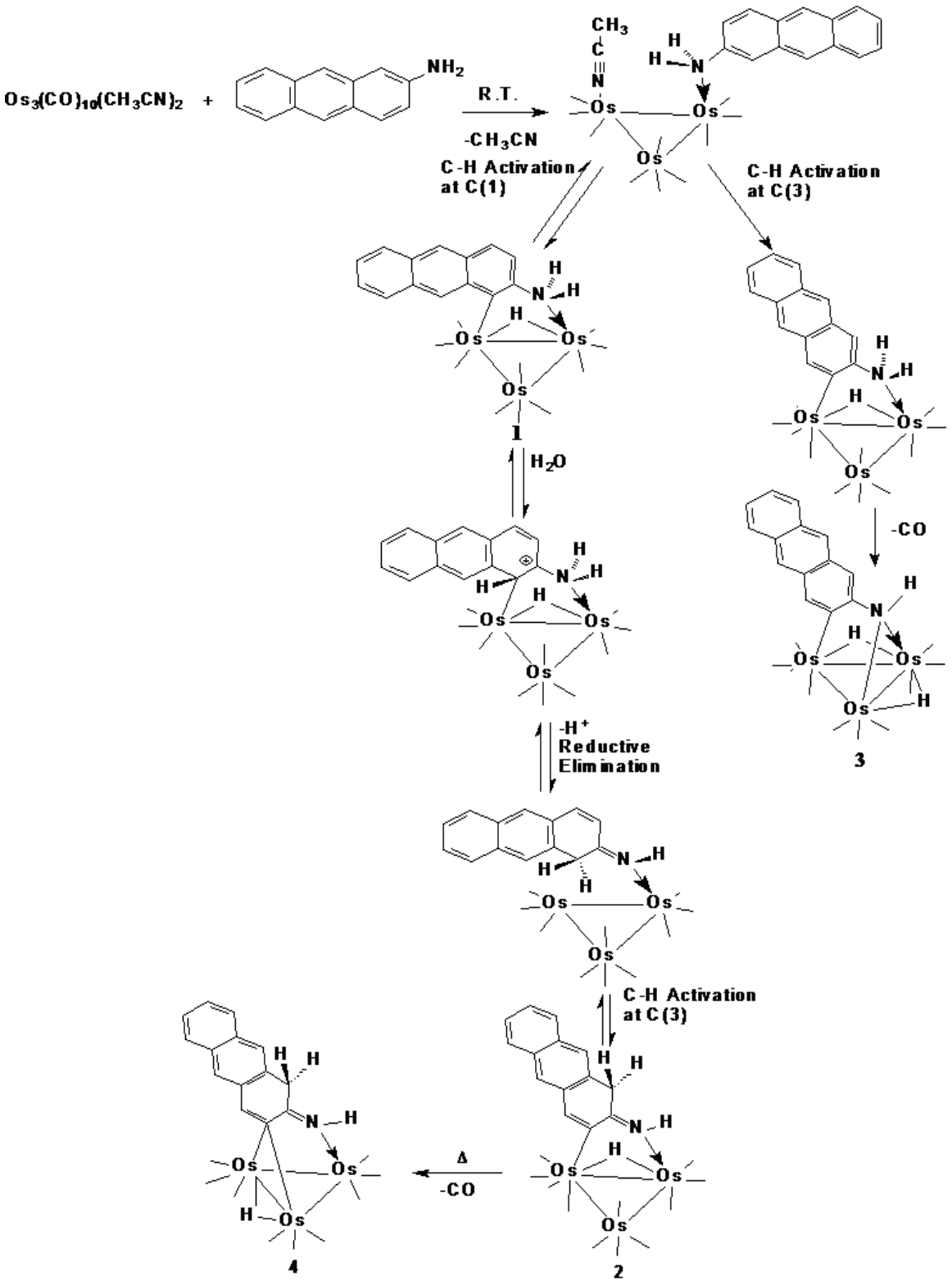
Os3(CO)10(CH3CN)2 +
NH2
R.T.
-CH3CN
C-H Activation at C(1)
C-H Activation at C(3)
1
H2O
-CO
3
-H+ Reductive Elimination
C-H Activation at C(3)
Δ
-CO
4
2

Scheme 2.1

The rearrangement of **1** to **2** involves an overall transfer of a proton from the amine nitrogen to the 1-position of the anthracene ring along with reductive elimination of the initially activated C(1)–H bond. The disruption of the aromatic character by the proton transfer to C(1) results in formation of a C(2)═N bond (Scheme 2.1). We noticed that conversion of **1** to **2** was accelerated by the addition of water. When D_2O is added to a solution of **1** in CD_2Cl_2 the onset of the conversion to **2** is noted immediately (Figure 2.1). In addition to the appearance of the hydride peak associated with **2** and the corresponding AB pattern for the C(1) methylene group we noted an additional broad singlet at δ 4.79 that is not present in either **1** or **2**. This resonance gradually disappears along with the resonances associated with **1** and conversion to **2** is >90% complete in 6 days (Figure 2.1). We can assign this peak to a C(1)HD group formed by initial deuteration of C(1) by D_2O followed by reductive elimination (Scheme 2.1). The disappearance of this peak with time and the simultaneous appearance of the $C(1)H_2$ of **2** indicates that these steps are reversible and that a thermodynamic isotope effect is operative due to the presence of H_2O in the sample (in our hands it was not possible to avoid the introduction of water during the preparation of $[Os_3(CO)_{10}(MeCN)_2]$ and/or during TLC purification). We suggest here that steric crowding at the osmium atom bound to the C(1) in **1** leads to an elongated Os–C(1) bond, negatively polarized toward C(1) which activates this position towards protonation by adventitious water. The proposed steric crowding arises from the disposition of the anthracene ring relative to the carbonyl groups on the Os bound to C(1). Clearly there are alternative possibilities for the proton catalyzed conversion of **1** to **2** but the pathway presented in Scheme 2.1 represents the most straightforward one based on the data at hand. As

expected at higher temperature the conversion of **1** to **2** is much faster and therefore only compounds **2** and **3** are observed.

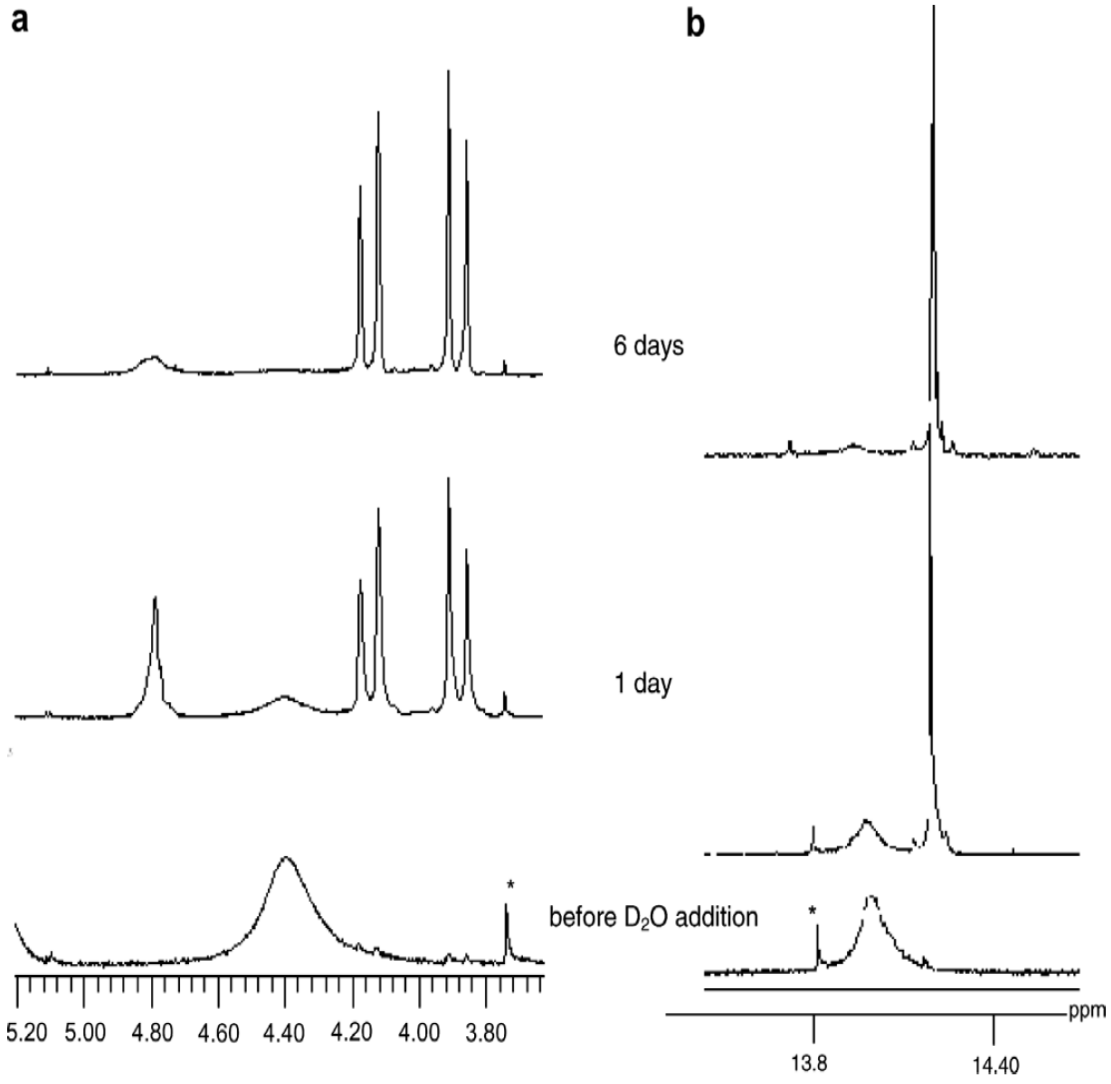

Figure 2.1: 400 MHz ^{1}H NMR in CD_2Cl_2 showing the room temperature conversion of $[Os_3(CO)_{10}(\mu\text{-}\eta^2\text{-}(N\text{-}C(1))\text{-}NH_2C_{14}H_8)(\mu\text{-}H)]$ (1) to$[Os_3(CO)_{10}(\mu\text{-}\eta^2\text{-}(N\text{-}C(3))\text{-}NHC_{14}H_9)(\mu\text{-}H)]$ (2) before and after the addition of D_2O in the aliphatic (a) and hydride proton (b) regions (* indicates a trace impurity).

Initial activation at C(3) leads to a less sterically encumbered adduct which then goes on to form **3** via N–H activation-decarbonylation. There is ample precedent for the room temperature formation of nonacarbonyl dihydrides from the reaction of aromatic hydrocarbons containing amine functionalities with $[Os_3(CO)_{10}(MeCN)_2]$ [19].

In our previous studies on the reactivity of decacarbonyl triosmium complexes of aromatic nitrogen heterocycles we found that decarbonylation either thermally or photochemically leads to the formation of nonacarbonyl complexes containing a μ_3-η^2 bonding mode for the nitrogen heterocycle with the osmium bound carbon involved in a 3-center-2-electron bond [1–2]. This is not the case for **2** where only thermolysis leads to decarbonylation while photolysis leads only to the formation of **3** along with nonspecific decomposition (Scheme 2.3). The reasons for this difference probably lie in the larger size and "vertical" orientation of the anthracene ring in **2**. Our recent computational studies on the transition states involved in the decarbonylation of related complexes revealed that considerable motion of the heterocyclic ring is involved in the reaction coordinate [20]. Thermal excitation of the large and vertically oriented anthracene ring is therefore required to access the decarbonylation pathway. This is thermally accessible for the smaller ring systems at ambient temperatures and thus decarbonylation can take place both thermally and photochemically.

2.3.2. Solid state structures of compounds 2 and 3

The solid state structure of **2** is shown in Figure 2.2, crystal data are given in Table 2.1 and selected distances and angles are given in Table 2.2. The structure consists

of an approximately equilateral triangle of osmium atoms with the 2-amino anthracene ligand bound to one edge of the triangle via the nitrogen atom and C(3) of the ring (C(24) in Figure 2.2). The ligand resides in a plane approximately perpendicular to the plane of the Os_3 triangle (N(1)–Os(3)–Os(2) = 92.49(12)° and C(24)–Os(1)–Os(2) = 90.65(14)°). The N(1)–C(11) (C(3)) bond length of 1.296(6) Å is consistent with this being a carbon–nitrogen double bond and the adjacent carbon–carbon bonds can be viewed as carbon–carbon single bonds (C(11)–C(24) = 1.467(7), C(11)–C(12) = 1.500(7), C(12)–C(13) = 1.508(7) Å). The C(23)–C(24) bond length of 1.357(7) Å is suggestive of double bond localization as a result of disruption of the aromaticity of the cluster bound ring while the carbon–carbon bonds in the remaining anthracene rings are all around 1.42 Å.

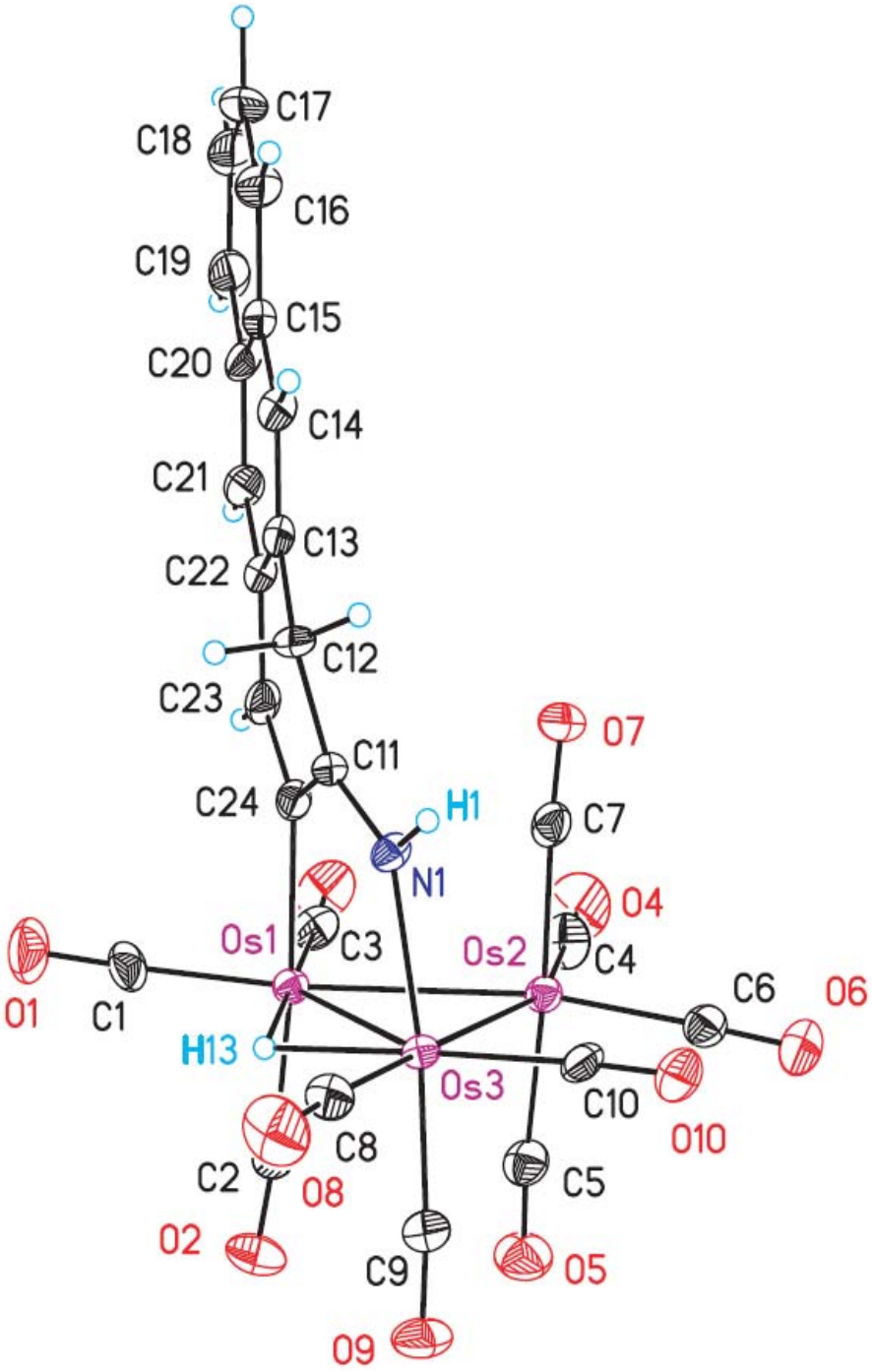

Figure 2.2: Solid state structure of $[Os_3(CO)_{10}(\mu\text{-}\eta^2\text{-}(N\text{-}C(3))\text{-}NHC_{14}H_9)(\mu\text{-}H)]$ (2) showing the 90% probability thermal ellipsoids and the calculated positions of the hydride and hydrogen atoms.

Table 2.1 Crystal data and structure refinement for 2 and 3

Compound	**2**	**3**
Empirical formula	$\mathbf{C_{24}H_{11}NO_{10}Os_3}$	$\mathbf{C_{23}H_{11}NO_9Os_3}$
Formula weight	1044.95	1015.93
Temperature (K)	173(2)	173(2)
Wavelength (Å)	0.71073	0.71073
Crystal system	triclinic	monoclinic
Space group	$P\bar{1}$	$P\ 2_1/c$
Unit cell dimensions		
a (Å)	8.4517(10)	8.9379(6)
b (Å)	8. 5215(10)	14.2536(10)
c (Å)	20.125(2)	19.0453(12)
α (º)	92.056(3)	90
β (º)	90.265(3)	93.805(2)
γ (º)	119.334(2)	90
Volume ($Å^3$)	1262.4(3)	2421.0(3)
Z	2	4
D_{calc} (Mg/m^3)	2.749	2.787
Absorption coefficient (mm^{-1})	15.119	15.760
F(000)	942	1824
Crystal size (mm)	0.20 X 0.12 X 0.02	0.19 X 0.12 X 0.08
0 Range for data collection (º)	2.03–28.33	1.79–28.34
Index ranges	$-11 \le h \le 11$ $-11 \le k \le 11$ $-26 \le l \le 26$	$-11 \le h \le 8$ $-18 \le k \le 19$ $-11 \le l \le 8$
Reflection collected	17528	16646
Independent reflections (Rint)	6285 (0.0304)	5862 (0.0304)
Completeness to $\theta = 28.34º$ (%)	99.5	97.2
Absorption correction	semi–empirical from equivalents	semi–empirical from equivalents
Maximum and minimum transmission	0.7519 and 0.1519	0.3654 and 0.1537
Refinement method	Full-matrix least-squares on F^2	Full-matrix least-squares on F^2
Data/restraints/Parameters	6285/0/343	5862/0/325
Goodness-of-fit on F^2	1.077	1.076
Final *R* indices [$I > 2\sigma(I)$]	$R_1 = 0.0297, wR_2 = 0.0681$	$R_1 = 0.0280, wR_2 = 0.0611$
R indices (all data)	$R_1 = 0.0337, wR_2 = 0.0697$	$R_1 = 0.0341, wR_2 = 0.0631$
Largest difference in peak and hole ($e\ Å^{-3}$)	2.037 and –1.288	2.162 and –0.841

Table 2.2 Selected bond distances (Å) and bond angles (°) for compound 2[a]

Distances (Å)			
Os(1)-Os(3)	2.9007(4)	C(11)-N(1)	1.296(6)
Os(1)-Os(2)	2.9098(4)	C(11)-C(24)	1.467(7)
Os(2)-Os(3)	2.8992(4)	C(11)-C(12)	1.500(7)
Os(3)-N(1)	2.112(4)	C(12)-C(13)	1.508(7)
Os(1)-C(24)	2.148(5)	C(23)-C(24)	1.357(7)
Os-CO[b]	1.918(6)	C(13)-C(22)	1.426(7)
C-O[b]1.138(7)			
Angles (°)			
Os(1)-Os(2)-Os(3)	59.912(7)	N(1)-C(11)-C(24)	120.3(5)
Os(1)-Os(3)-Os(2)	60.225(10)	N(1)-C(11)-C(12)	118.5((5)
Os(2)-Os(2)-Os(3)	59.863(9)	C(24)-C(11)-C(12)	121.4(4)
N(1)-Os(3)-Os(2)	92.49(12)	C(11)-C(12)-C(13)	115.0(4)
N(1)-Os(3)-Os(1)	81.10(11)	C(11)-C(24)-C(23)	114.5(5)
C(24)-Os(1)-Os(2)	90.65(14)	C(22)-C(23)-C(24)	126.8(5)
C(24)-Os(1)-Os(3)	84.37(14)	Os-C-O[b]	176.2(5)

[a] Numbers in parentheses are average standard deviations.

[b] Average values.

The solid state structure of **3** is shown in Figure 2.3 crystal data are given in Table 2.1 and selected distances and bond angles are given in Table 2.3. The structure consists of an isosceles triangle of osmium atoms with one elongated edge (Os(1)–Os(2) = 2.9881(3) Å) and two shorter approximately equal edges (Os(1)–Os(3) = 2.8102(3), Os(2)–Os(3) = 2.8030(3) Å). The longer edge has an in-plane bridging hydride, H2H, as determined by the program XHYDEX [17]. The doubly bridged

edge has the calculated position of the hydride, H1H tucked well below the plane of the Os_3 triangle at 79.9° and as expected directly *trans* to two carbonyl groups on Os(1) and Os(3). The 2-aminoanthracene ligand is approximately perpendicular to the Os_3 plane and the symmetrical nitrogen bridge across the Os(1)–Os(3) edge Os(10)–N(1) = 2.131(4) and Os(3)–N(1) = 2.139(4) Å) results in the ligand bisecting this edge. There is evidence for double bond localization for the double bond associated with the nitrogen atom and the one involving the carbon atom bound to Os(2) (C(1)–C(2) = 1.359(7) and C(13)–C(14) = 1.370(8) Å) but the C–N bond is clearly a single bond (C(1)–N(1) = 1.439(7) Å). The overall geometry of the complex is very similar to that observed for related dihydrides where nitrogen is part of the aromatic ring system [19].

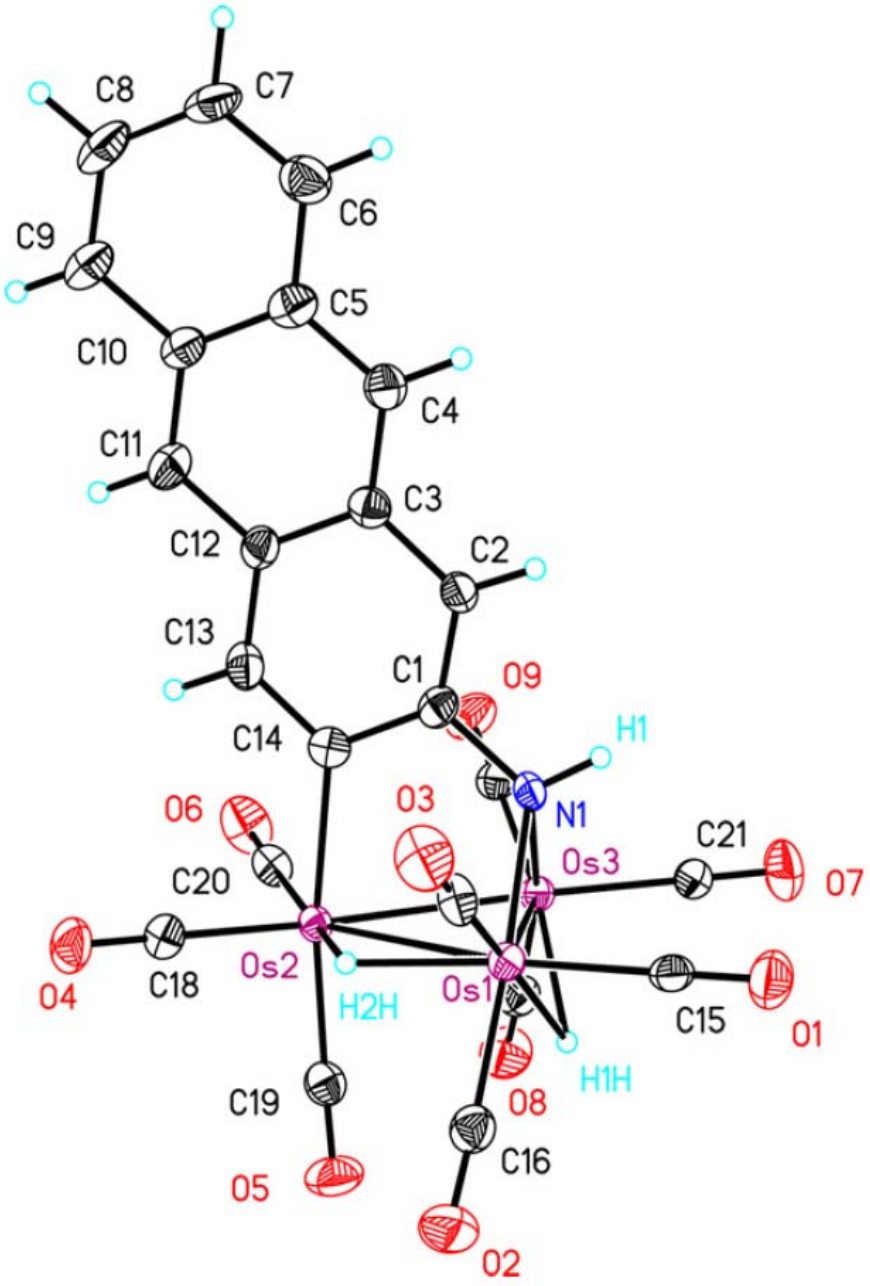

Figure 2.3: Solid state structure of $[Os_3(CO)_9(\mu\text{-}\eta^2\text{-}(N\text{-}C(3))\text{-}NHC_{14}H_8)(\mu\text{-}H)_2]$ (3) showing the 90% probability thermal ellipsoids and the calculated positions of the hydride and hydrogen atoms.

Table 2.3 Selected bond distances (Å) and bond angles (°) for compound 3[a]

Distances (Å)			
Os(1)-Os(3)	2.8102(3)	C(1)-N(1)	1.439(7)
Os(1)-Os(2)	2.9881(3)	C(1)-C(2)	1.359(7)
Os(2)-Os(3)	2.8030(3)	C(1)-C(14)	1.431(7)
Os(1)-N(1)	2.131(4)	C(2)-C(3)	1.420(8)
Os(3)-N(1)	2.139(4)	C(13)-C(14)	1.370(8)
Os(2)-C(14)	2.135(6)	C(12)-C(13)	1.411(8)
Os-CO[b]	1.914(6)		
C-O[b]	1.136(7)		
Angles (°)			
Os(1)-Os(2)-Os(3)	57.954(7)	N(1)-C(1)-C(2)	119.8(5)
Os(1)-Os(3)-Os(2)	64.327(8)	N(1)-C(11)-C(12)	117.0((5)
Os(2)-Os(1)-Os(3)	57.719(8)	C(2)-C(1)-C(14)	123.2(5)
N(1)-Os(3)-Os(2)	77.48(11)	C(13)-C(14)-C(1)	116.4(5)
N(1)-Os(1)-Os(2)	73.40(11)	C(12)-C(13)-C(14)	122.6(5)
C(14)-Os(2)-Os(1)	82.39(14)	C(2)-C(3)-C(12)	117.6(5)
C(14)-Os(2)-Os(3)	83.27(15)	Os-C-O[b]	177.2(5)

[a] Numbers in parentheses are average standard deviations.

[b] Average values.

2.3.3. Hydride ligand dynamics for 1 and 3

Although the monohydride complex **2** is stereochemically rigid, the related complex **1** exhibits a dynamic process which we interpret as simple edge to edge migration of the hydride ligand. This hydride migration averages the major isomer where the hydride bridges the same edge as the anthracene ligand, as in **2**, with a minor isomer

where the bridge is either to the carbon bound osmium atom or the nitrogen bound osmium atom and the $Os(CO)_4$ group (Scheme 2.2 and Figure 2.4). The ratio of the two isomers is 6.1:1 with the major isomer appearing at δ −14.06 and the minor isomer appearing at δ −13.02 as a broad signal at −4 °C. Similar edge hopping processes have been observed for $Os_2(CO)_{10}(L)(\mu\text{-}H)$ systems where L is a nitrogen containing ligand [21].

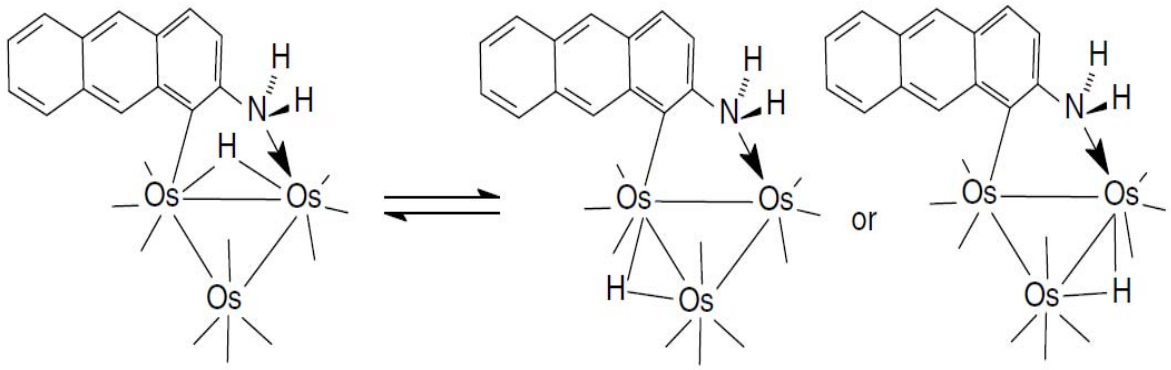

Scheme 2.2

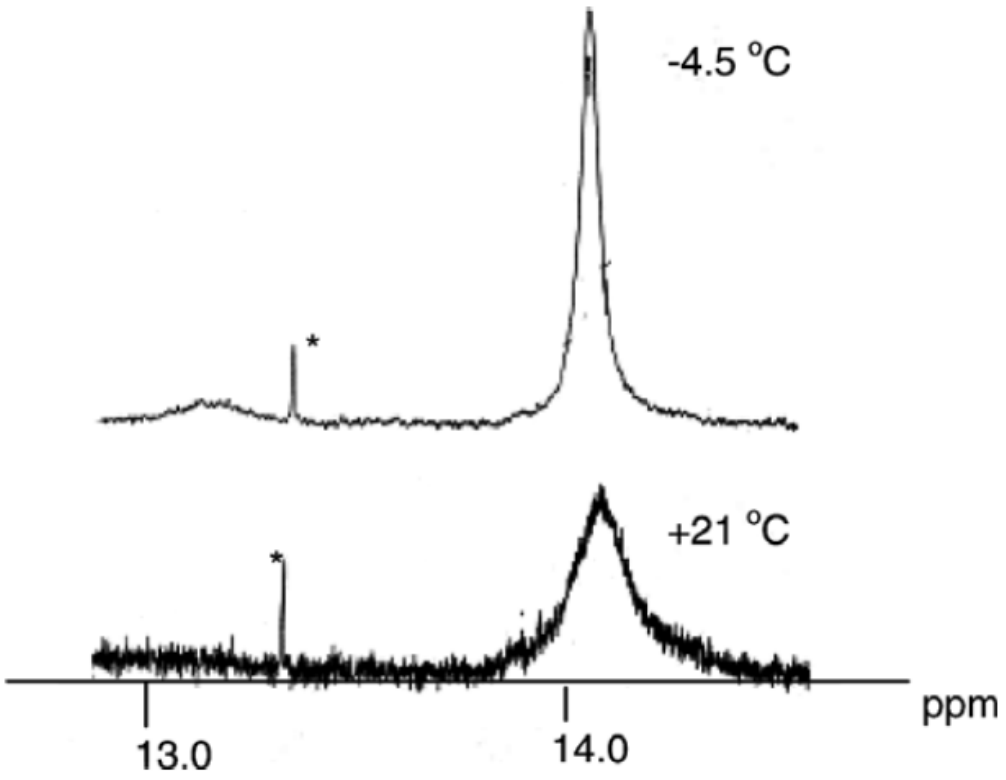

Figure 2.4: 500 MHz ^{1}H NMR of [$Os_3(CO)_{10}$(μ-η^2-(N-C(1))-$NH_2C_{14}H_8$)(μ-H)] (1) in the hydride region at ambient temperature and −4.5 °C (*indicates a trace impurity).

Complex **2** also shows a dynamical process common to hydrido triosmium clusters. At room temperature a single sharp hydride resonance of relative intensity 2 is observed at δ −14.62. Given that the two hydride ligands in **2** are not magnetically equivalent in the solid state structure there must be an exchange process which passes through a symmetrical intermediate (Scheme 2.3). As the temperature is lowered to −12.5 °C the resonance at δ −14.62 broadens and is resolved into two resonances at δ−14.56 and δ −14.69 of equal intensity (Figure 2.5). This type of hydride edge hopping is quite common for nonacarbonyl dihydrido triosmium clusters [19].

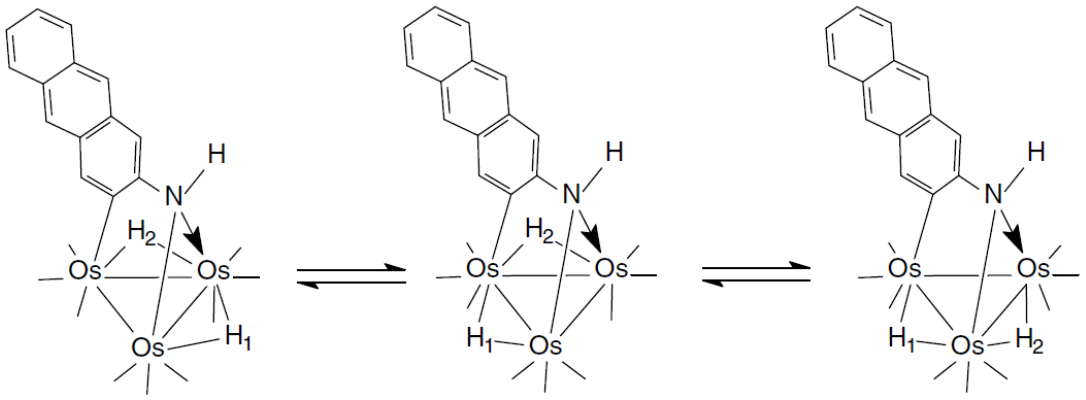

Scheme 2.3

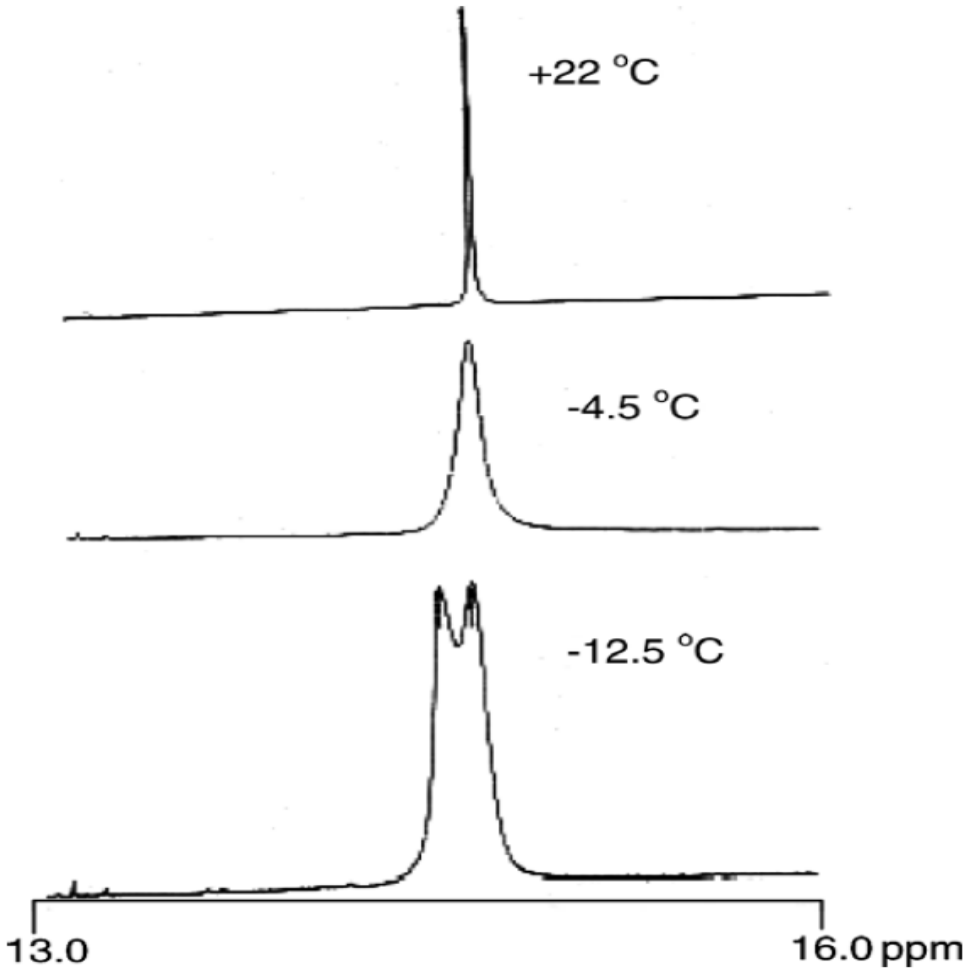

Figure 2.5: Variable temperature 500 MHz ^{1}H NMR of $[Os_3(CO)_9(\mu\text{-}\eta^2\text{-}(N\text{-}C(3))\text{-}NHC_{14}H_8)(\mu\text{-}H)_2]$ (3) in the hydride region.

2.3.4 Photophysical properties of 1–4

The complexes **1**–**4** all show several absorption bands in the near UV–Vis region 260–430 nm and in addition **1** shows a band in the visible at 470 nm and **4** shows a band at 615 nm (Table 2.4). The similarity between the spectra in the 260–430 nm region and that of the free ligand, 2-aminoanthracene, suggest that the absorptions in this region are due to π to π^* transitions. This is further supported by the emission spectra of the complexes where almost identical emissions are observed for **1**–**4** and for 2-amino anthracene in the range of 476–490 nm when they are irradiated in the π to π^* region (Table 2.4). Excitation spectra of the complexes and of 2-amino-anthracene show that the major contributions to the emissions are from the bands at 261 nm and in the 385–430 nm range. The major difference between the emissions of the complexes and the emission of the free ligand is that the intensity of the emission from the complexes is significantly attenuated with respect to the free ligand. This is not surprising in that binding of the ligand to the cluster would be expected to mix in metal orbitals with π and/or π^* ligand MO's thereby deceasing the π to π^* transition probability. Irradiation of **1** at 470 nm led to no emission and irradiation of **4** at 615 nm also led to no emission. We assign the low-energy band to an n to σ^* transition based on its similar wavelength and intensity compared with the large series of previously reported complexes with similar bonding modes to **4** [22]. Thus, it appears that the overall photophysical properties of the anthracene ligand undergo only slight modification on binding to the triosmium cluster in a variety of bonding modes.

Table 2.4 UV–Vis absorption and emission data for 1–4 and 2-aminoanthracene

Compound	π- π^* (nm)	MLCT (nm)	n-σ^* (nm)	Excitation (nm)	Emission (nm)	lifetime (ns)
2-amino anthracene	261, 316, 334, 352, 405			410	488	
1	261, 324, 364, 383	470		324	485	
2	260, 320, 352, 385, 434			434	490	7.5
3	269, 312, 353, 372, 395			395	476	5.8
4	268, 310, 386		615	386	480	

2.3.5. Electrochemical behavior of 1–4

Complexes **1**–**3** all show irreversible $1e^-$ reductions in the range of −1.85 to −2.14 V while **4** shows a nicely reversible $1e^-$ wave at −1.16 V ($\Delta E^{1/2}$ = 39 mV at scan rates of 50–800 mV/s) and a quasi-reversible second reduction at −1.62 V ($\Delta E^{1/2}$ = 200 mV at a scan rate of 400 mV/s; Table 2.5, Figure 2.6). The large $\Delta E^{1/2}$ and lower peak area for this second reduction suggest that reaction/decomposition of the resulting dianion is rapid on the chemical and electrochemical time scale. Indeed at scan rates less than 400 mV/s this second reduction becomes irreversible while the peak to peak separation for the first reduction remains the same at scan rates of 50–800 mV/s. In CH_2Cl_2 no reduction of 2-amino anthracene is observed up to −2.45 V (relative to $FeCp/FeCp^+$). The irreversible reduction potentials observed for **2** and **3** are similar to that observed for anthracene (−2.07 V) in CH_3CN but apparently significantly lower than the free ligand in CH_2Cl_2 [23, 24]. This is in spite of the fact that in the case of **2** the aromaticity has been interrupted by the proton transfer to the ring (vide supra). This

suggests some significant delocalization of electron density onto the cluster in the radical anion but unlike the free ligand, where the reduction is reversible, the resulting radical goes on to react further [23, 24]. The slightly lower reduction potential observed for **1** is consistent with the proposed structure where the aromaticity of the anthracene ligand is preserved. The oxidation potentials for **1** and **3** are slightly more positive than for the free ligand, again consistent with some delocalization of ligand electron density while **2** shows a slightly less positive oxidation potential possibly because of the replacement of a CO by the better electron donors NH and H.

Table 2.5 Polarographic half wave potentials (in V vs. $FeCp_2$/ $FeCp_2^+$ in CH_2Cl_2) for complexes 1–4

Compound	Oxidation	Reduction
2-Amino-anthracene	+0.35 (E_{IRR}), + 0.85 (E_{IRR})	>-2.45[a]
1	+0.42 (E_{IRR})	-1.85 (E_{IRR})
2	+0.35 (E_{IRR})	-2.14(E_{IRR})
3	+0.42 (E_{IRR})	-2.05 (E_{IRR})
4	+0.49 (E_{IRR})	-1.16(E_{REV}), -1.62(E_{QREV})

[a] The limit of the solvent, CH_2Cl_2, is −2.45 V.

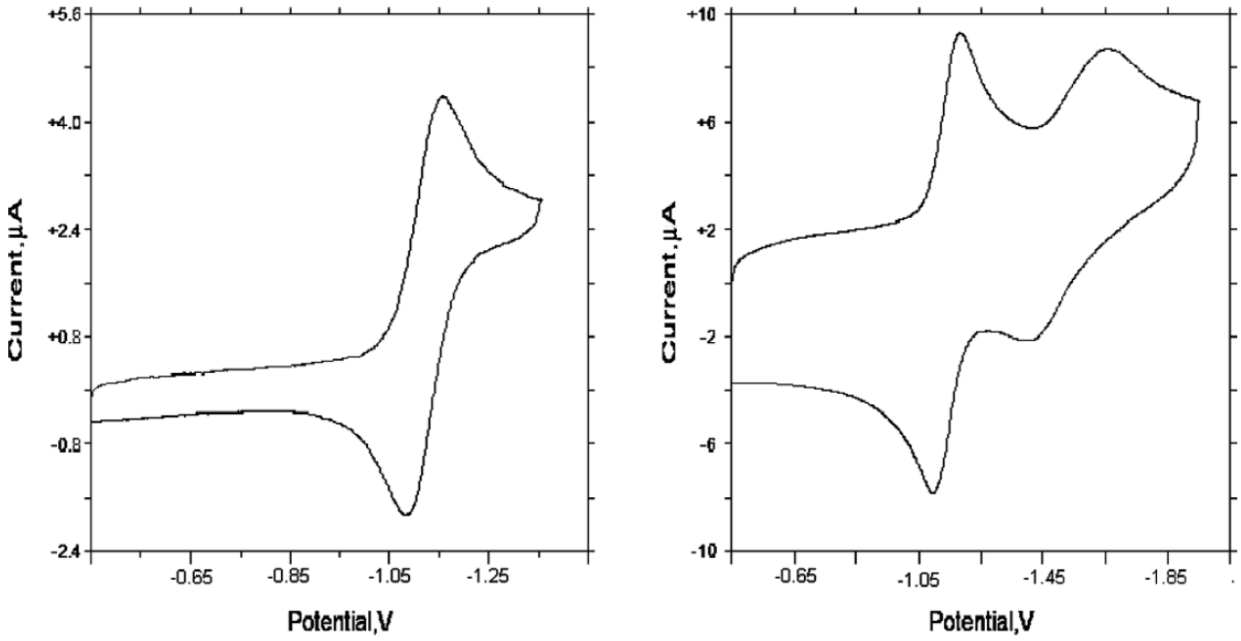

Figure 2.6 Cyclic voltamograms for $[Os_3(CO)_9(\mu_3\text{-}\eta^2\text{-}C_{14}H_8NH)(\mu\text{-}H)]$ (4): (a) the first reversible $1e^-$ reduction at a scan rate of 50 mV/s ($\Delta E^{1/2}$ = 39 mV); (b) the first reversible ($\Delta E^{1/2}$ = 39 mV) and second quasi-reversible electron reduction ($\Delta E^{1/2}$ = 200 mV) at a scan rate of 400 mV/s.

The first reversible $1e^-$ reduction observed for **4** is reminiscent of the previously reported triosmium cluster complexes of aromatic nitrogen heterocycles containing a formally 3-center-2-electron bond with a carbocyclic ring in a $46e^-$ species [6, 22] and generalizes the electron acceptor properties of this bonding mode to complexes containing exocyclic as well as endocyclic amine groups [8]. However, within this class of molecules only one example of a complex that has two reversible reductions exists; a 4-carboxaldehyde quinoxaline complex. However, the behavior of **4** is distinctly different in that the second reduction only approaches reversibility at CV scan rates of 400 mV/s

[6]. The lower reduction potential of **4** relative to the other complexes and to the free ligand also reflects this electron deficiency.

2.3.4 Reactivity of complex 4 towards phosphines

The application of metal clusters as DNA intercalator requires the attachment of water-solublizing ligands to the metal core. E. Rosenberg *et al.* [7, 10-11] have previously reported water-soluble phosphine substituted clusters have good solubility in water. Our group has now developed an effective method for synthesizing $[Os_3(CO)_9\{\mu-\eta_2-(L-H)\}\ (\mu-H)(PR_3)]$ from $[Os_3(CO)_{10}(MeCN)_2]$ via the reaction of phosphines with the electron-deficient cluster $[Os_3(CO)_9\{\mu_3-\eta_2-(L-H)\}(\mu-H)]$. We have studied the reactivity of the electron-deficient cluster $[Os_3(CO)_9(\mu_3-\eta^2\text{-}(N\text{-}C(3))\text{-}NHC_{10}H_9)(\mu\text{-}H)]$ **4** towards phosphines.

The complex **4** reacts rapidly with $(CH_3O)_3P$ at room temperature. The NMR spectra of the product showed that the anthracene ligand was replaced by two phosphines. The reaction of **1** with $(C_2H_5O)_3P$ at room temperature yielded the product containing both anthracene and phosphine ligands (Scheme 2.4).

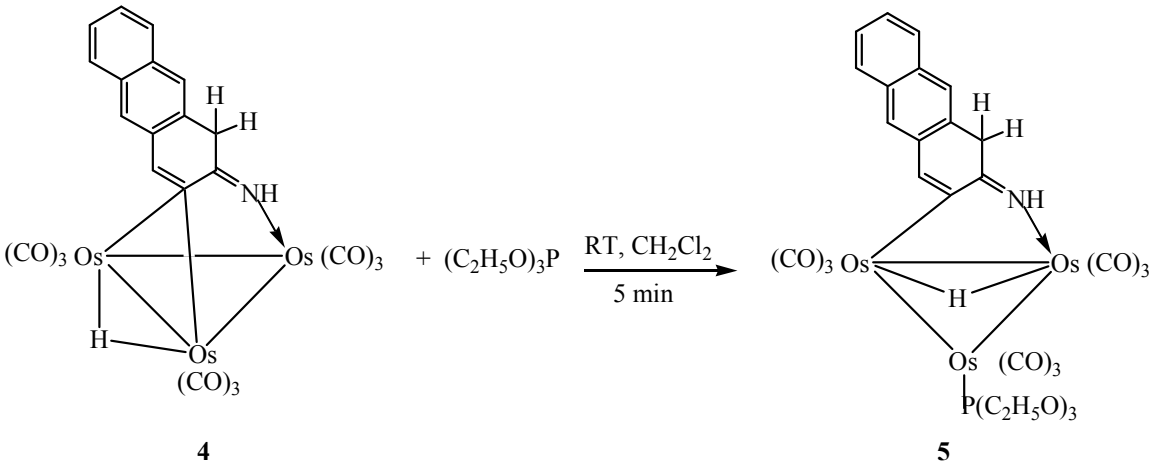

4 **5**

Scheme 2.4

The ^{1}H NMR showed the presence of both 2-amino-anthracene and the $P(C_2H_5O)_3$ ligands. However, the complex multiple signals in the hydride region indicates that the sample is a mixture of complexes. The strong absorption at 1712 cm^{-1} in the IR spectrum indicates possibility of a bridging carbonyl ligand in this mixture of complexes. This reaction indicates that the synthesis of water-soluble phosphine containing 2-amino-anthracene substituted cluster could be very difficult due to the poor yield and decomposition. However, the reaction conditions for an efficient addition of water-soluble phosphines have yet to be determined.

2.4 Conclusions

Perhaps the most interesting result of this study is the observation of the proton transfer reaction involved in the conversion of **1** to **2**. This represents a disruption of the aromatic ring of anthracene under very mild conditions. The pathway proposed for this

conversion is by no means a unique explanation of this observation but the increased rate of the conversion in the presence of D_2O and the detection of what appear to be a deuterium containing peak seems to at least point to water as the catalyst for this process. The formation of **4** from **2** and its reversible $1e^-$ electrochemical behavior further illustrates the generality of the electron acceptor properties of the μ_3-η^2-electron deficient bonding mode [2, 8]. Overall the photophysical properties and the electrochemical properties of the reported complexes do not differ drastically from the free ligand except in the case of **4**. Poor yield and mixtures of products obtained from the reaction of complex **4** with $(C_2H_5O)_3P$ discouraged us from pursuing with this complex to be converted as a water soluble luminescent DNA labeling agents.

References

1. B. Bergman, R.H. Holmquist, R. Smith, E. Rosenberg, K.I. Hardcastle, M. Visi and J. Ciurash, *J. Am. Chem. Soc.* **120** (1998), p. 12818.
2. J. Abedin, B. Bergman, R. Holmquist, R. Smith, E. Rosenberg, J. Ciurash, K. Hardcastle, J. Roe, V. Vazquez, C. Roe, S. Kabir, B. Roy, S. Alam and K.A. Azam, *Coord. Chem. Rev.* **190–192** (1999), p. 975.
3. E. Rosenberg, S.E. Kabir, Md.J. Abedin and K.I. Hardcastle, *Organometallics* **23** (2004), p. 3982.
4. D.G. Musaev, T. Nowroozi-Isfahani, K. Morokuma, J. Abedin, E. Rosenberg and K.I. Hardcastle, *Organometallics* **25** (2006), p. 203.
5. E. Rosenberg, D. Rokhsana, C. Nervi, R. Gobetto, L. Milone and A. Viale, *Chem. Eur. J.* **9** (2003), p. 5749.
6. E. Rosenberg, D. Rokshsana, C. Nervi, R. Gobetto, L. Milone, A. Viale and J. Fiedler, *Organometallics* **23** (2004), p. 215.
7. E. Rosenberg, F. Spada, D. Rokhsana, C. Nervi, R. Gobetto, L. Milone and A. Viale, *J. Organomet. Chem.* **689** (2004), p. 1796.
8. J.A. Cabeza, I. da Silva, I. del Rio, S. Garcia-grande, V. Riera and M.G. Sánchez-Vega, *Organometallics* **22** (2003), p. 1519.
9. H. Chen, J.A. Parkinson, S. Parsons, R.A. Coxall, R.O. Gould and P.J. Sadler, *J. Am. Chem. Soc.* **124** (2002), p. 3064.
10. E. Rosenberg, F. Spada, K. Sugden, B. Martin, R. Gobetto, L. Milone and A. Viale, *J. Organomet. Chem.* **689** (2004), p. 4729.

11. E. Rosenberg, F. Spada, K. Sugden, B. Martin, L. Milone, R. Gobetto, A. Viale and J. Fiedler, *J. Organomet. Chem.* **668** (2003), p. 51.

12. B.F.G. Johnson, J. Lewis and D.A. Pippard, *J. Chem. Soc., Dalton Trans.* (1881), p. 407.

13. SMART Version 5.628, 2003, Bruker AXS, Inc., Analytical X-ray Systems, 5465 East Cheryl Parkway, Madison, WI 53711-5373.

14. SAINT Version 6.36A, 2002, Bruker AXS, Inc., Analytical X-ray Systems, 5465 East Cheryl Parkway, Madison, WI 53711-5373.

15. SADABS Version 2.10, 2003, George Sheldrick, University of Göttingen, Göttingen, Germany.

16. SHELXTL V6.12, 2002, Bruker AXS, Inc., Analytical X-ray Systems, 5465 East Cheryl Parkway, Madison, WI 53711-5373.

17. A.G. Orpen XHYDEX, *J. Chem. Soc., Dalton Trans.* (1980), p. 2509.

18. In: A.J.C. Wilson, Editor, *International Tables for X-ray Crystallography* **vol. C**, Kynoch Academic Publishers, Dordrecht (1992) Tables 6.1.1.4 (pp. 500–502) and 4.2.6.8 (pp. 219–222).

19. E. Rosenberg, D.S. Kolwaite, S.E. Kabir, K.I. Hardcastle, T. McPhillips, R. Duque and M. Day, *Organometallics* **15** (1996), p. 1979.

20. D.G. Musaev, T. Nowroozi-Isfahani, K. Morokuma and E. Roseneberg, *Organometallics* **24** (2005), p. 5973.

21. E. Rosenberg, D. Espitia, S.E. Kabir, T. McPhillips, M.W. Day, K.I. Hardcastle, R. Gobetto, D. Osella and L. Milone, *Organometallics* **10** (1991), p. 3550.

22. E. Rosenberg, L. Milone, C. Nervi, D. Osella, J. Fiedler, Md.J. Abedin and D. Rokhsana, *Inorg. Chim. Acta* **300–302** (2000), p. 769.

23. T.A. Gough and M.E. Power, Polarography 1964. In: G.J. Hills, Editor, *Proceedings of the Third International Congress, Southampton*, Macmillan, New York (1964), p. 1017.

24. D.F. Zigler, M.C. Elvington, J. Heinecke and K.J. Brewer, *Inorg. Chem.* **45** (2006), p. 6565.

CHAPTER 3: TUNING PHOTOPHYSICAL PROPERTIES WITH ANCILLARY LIGANDS IN Ru(II) MONO-DIIMINE COMPLEXES

3.1 Introduction

Transition metal luminescent complexes containing one or more diimine ligands typically have excited-state lifetimes ranging from about 100 ns to 10 μs. Because the lifetimes of these luminophores are long compared to fluorescent dyes that are used as biological probes, time-gated detection can be used to suppress interfering auto-fluorescence from the biological sample. In addition, highly polarized emission from some of these complexes has stimulated interest in using them as biophysical probes for studying the dynamics of macromolecular assemblies and interactions on membranes [1–4]. The luminescent behavior of these complexes arises from the MLCT (metal-to-ligand charge-transfer) band. Because the emission of metal–ligand complexes (MLCs) is dominated by the MLCT transition, the MLCs behave like a single chromophoric unit, and they have high chemical and photochemical stabilities under physiological conditions. As a result of these favorable properties, MLCs are finding new applications in biophysical chemistry, clinical chemistry and DNA diagnostics [5, 6].

Because the energy gap law determines the luminescent properties of these complexes, several criteria must be satisfied to observe luminescence from their MLCT state [7 –10]. The ligand field must be strong enough to raise the d–d state above the

MLCT state [11]. This is the reason why $[Fe(L–L)_3]^{2+}$ are not luminescent (non-radiative decay), but $[Ru(L–L)_3]^{2+}$ show radiative decay and hence useful luminescence (L–L = 2,2 bipyridyl, 1,10-phenanthroline and their derivatives). However, the energy of the excited-state is closer to the ground state for the Os–MLCs. Consequently, they typically show weak luminescence; the smaller energy gap facilitates non-radiative decay [5]. The luminescence of these complexes is phosphorescence from the triplet state. Because of the strong spin–orbit coupling, the intersystem crossing from the initially excited singlet state is very efficient, and the triplet excited-state yield is close to unity. In addition, the degree of singlet–triplet mixing directly affects the radiative vs. non-radiative decay rates, and thus affects the lifetime of the resulting triplet excited-state. In particular, increased singlet–triplet mixing results in shorter triplet excited-state lifetimes.

When excited with polarized light, the emission from asymmetric MLCT complexes is also polarized, which makes these complexes useful for studying dynamics; in general, complexes with non-identical diimine ligands show higher fundamental anisotropies than the more symmetrical complexes. The first such complex reported was $[Ru(bpy)_2(dcbpy)]^{2+}$ (dcbpy = 4,4′-dicarboxy-2,2′-bipyridyl). This dicarboxy derivative showed higher fundamental anisotropies than $[Ru(bpy)_3]^{2+}$. Introducing electron withdrawing groups on the diimine ligand resulted in red-shifted emission and an increase in emission anisotropy, which suggests that one ligand is accepting an electron preferentially in the MLCT transition [1, 12–14]. The possibility of improving the fundamental anisotropy with a single chromophoric ligand in metal–ligand complexes is based on results for Re(I) complexes (e.g. $[Re(4,7\text{-dimethyl-phen})(CO)_3(4\text{-carboxy-Py})(PF_6)]$) [4, 15].

A limitation of most metal–ligand complexes is low quantum yield. However, the electronic effect of ligands on the energy gap can be utilized to increase quantum efficiency. Previous studies [16] have shown that replacing diimines with chelating phosphine ligands results in increased quantum yields of $[Os(phen)(dppene)]^{2+}$ and $[Os(phen)_2(dppene)]^{2+}$ (dppene = diphenylphosphinoethylene) compared to $[Os(phen)_3]^{2+}$ (Q = 0.518, 0.138 and 0.016 respectively). Therefore, careful selection of metal and ligands can generate MLCs with spectroscopic and physical properties useful for the study of specific biological systems [5, 9, 17–20]. For example, we recently reported the synthesis, electrochemical and electrogenerated chemiluminescence studies of $[Ru(bpy)_2\{2\text{-}(4\text{-methylpyridine-2-yl})benzo[d]\text{-}X\text{-}azole\}(PF_6)_2]$ [21]. This study focused on the development of novel electrogenerated chemiluminescence devices suitable for the detection of different biological analytes of clinical and environmental interest. Also, Lakowicz and coworkers have reported the use of the long-lifetime probe $[Re(4,7\text{-dimethyl-phen})(CO)_3(4\text{-carboxy-Py})(PF_6)]$ to study overall rotational motion in lipid vesicles and microsecond dynamics of cell membranes [2–4]. The limitation of this type of complex is that the ligation around the metal is not amenable to further modification because the carbonyls are difficult to substitute, making it difficult to further alter the excited-state lifetime.

To develop better MLC probes for application to specific biological systems, a deeper understanding of the probe's photophysical properties is required. Recently, we reported photophysical and computational studies of $[Re(CO)_3\{2\text{-}(4\text{-methyl pyridine-2-yl})benzo[d]\text{-}X\text{-}azol\}L]$ and $[Re(CO)_3\{2\text{-}(4\text{-methylpyridine-2-yl})benzo[d]\text{-}X\text{-}azol\text{-}2\text{-}yl\}(4\text{-methylquinolin})L]^{+}$. The purpose of these studies was to investigate the effect of the

organic ligand on the optical properties and electronic structure of the reported complexes [22]. The results showed that the photophysical properties depended on the nature of X (N > S > O) and L (py and Cl). The pyridinyl nitrogen is a better electron donor for the Ru(II), and this donor results in a higher quantum yield and longer excited-state lifetime relative to the S and O containing heterocycles.

Ideally, one would like to develop a series of complexes where the MLCT band is red-shifted and well-separated from the intra-ligand transitions and where the intensity of the MLCT transition is stronger than observed for previously reported Ru(II) diimine complexes. It would be desirable to have the ability to tune the lifetime of the excited-state so that one could tailor a particular probe to a particular dynamic process in a bio-macromolecule. It would also be desirable to have complexes that contain only one chelating heterocycle, because this would decrease the molecular symmetry, which would have the effect of increasing the anisotropy of the luminescence. Combining all of these desired features into the synthesis of a luminescent probe is a challenging task. However, by making use of the easily-substituted ruthenium complex $K[Ru(CO)_3(TFA)_3]$ [23] and the well-known fact that the incorporation of π-acid ligands [5,16 and 24] into complexes containing chelating nitrogen heterocycles has the effect of prolonging the excited-state lifetime [16], we have developed synthetic pathways to complexes having most, if not all, of the desired photophysical properties. In this study, we report the synthesis of a series of complexes $[XRu(CO)(L–L)(L')_2][PF_6]$ (X = H, TFA, Cl; L–L = 2,2′-bipyridyl, 1,10-phenanthroline, 5-amino-1,10-phenanthroline and 4,4′-dicarboxylic-2,2′-bipyridyl; $(L')_2 = 2PPh_3$, $Ph_2PC_2H_4PPh_2$, $Ph_2PC_2H_2PPh_2$).

3.2 Experimental

3.2.1 General methods and materials

Reactions were carried out under a nitrogen atmosphere, but purification was carried out in air using preparative thin layer chromatography (10 × 20 cm plates coated with 1 mm silica gel PF 60254-EM Science). Activated neutral alumina (150 mesh, 58 Å) was also used to purify compounds by column chromatography. Solvents were reagent grade. Tetrahydrofuran was distilled from benzophenone ketyl and methylene chloride and acetonitrile were distilled from calcium hydride. Ruthenium carbonyl was purchased from Strem Chemicals. 2,2-bipyridyl, 1,10-phenantroline, 4,4′-dicarboxy-2,2-bipyridyl and 5-amino-1,10-phenanthroline (Aldrich) were used as received.

General crystallization method: Sample was dissolved in minimum volume of CH_2Cl_2 or acetone in a clean test tube. n-Hexane was added slowly by dripping down the side of the test tube to form a discreet layer of hexane. The test tube was covered and placed in refrigerator at 4 ºC to obtain single crystals suitable for X-ray crystallography.

^{1}H NMR spectra were obtained on a Varian 400 MHz Unity Plus or a Varian NMR Systems 500 MHz spectrometer. Infrared spectra were obtained on a Thermo-Nicolet 633 FT-IR spectrometer. Elemental analyses were performed by Schwarzkopf Microanalytical Labs, Woodside, NY. ESI-MS spectra ware obtained on a Watts/Micromass LCT using 80% MeCN as carrier solvent. Some of the spectra showed the presence of Na^+ associated with the molecular ion due to the extensive use of salt solutions with this instrument which has contaminated the analyzer.

3.2.2 Crystal structure analysis

Suitable crystals of **5**, **6** and **10** were coated with Paratone N oil, suspended in a small fiber loop and placed in a cooled nitrogen gas stream at 173 K on a Bruker D8 smartAPEX CCD sealed tube diffractometer with graphite-monochromated Mo Kα (0.71073 Å) radiation. Data were measured using a series of combinations of phi and omega scans with 10 s frame exposures and 0.30 frame widths. Data collection, indexing and initial cell refinements were all carried out using SMART [25] software. Frame integration and final cell refinements were done using SAINT [26] software. The final cell parameters were determined from least-squares refinement on 2481 and 5705 reflections, respectively. The SADABS [27] program was used to carry out absorption corrections. The structure was solved using the Patterson method and difference Fourier techniques (SHELXTL, V6.12) [28]. Hydrogen atoms were placed in their expected chemical positions using the HFIX command and were included in the final cycles of least-squares with isotropic Uij's related to the atom's ridden upon. All non-hydrogen atoms were refined anisotropically. Scattering factors and anomalous dispersion corrections are taken from the *International Tables for X-ray Crystallography* [29]. Structure solution, refinement, six graphics and generation of publication materials were performed by using SHELXTL, V6.12 software. Additional details of data collection and structure refinement are given in Table 3.2.

3.2.3 Electrochemistry

A PAR 263A electrochemical analyzer (EG&G Princeton Applied Research, Oak Ridge, TN, USA) interfaced to a personal computer running PAR M270 electrochemical software was used for the electrochemical measurements. A standard three-electrode cell was designed to allow the tip of the reference electrode (saturated calomel electrode, SCE) to closely approach the working (a glassy carbon disk, diameter 0.1 cm, sealed in epoxy resin), and the auxiliary (a Pt wire) electrodes. All measurements were carried out under nitrogen in CH_2Cl_2 solutions containing 0.1 M $[NBu_4]PF_6$ as supporting electrolyte and the metal complexes at 1.0×10^{-3} M. All potentials are reported vs. the ferrocene/ferrocinium redox couple, added as an internal standard ($E°'$ (Fc/Fc^+) = +0.41 V vs. SCE [i]). Positive-feedback IR compensation was applied routinely [30].

3.2.4 Luminescence spectroscopy

Steady state UV–Vis absorption spectra and emission spectra were recorded on a Molecular Devices Spectra Max M2. The quantum yields (φ) for the luminescent complexes in the presence of oxygen were calculated using Eq. (1), relative to a Rhodamine B standard (φ = 0.73, in ethanol), where abs is the absorbance (<0.05) at the excitation wavelength (420 nm), and area is the integrated emission spectrum corrected for the wavelength-dependent quantum efficiency of the instrument [31].

$$\varphi = \frac{\text{abs Rhodamine}}{\text{area Rhodamine}} \text{ X } \frac{\text{area Ru}}{\text{abs Ru}} \text{ X } 0.73 \qquad (1)$$

Time-resolved luminescence decay and anisotropy decay measurements were performed by time-correlated single-photon counting (TCSPC), using the Quantum Northwest FLASC 1000 sample chamber (Spokane, WA). In the FLASC 1000, the vertical (V or 0° to vertically polarized excitation) and horizontal (H or 90°) emission components are separated on one side of the sample cuvette, orthogonal to the excitation path, by a beam-splitting Glan-Thompson polarizer (Karl Lambrecht, Chicago, IL). This allows *simultaneous* detection of the V and H anisotropy decay components by separate detectors, which assures data collection under identical excitation conditions. A variable-angle polarizer, in the emission path on the opposite side of the sample cuvette, was set at the magic angle (54.7° to vertically polarized excitation) for determination of the luminescence lifetime. The fluorescence intensity decay was calculated by fitting the data to a single exponential decay model; here I(t) is the time dependent intensity and I_0 is the intensity at time 0 and τ is the excited-state lifetime.

$$I(t)=I_0\exp(-t/\tau) \qquad (2)$$

In the time-resolved anisotropy experiment, the depolarization of the emitted light that results from molecular rotation is given by

$$r(t) = \frac{I_{VV}(t) - I_{VH}(t)}{I_{VV}(t) + 2I_{VH}(t)} = \sum_{j=1}^{5} \beta_j e^{-t/\phi_j} \qquad (3)$$

where $I_{VV}(t)$ and $I_{VH}(t)$ represent the vertical and horizontal decays, respectively, obtained using vertical excitation. The pre-exponential factors, β_j, are trigonometric functions of the angles between the excitation and emission transition dipole moments of the probe and the symmetry axes of the ellipsoid of revolution [32], and the sum of β_j is the limiting

anisotropy at zero time, r_0, when no motion has occurred. The denominator of Eq. (3) is the total intensity decay, $I(t)$,

$$I_{VV}(t) + 2I_{VH}(t) = I(t) = \sum_{i=1}^{n} \alpha_i e^{-t/\tau_i} \qquad (4)$$

where τ_i is the lifetime and α_i is the amplitude of the ith component; the magic angle decay is $I(t)/3$. The anisotropy decay data were analyzed using the software package FLUOFIT PRO (PicoQuant, Berlin). For anisotropy analysis, the individual vertical and horizontal decays,$I_{VV}(t)$ and $I_{VH}(t)$, respectively, were fit simultaneously according to the following relationships:

$$I_{VV}(t) = G \frac{1}{3} \sum_{i=1}^{n} \alpha_i e^{-t/\tau_i} \left[1 + 2(r_\infty + \sum_{j=1}^{n} \beta_j e^{-t/\phi_j} \right] \qquad (5a)$$

$$I_{VH}(t) = \frac{1}{3} \sum_{i=1}^{n} \alpha_i e^{-t/\tau_i} \left[1 - (r_\infty + \sum_{j=1}^{n} \beta_j e^{-t/\phi_j} \right] \qquad (5b)$$

where r_∞ is the anisotropy at infinite time [33], and $G = \int I_{HV}\, dt / \int I_{HH}\, dt$ is a factor, obtained using horizontal excitation, that corrects for the difference in the efficiencies of the V and H detection channels; under ideal conditions $G \sim 1$ [34] and [35].

3.2.6 Synthesis

The reactive starting complex $K[Ru(CF_3CO_2)_3(CO)_3]$ (**1**) was synthesized according to the published procedure [23]. Spectroscopic data for the new compounds are summarized in Table 3.1. Elemental analyses were obtained only for the final diimine complexes. In some cases the lability of the TFA ligand led to elemental analyses slightly

out of the required range for carbon content (>0.5%, compounds **7**, **11**, **15**). Mass spectral and spectroscopic data verify identity and purity of these complexes (Table 3.1).

3.2.7 Synthesis of $[Ru\{P(C_6H_5)_3\}_2(CO)_2(TFA)_2]$ (2), $[Ru(\eta^2(C_6H_5)_2PC_2H_4P(C_6H_5)_2)(CO)_2(TFA)_2]$ (3) and $[Ru\{\eta^2(C_6H_5)_2PC_2H_2P(C_6H_5)_2\}(CO)_2(TFA)_2]$ (4)

An acetone solution (30 mL) of $K[Ru(CF_3CO_2)_3(CO)_3]$ (**1**) (100 mg, 0.18 mmol) and triphenylphosphine (94 mg, 0.36 mmol) was refluxed for 24 h. The solvent was removed by a rotary evaporator and the residue was purified by using thin layer chromatography on silica gel. Elution with hexane/acetone (9:1 v/v) gave two bands. The slower moving band afforded $[Ru\{P(C_6H_5)_3\}_2(CO)_2(TFA)_2]$ (**2**) (66 mg, 41%) as a white powder after recrystallization from acetone/hexane at RT.

A mixture of **1** (250 mg, 0.44 mmole) and diphenylphosphinoethane (dppe) (195 mg, 0.48 mmole) was refluxed in an ether–acetone (10 mL/10 mL) solvent for 2 h under N_2. The color of the solution changed from yellow to green. The solvent was removed by a rotary evaporator and the residue was purified by using thin layer chromatography on silica gel. Elution with acetone/hexane [1:3 (v/v)] developed two bands. The faster moving yellow band yielded a small amount of **1** and the slower moving green band afforded $[Ru(\eta^2(C_6H_5)_2PC_2H_4P(C_6H_5)_2)(CO)_2(TFA)_2]$ (**3**) (120 mg, 35%).

Reaction of **1** (250 mg, 0.44 mmol) with diphenylphosphinoethylene (194 mg, 0.48 mmol) in refluxing ether–acetone (10 mL/10 mL) solvent followed by similar

purification by using thin layer chromatography on silica gel afforded $[Ru(\eta^2(C_6H_5)_2PC_2H_2P(C_6H_5)_2)(CO)_2(TFA)_2]$ (**4**) (140 mg, 40%).

3.2.8 Reaction of $[Ru\{P(C_6H_5)_3\}_2(CO)_2(TFA)_2]$ (2) with 1,10-phenanthroline and 2,2′-bipyridyl

The reaction of **2** (100 mg, 0.11 mmole) with 1,10-phenanthroline (40 mg, 0.22 mmole) in refluxing toluene for 72 h resulted in an orange solution. The solvent was removed on a rotary evaporator and the oily residue was dissolved in acetone and placed onto a column of neutral alumina. Elution with hexane/CH_2Cl_2 [3:1 (v/v)] gave two bands. The slower moving orange band gave $[Ru\{P(C_6H_5)_3\}_2$(1,10phenanthroline) (CO)Cl][PF_6] (**5**) (35 mg, 36%) as orange crystals after adding aqueous ammonium hexafluorophosphate and recrystallization from hexane/CH_2Cl_2 (Anal. Calc. for $C_{49}H_{38}O_1P_3F_6Ru_1N_2Cl_1$: C, 58.5; H, 3.83; N, 2.78. Found: C, 58.2; H, 3.62, N, 3.06%). The faster moving yellow band yielded $[Ru\{P(C_6H_5)_3\}$(1,10-phenanthroline) (CO)($(TFA)_2$] (**6**) (25 mg, 29%) as yellow crystals from hexane/CH_2Cl_2 (Anal. Calc. for $C_{35}H_{23}N_2P_1O_5F_6Ru_1$: C, 53.77; H, 2.97. Found: C, 54.16; H, 2.78%).

The reaction of **2** (100 mg, 0.11 mmole) with 2,2′-bipyridyl (35 mg, 0.22 mmole) in ethylene glycol (15 mL) at 140 °C for 72 h produced an orange solution. A deep yellow precipitate was obtained by the addition of aqueous NH_4PF_6 (1.0 g/10 mL). The precipitate was dissolved in CH_2Cl_2 and chromatographed on a column of activated alumina (Hexane/CH_2Cl_2, [1:1 v/v]) yielding the compound $[Ru\{P(C_6H_5)_3\}_2$(2,2′-

bipyridyl)(CO)TFA][PF_6] (**7**) (48 mg, 47%) as a deep yellow powder (Anal. Calc. for $C_{49}H_{38}O_3P_3F_9Ru_1N_2$: C, 55.44; H, 3.68, N, 2.69. Found: C, 56.06; H, 3.88, N, 3.28%).

Reaction of **2** (210 mg, 0.23 mmol) with 4,4′-dicarboxy-bipyridyl (56 mg, 0.23 mmol) in ethylene glycol (25 mL) at 140 °C for 72 h followed by addition of aqueous NH_4PF_6(1.0 g/10 mL) resulted in a mixture of [Ru{$P(C_6H_5)_3$}$_2$(4,4′-dicarboxy-bipyridyl)(CO)TFA][PF_6] (**8**) and [HRu{$P(C_6H_5)_3$}$_2$(4,4′-dicarboxy-bipyridyl)(CO)][PF_6] (**9**). Dissolving the mixture in hot ethanol yielded only [HRu{$P(C_6H_5)_3$}$_2$(4,4′-dicarboxy-bipyridyl)(CO)][PF_6] (**9**) (102 mg, 54%) (Anal. Calc. for $C_{49}H_{39}O_5P_3F_6Ru_1N_2$: C, 56.38; H, 3.77, N, 2.69. Found: C, 57.1; H, 3.88, N, 2.62%). Recrystallization of **7** from hot ethanol gave pale yellow crystals of [HRu{$P(C_6H_5)_3$}$_2$(2,2′-bipyridyl)(CO)][PF_6] (**10**).

3.2.9 Reaction of of [Ru{$\eta^2(C_6H_5)_2PC_2H_4P(C_6H_5)_2$}$(CO)_2(TFA)_2$] (3) with 1,10-phenanthroline and 2,2′-bipyridyl

Compound **3** (120 mg, 0.153 mmole) was heated with 1,10-phenanthroline (83 mg, 0.461mmole) in ethylene glycol (15 mL) at 140 °C for 72 h, The color of the reaction mixture turned to deep orange. An orange precipitate of [(CO)(TFA)Ru{$\eta^2(C_6H_5)_2PC_2H_4P(C_6H_5)_2$}($\eta^2C_{12}H_8N_2$)][$PF_6$] (**11**) (84 mg, 56%) was obtained by adding aqueous NH_4PF_6 (1.0 g/10 mL) to the reaction mixture. The residue was then filtered and washed three times with DI water and three times with diethyl ether and dried under vacuum (Anal. Calc. for $C_{41}H_{32}O_3P_3F_9Ru_1N_2$: C, 51.0; H, 3.33, N, 2.91. Found: C, 51.9; H, 3.65, N, 3.21%).

A similar reaction of compound **2** (120 mg, 0.153 mmole) with 2,2′-bipyridyl (71 mg, 0.46 mmole) in ethylene glycol (15 mL) at 140 °C for 72 h followed by addition of aqueous NH_4PF_6 (1.0 g/10 mL) gave $[(CO)(TFA)Ru\{\eta^2(C_6H_5)_2PC_2H_4P(C_6H_5)_2\}(\eta^2C_{10}H_8N_2)][PF_6]$ (**12**) (80 mg, 55%) as yellow precipitate. The residue was then filtered and washed three times with DI water and three times with diethyl ether and dried under vacuum (Anal. Calc. for $C_{39}H_{32}O_3P_3F_9Ru_1N_2$: C, 49.7; H, 3.41. Found: C, 50.1; H, 3.72%).

3.2.10 Reaction of of $[Ru\{\eta^2(C_6H_5)_2PC_2H_2P(C_6H_5)_2\}(CO)_2(TFA)_2]$ (4) with 1,10-phenanthroline, 2,2′-bipyridyl and 5-amino-1,10-phenanthroline

A mixture of **4** (130 mg, 0.167 mmole) and 1,10-phenanthroline (86 mg, 0.48 mmole) in ethylene glycol (15 mL) was heated at 140 °C for 72 h. Addition of aqueous NH_4PF_6(1.0 g/10 mL) to the reaction mixture yielded the yellow precipitate of $[(CO)(TFA)Ru\{\eta^2(C_6H_5)_2PC_2H_2P(C_6H_5)_2\}(\eta\text{-}^2C_{12}H_8N_2)][PF_6]$ (**13**) (95 mg, 59%). The residue was then filtered and washed tree times with DI water and three times with diethyl ether and dried under vacuum (Anal. Calc. for $C_{41}H_{30}O_3P_3F_9Ru_1N_2$: C, 51.1; H, 3.11. Found: C, 51.6; H, 2.97%).

A similar reaction of compound **4** (140 mg, 0.18 mmole) with 2,2′-bipyridyl (71 mg, 0.46 mmole) in ethylene glycol (15 mL) at 140 °C for 72 h followed by addition of aqueous NH_4PF_6 (1.0 g/10 mL) afforded $[(CO)(TFA)Ru\{\eta^2(C_6H_5)_2PC_2H_4P(C_6H_5)_2\}(\eta^2C_{10}H_8N_2)][PF_6]$ **14** (65 mg, 45%). The residue was then filtered and washed three

times with DI water and three times with diethyl ether and dried under vacuum (Anal. Calc. for $C_{39}H_{30}O_3P_3F_9Ru_1N_2$: C, 49.89; H, 3.19. Found: C, 50.26; H, 3.42%).

The reaction of compound **4** (140 mg, 0.18 mmole) with 5-amino-1,10-phenanthroline (39 mg, 0.19 mmole) in ethylene glycol (15 mL) at 140 °C for 72 h followed by addition of aqueous NH_4PF_6 (1.0 g/10 mL) and purification on an activated alumina column (elution with CH_2Cl_2/MeCN, [2:1 v/v]) gave [(CO)Ru{$\eta^2(C_6H_5)_2PC_2H_2P(C_6H_5)_2$}(TFA)($\eta^2C_{10}H_9N_3$)][$PF_6$] (**15**) (80 mg, 55%). It was not possible to obtain good elemental analysis for this compound probably owing to the lability of the TFA.

The addition of conc. hydrochloric acid or aqueous NaCl to a methanol solution of **15** afforded hydride complex [HRu({$\eta^2(C_6H_5)_2PC_2H_4P(C_6H_5)_2$}(CO)($\eta^2C_{10}H_9N_3$)][$PF_6$] (**16**). The mass spectra showed trace of the chloride product [ClRu({$\eta^2(C_6H_5)_2PC_2H_4P(C_6H_5)_2$}(CO)($\eta^2C_{10}H_9N_3$)][$PF_6$] present with the hydride complex. ESI-MS: *m*/*z* 924 [M+Na] (Calc. M = 902).

3.3. Results and discussion

3. 3.1 Compound synthesis and reaction pathways

The phosphine complexes [Ru{$P(C_6H_5)_3$}$_2$(CO)$_2$(TFA)$_2$] (**2**), [Ru($\eta^2(C_6H_5)_2PC_2H_4P(C_6H_5)_2$)(CO)$_2(TFA)_2$] (**3**) and [Ru{$\eta^2(C_6H_5)_2PC_2H_2P(C_6H_5)_2$}(CO)$_2(TFA)_2$] (**4**) were prepared (Scheme 3.1), and a series of stepwise reactions shown in Scheme 2–7, show the preparation of the luminescent ruthenium MLC complexes of formula [XRu(CO)(diimine)$(L)_2$][PF_6] as well as the non-luminescent [$(TFA)_2$Ru(CO)(2,2′-

bpy)(PPh_3)]. The stepwise carbonyl and TFA (TFA = trifluoroacetate) ligand replacement reactions were monitored by IR and ^{31}PNMR spectroscopic methods.

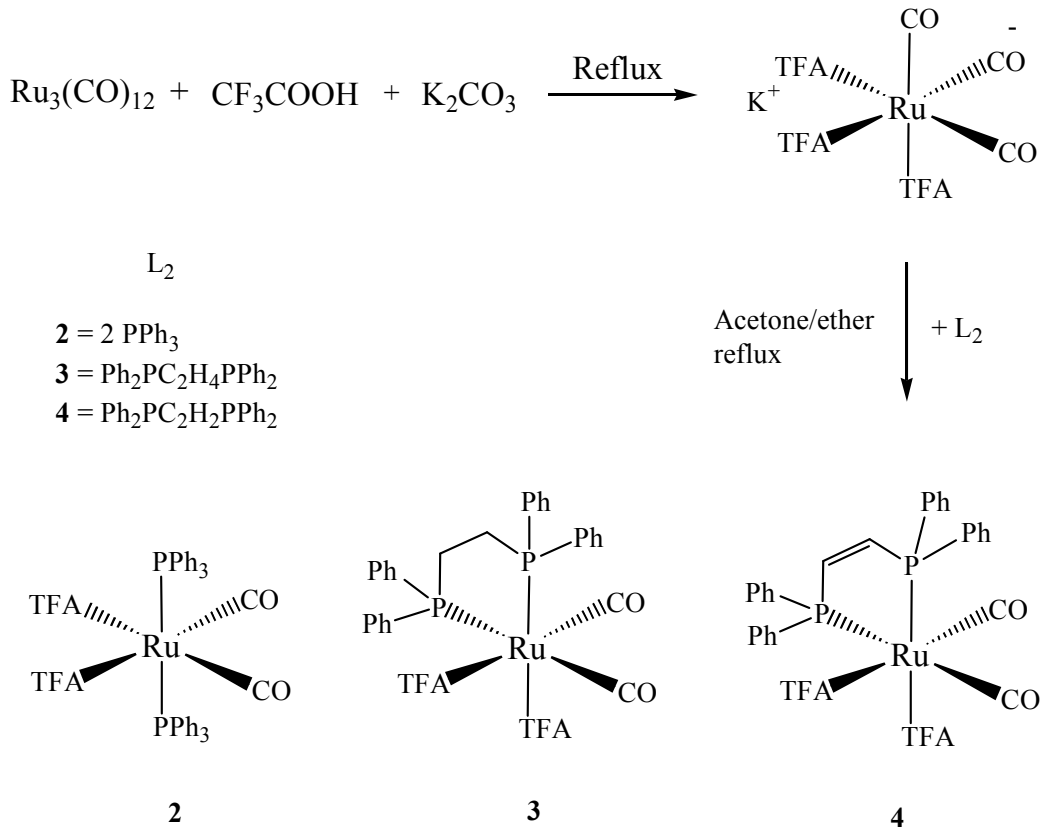

2 **3** **4**

Scheme 3.1

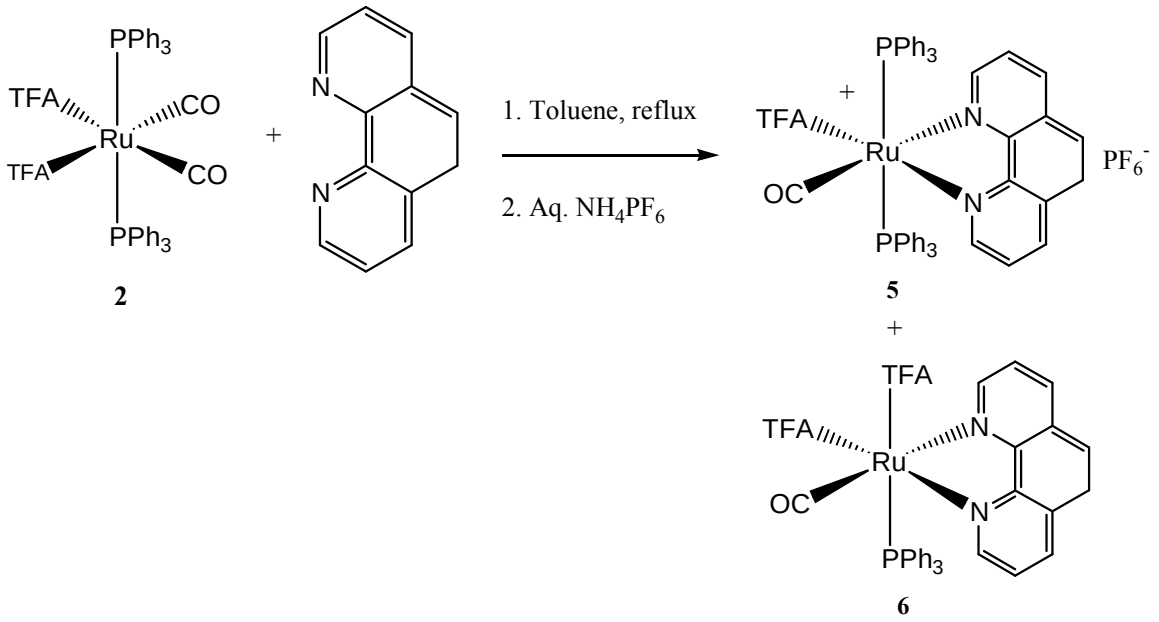

Scheme 3.2

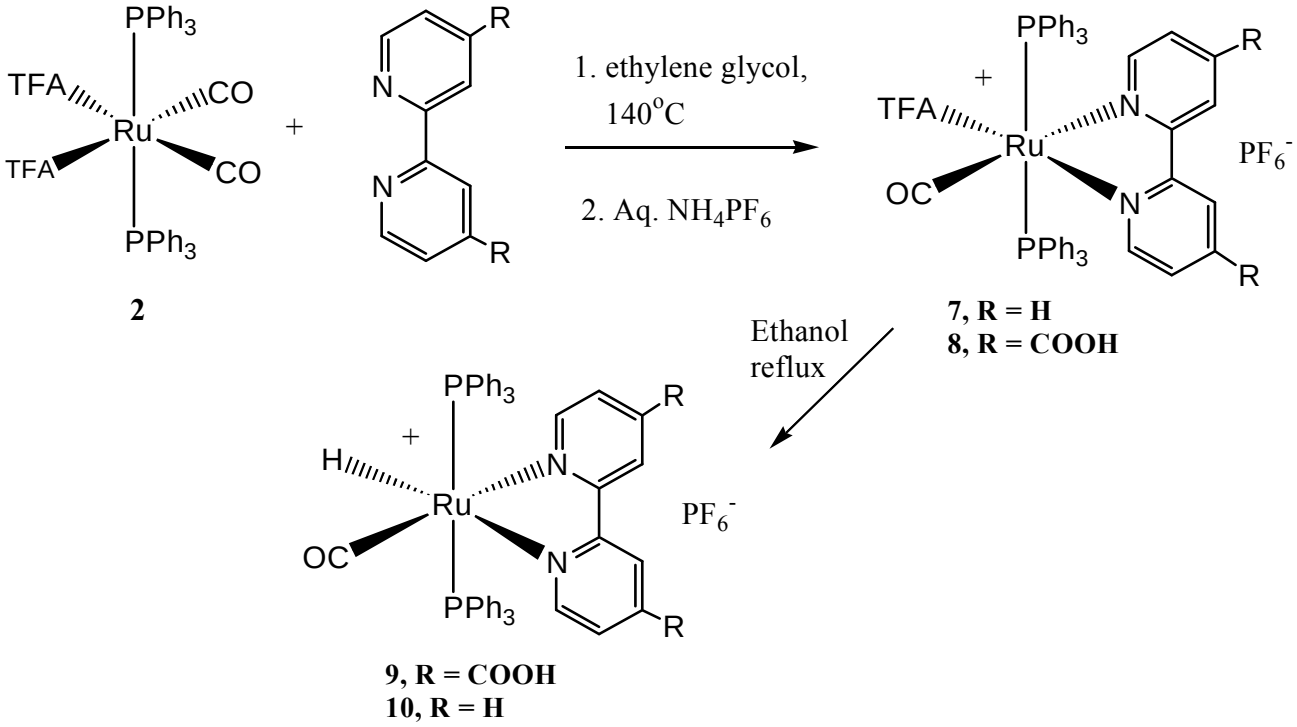

Scheme 3.3

The Reaction of **2** with 1,10-phenanthroline in refluxing toluene for 72 h followed by chromatographic separation with an alumina column and crystallization from CH_2Cl_2/hexane yielded $[Ru\{P(C_6H_5)_3\}_2$(1,10-phenanthroline)(CO)Cl][PF_6] (**5**) and [Ru{$P(C_6H_5)_3$}(1,10-phenanthroline)(CO)(($TFA)_2$] (**6**) in 36% and 29% yields, respectively (Scheme 3.2). The reaction of Compound **2** with 2,2′-bipyridyl or 4,4′-dicarboxy-2,2′-bipyridyl in ethylene glycol at 140 °C gave $[Ru\{P(C_6H_5)_3\}_2$(2,2′-bipyridyl)(CO)TFA][PF_6] (**7**) and $[Ru\{P(C_6H_5)_3\}_2$(4,4′-dicarboxy-bipyridyl)(CO)TFA] [PF_6] (**8**) with a small amount of $[HRu\{P(C_6H_5)_3\}_2$(4,4′-dicarboxybipyridyl)(CO)][PF_6] (**9**), respectively. Crystallization of **7** and the mixture of **8** and **9** from hot ethanol yielded only the hydride complexes as $[HRu\{P(C_6H_5)_3\}_2$(2,2′-bipyridyl)(CO)][PF_6] (**10**) and $[HRu\{P(C_6H_5)_3\}_2$(4,4′-dicarboxy-bipyridyl)(CO)][PF_6] (**9**), respectively (Scheme 3.3). All these complexes were characterized by elemental analysis, infrared, ^{1}H NMR, ^{31}P–{^{1}H} NMR, UV–Vis and mass spectral data (Table 3.1). The structures of complexes **5**, **6** and **10** were further investigated by single crystal X-ray diffraction analysis.

Complex **7** contains the labile ligand TFA (trifluoroacetate) *trans* to the N of the bipyridyl ligand. In solution, the complex can lose the TFA ligand to form the trigonal–bipyramidal intermediate with a vacant coordination site. Coordinative solvents like alcohols can coordinate to the vacant site *trans* to the N of the bipyridyl ligand, which then undergoes ejection of a proton to form a methoxide complex, and then β-elimination to give the hydride complex. A proposed mechanism for hydride formation is shown in Scheme 3.4.

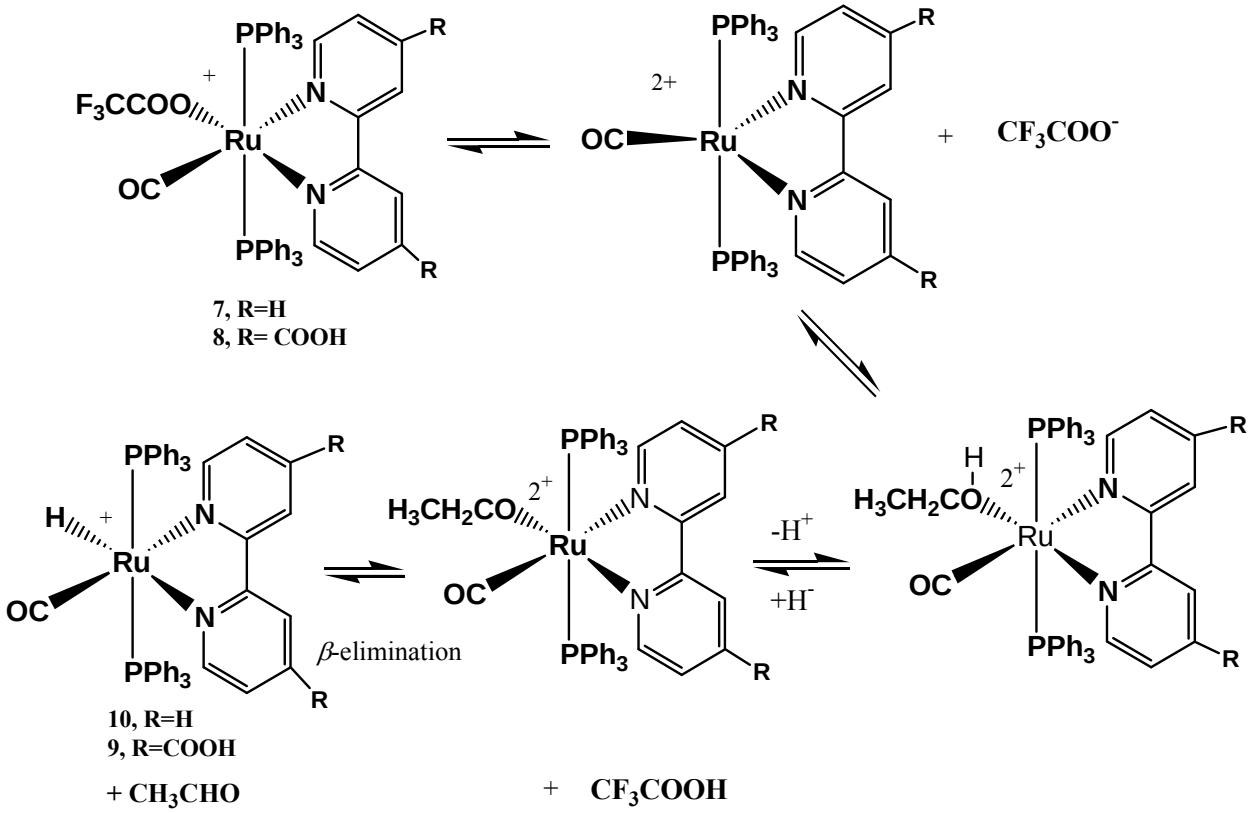

Scheme 3.4

3.3.2. Reaction of the chelating phosphine complexes with the diimine ligands

The reactions of complex **3** with 1,10-phenanthroline or 2,2′-bipyridyl in ethylene glycol formed $[(CO)(TFA)Ru\{\eta^2(C_6H_5)_2PC_2H_4P(C_6H_5)_2\}(\eta^2C_{12}H_8N_2)][PF_6]$ (**11**) and $[(CO)(TFA)Ru\{\mu\text{-}\eta^2(C_6H_5)_2PC_2H_4P(C_6H_5)_2\}(\eta^2C_{10}H_8N_2)][PF_6]$ (**12**) in 56% and 55% yield, respectively (Scheme 3.5). Similarly, heating complex **4** with 1,10-phenanthroline or 2,2′-bipyridyl in ethylene glycol at 140 °C afforded $[(CO)(TFA)Ru\{\eta^2(C_6H_5)_2PC_2H_2P(C_6H_5)_2\}(\eta^2C_{12}H_8N_2)][PF_6]$ (**13**) and $[(CO)(TFA)Ru\{\eta^2(C_6H_5)_2PC_2H_4P(C_6H_5)_2\}(\eta^2C_{10}H_8N_2)][PF_6]$ (**14**) in 59% and 45% yields, respectively (Scheme 3.6). Reaction

of **4** with bio-conjugable ligand 5-amino-1,10-phenanthroline in ethylene glycol at 140 °C gave $[(CO)Ru(\{\eta^2(C_6H_5)_2PC_2H_4P(C_6H_5)_2\}TFA(\eta^2C_{10}H_9N_3)][PF_6]$ (**15**) in 55% yield (Scheme 3.6).

All these complexes were characterized by elemental analysis, infrared, ^1H NMR, $^{31}P-\{^1H\}$ NMR, UV–Vis and mass spectral data (Table 3.1). Due to the presence of the labile ligand TFA, these complexes are unstable in solution, and we were not able to obtain good quality crystals for X-ray crystallographic analysis. Addition of Conc. HCl or aqueous NaCl solution to the methanol solution of **15** produced complex $[HRu\{\eta^2(C_6H_5)_2PC_2H_4P(C_6H_5)_2\}(CO)(\eta^2C_{10}H_9N_3)][PF_6]$ (**16**) along with trace amount of $[Ru\{\eta^2(C_6H_5)_2PC_2H_4P(C_6H_5)_2\}(CO)(\eta^2C_{10}H_9N_3)Cl][PF_6]$. The ESI-MS gave an $m/z = 924$, due to formation of the Na^+ adduct, shows the presence of this compound as a mixture with the hydride compound (Scheme 3.7).

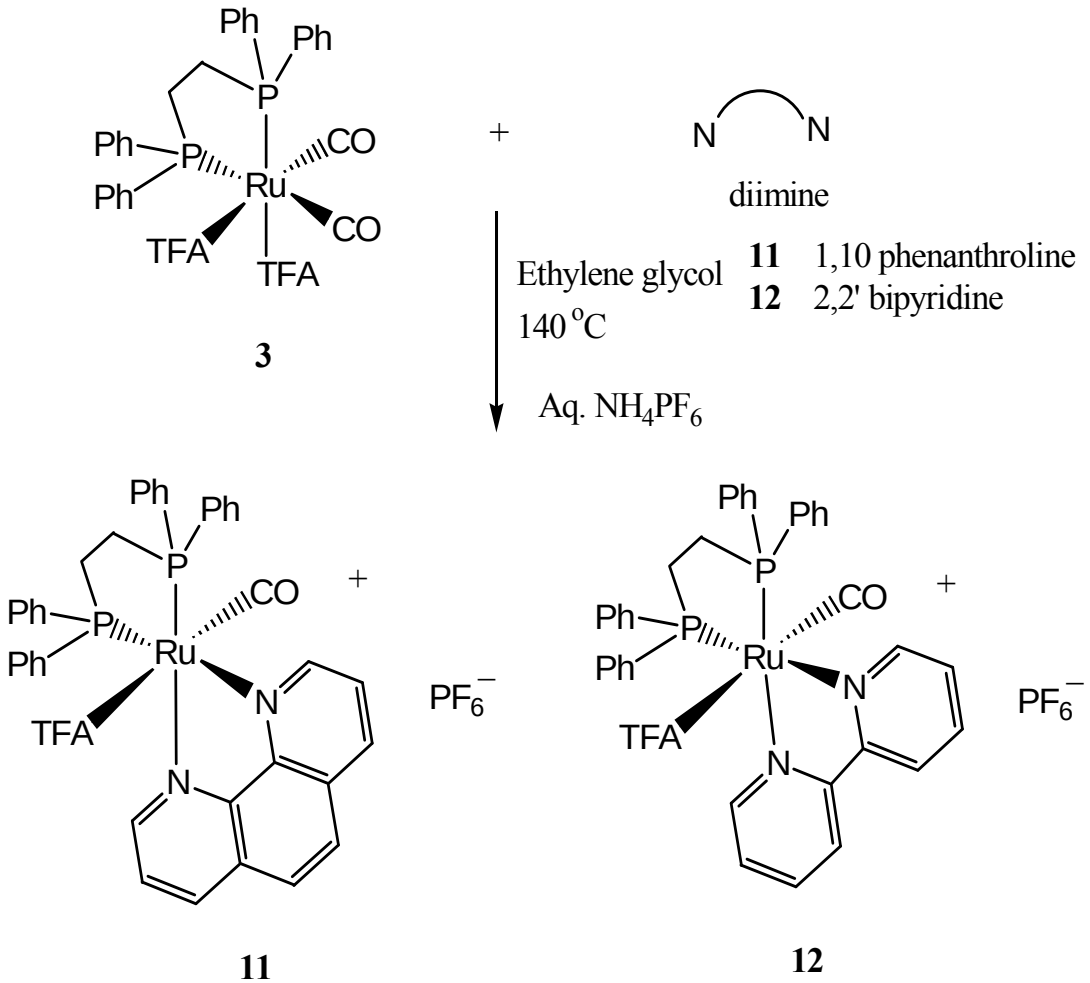
Ph
Ph
P
Ph
P
CO
Ph
Ru
Ph
CO
TFA
TFA
3
+
N
N
diimine
Ethylene glycol
140 °C
11 1,10 phenanthroline
12 2,2' bipyridine
Aq. NH4PF6
Ph
Ph
P
Ph
P
CO
Ph
Ru
TFA
N
N
+
PF6−
11
Ph
Ph
P
Ph
P
CO
Ph
Ru
TFA
N
N
+
PF6−
12

Scheme 3.5

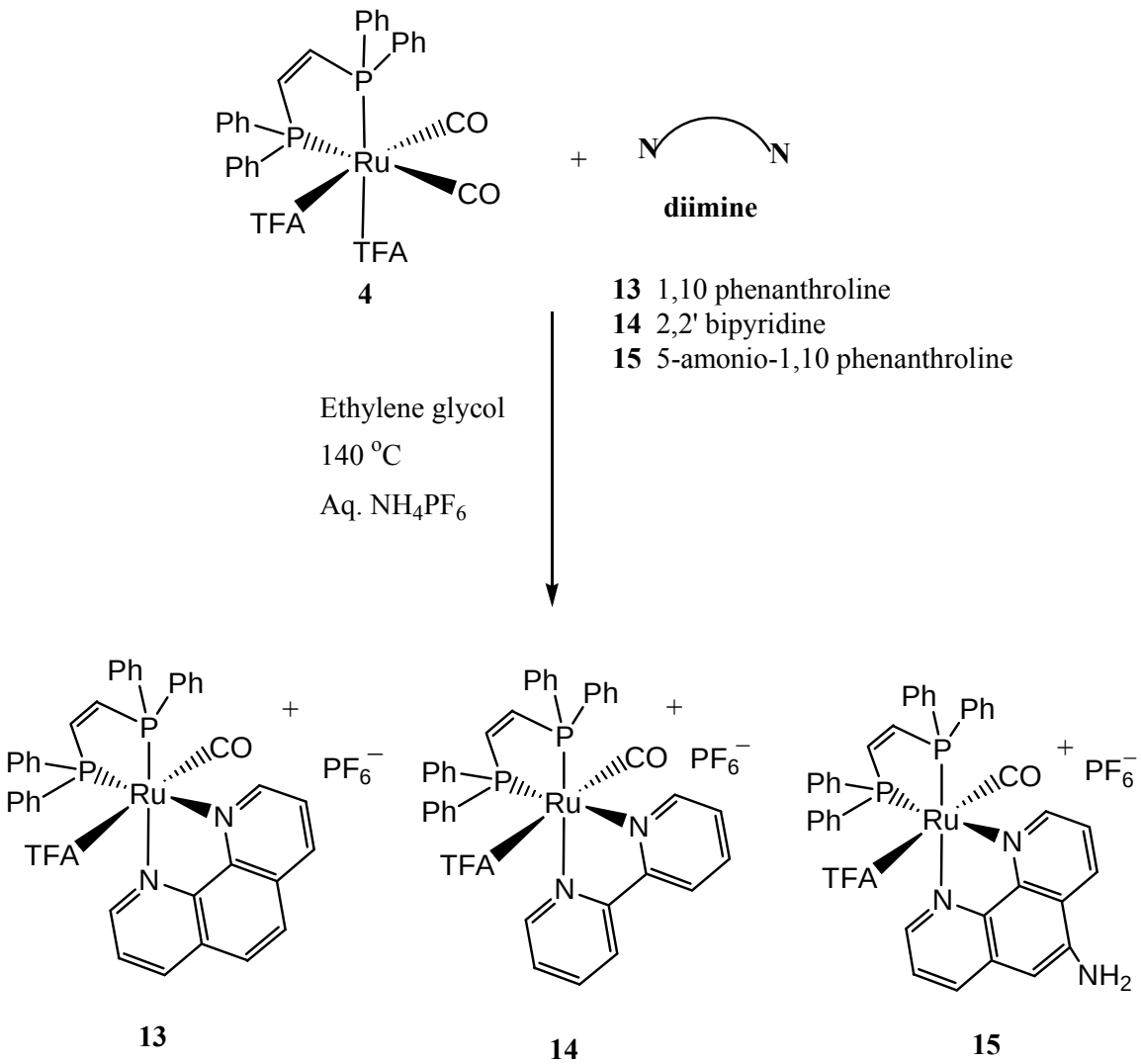
Ph
Ph
P
Ph
P
Ph
Ru
CO
CO
TFA
TFA
4
+
N
N
diimine
13 1,10 phenanthroline
14 2,2' bipyridine
15 5-amonio-1,10 phenanthroline
Ethylene glycol
140 °C
Aq. NH4PF6
PF6−
NH2
13
14
15

Scheme 3.6

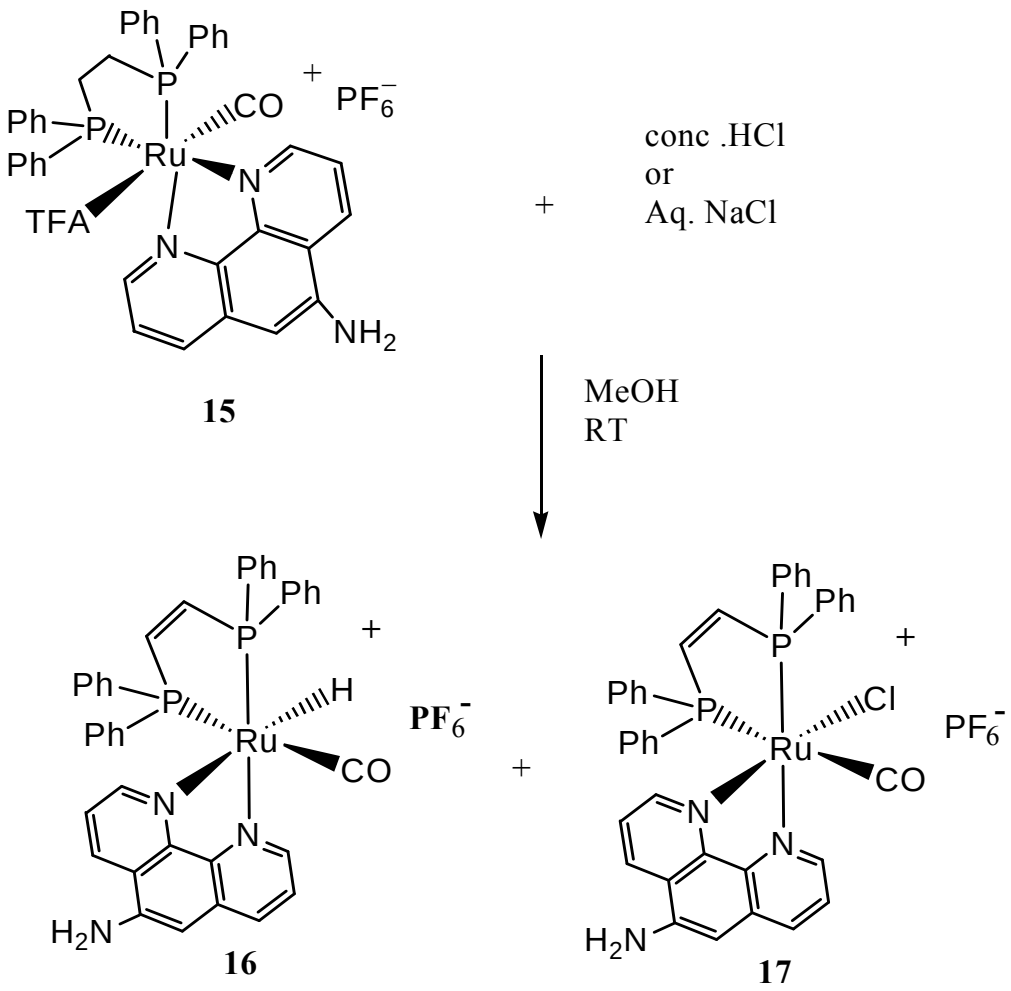

Scheme 3.7

The hydride complex was confirmed by the observed pentaplet at −7.8. A probable route to hydride formation in the H_2O/MeOH solution is shown in Scheme 3.8. There is a possibility that the reaction with HCl and NaCl is catalyzed by the H^+ present in the solution. It is predicted that the complex **15** loses the labile ligand, TFA, followed by the coordination of H_2O. Protonation of this bound water molecule then facilitates hydride transfer to the metal center (Scheme 3.8).

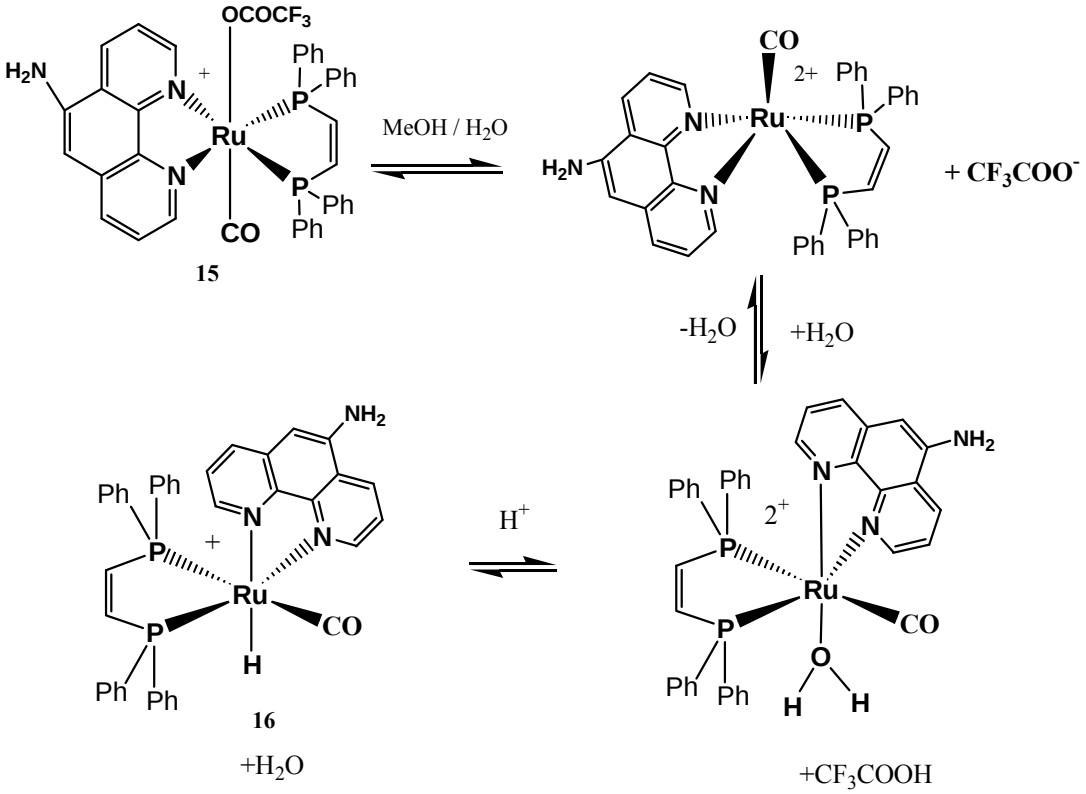

15

16

Scheme 3.8

Table 3.1 IR, NMR and ESI-MS data

Compound	IR (ν_{CO}, cm^{-1})[a]	^{1}H NMR (δ, ppm)[b]	$^{31}PNMR$ (δ, ppm)[b]	ESI-MS[c] (m/Z)
2	2061vs, 2001vs, 1692vs	7.8-7.2 (30H)	29.52(s, 2P)	794 [M-TFA]
3	2066vs, 2004vs, 1691vs	7.8-7.0 (20H), 3.6-3.4 (2H), 2.01 (2H)	45.8 (s, 1P), 44.07(s, 1P)	-----
4	2077vs, 2006vs, 1692vs	7.8-6.9 (22H)	53.99(s, 1P), 53.47(s, 1P)	**-----**
5	1993vs, 1688s	8.9-8.2 (6H), 7.9-6.8 (32H)	26.6(s, 2P), -155(1P)	869 [M-PF_6]
6	1982s, 1703vs	9.4-8.2 (6H), 7.8-6.9 (17H)	28.3(s, 1P), -155(1P)	685 [M-TFA]
7	1992vs, 1680s	9.1-8.4 (6H), 7.8-6.9 (32H),	28.98 (s, 2P), -155 (1P)	923 [M-PF_6]
8	1992s, 1727s, 1680m	--------	**---------**	**--------**
9	1944s, 1730s	11.7(2H), 9.1-8.5 (4H), 6.9-8.1 (32H), -11.09 (1H)	50.9 (2P), -155 (1P)	943 [M-PF_6+2Na^+]
10	1942s	9.0-8.2 (6H), 7.8-6.9 (32H), -11.07 (1H)	50.45 (2P), -155 (1P)	811 [M-PF_6]
11	1988vs, 1692m	8.6-7.9 (4H), 7.7-6.6 (23H), 3.6-3.3 (2H), 2.04 (2H)	45.24 (2P), -155 (1P)	967 [M + H^+]
12	1987vs, 1704m	9.4-8.2 (6H), 8.0-6.7 (22H), 3.5-3.3 (2H), 2.04 (2H)	53.96 (2P), -155 (1P)	941 [M^+]
13	1992vs, 1691m	8.8-8.2 (4H), 7.9-7.2 (23H), 7.0-6.8 (3H)	49.93 (2P), -155 (1P)	965 [M+H^+]
14	1988vs, 1706m	8.9-8.1 (6H), 7.8-6.8 (24H)	53.93 (2P), -155 (1P)	939 [M^+]
15	1990vs, 1685m	8.75-8.05 (5H), 7.8-7.0 (22H), 4.9-4.6 (2H)	53.9 (2P), -155 (1P)	835 [M-PF_6]
16	1977s	8.3-7.9 (5H), 7.8-6.8 (22H), 4.0 (2H), -7.8 (1H)	74.8 (2P), -155 (1P)	723 [M-PF_6]

[a.] Data were collected in KBr,
[b.] Data were collected in acetone d^6
[c.] Data were collected 80% acetonitrile

3.3.3 Solid state structures of compounds 5, 6 and 10

The solid state structures of **5**, **6** and **10** are shown in Figure 3.1, crystal data are given in Table 3.2 and selected distances and angles are given in Table 3.3–3.5. Complexes **5** and **10** contain two mono-dentate triphenylphosphine ligands *trans* to each other and complex **6** contains only one triphenylphosphine ligand. The presence of $[PF_6]$ anion assures the positive charge on **5** and **10** whereas complex **6** is a neutral complex as it contains two TFA ligands *cis* with respect to each other. The ligands in these complexes are arranged in close to octahedral geometry around the Ru atom. The chelating bi-dentate diimine ligands in **5**, **6** and **10** are bound to the Ru(II) with a bite angle 78.19(13), 79.2(13) and 74.5(17)°, respectively. This structural feature is similar to other Ru–diimine complexes [23] and [36]. The Ru–N phenanthroline (2.06–2.13 Å) and Ru–N bipyridine (2.10–2.16 Å) bond lengths of the coordinated diimine ligands are also comparable to those observed in other Ru–diimine complexes [36]. All these complexes contain one carbonyl ligand attached to the metal center and the Ru–C bond lengths of **5**, **6** and **10** [1.866(9), 1.864(4) and 1.816(15) Å] are similar to those observed for similar Os and Re complexes [36-38]. The exchange of Cl for TFA ligand in complex **5** resulted in disordering of the CO and Cl ligands. The hydride ligand in the equatorial position of complex **10** is *trans* to N(2) of the bipyridine ligand and Ru–H bond length is 2.04(5). The presence of this hydride was confirmed by ^{1}H NMR.

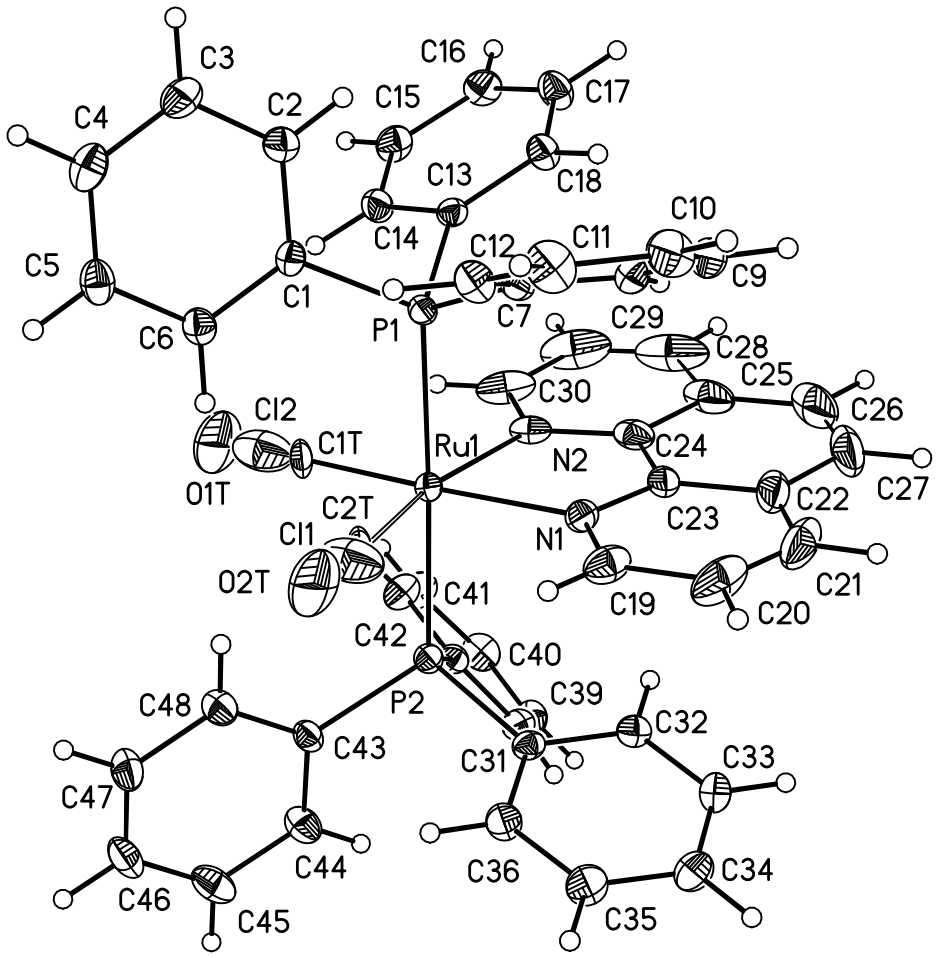

Figure 3.1: (a) Solid state structure of [Ru{P(C_6H_5)$_3$}$_2$(1,10-phenanthroline)(CO)Cl][PF_6] (5) showing the 90% probability thermal elipsoids and the calculated positions of the hydride and hydrogen atoms

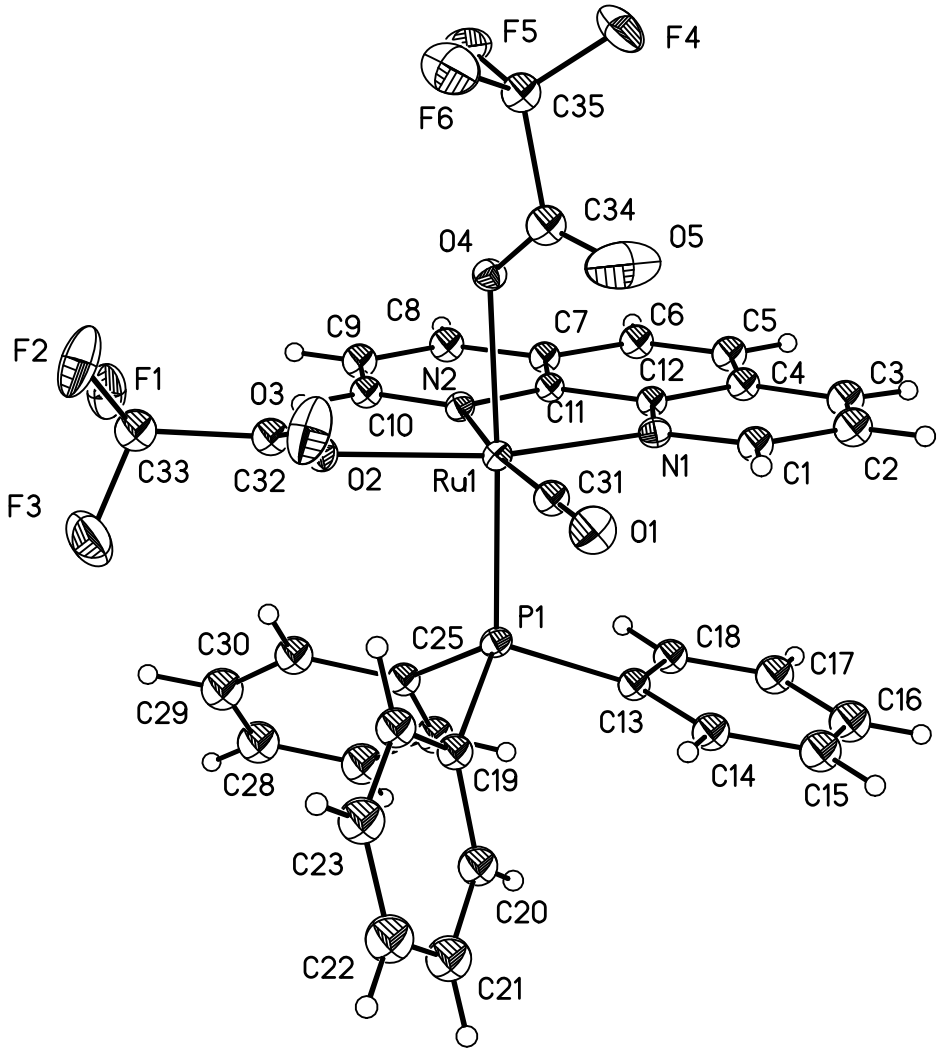

Figure 3.1: (b) Solid state structure of [Ru{P(C_6H_5)$_3$}(1,10-phenanthroline)(CO)((TFA)$_2$] (6) showing the 90% probability thermal elipsoids and the calculated positions of the hydride and hydrogen atoms

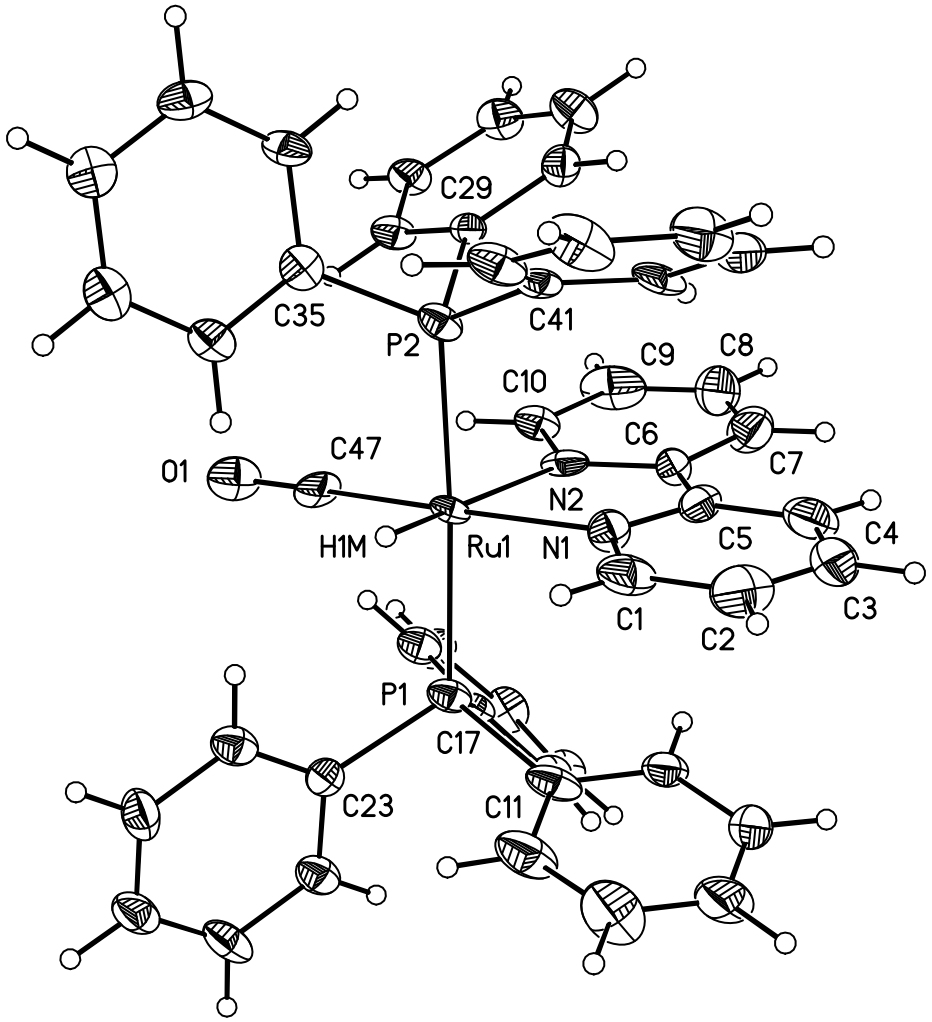

Figure 3.1: Solid state structure of (c) [HRu{P(C_6H_5)$_3$}$_2$(2,2′-bipyridyl)(CO)][PF_6] (10) showing the 90% probability thermal elipsoids and the calculated positions of the hydride and hydrogen atoms.

Table 3.2 Crystal data and structure refinement for compound 5, 6 and 10.

Compound	**5**	**6**	**10**
Empirical formula	$C_{49}H_{38}ClF_6N_3O_4P_3Ru$	$C_{35}H_{23}F_6N_2O_5PRu$	$C_{47}H_{39}F_6N_2OP_3Ru$
Formula weight	1076.25	797.59	955.78
Temperature (K)	173(2)	173(2)	173(2)
Wavelength (Å)	0.71073	0.71073	0.71073
Crystal system	triclinic	monoclinic	triclinic
Space group	*P* ī	*P 2(1)/n*	*P* ī
Unit cell dimensions			
a (Å)	12.0192(8)	11.0644(2)	11.848(3)
b (Å)	13.8790(9)	20.2377(4)	13.558(3)
c (Å)	14.7094(9)	15.1820(3)	14.869(4)
α (º)	92.1380(10)	90	89.908(4)
β (º)	99.2250(10)	93.896	81.975(4)
γ (º)	103.3140(10)	90	79.685(4)
Volume ($Å^3$)	1349.9(3)	3391.67(11)	2326.2(9)
Z	2	4	2
D_{calc} (Mg/m^3)	1.521	1.562	1.365
Absorption coefficient (mm^{-1})	0.565	4.882	0.500
F(000)	1090	1600	972
Crystal size (mm)	0.28 X 0.23 X 0.13	0.35 X 0.15 X 0.15	0.19 X 0.12 X 0.12
θ Range for data collection (º)	1.41–28.37	1.41–28.37	1.76–23.82
Index ranges	$-16 \le h \le 16$ $-18 \le k \le 18$ $-19 \le l \le 19$	$-12 \le h \le 13$ $-23 \le k \le 23$ $-17 \le l \le 17$	$-13 \le h \le 13$ $-15 \le k \le 15$ $-16 \le l \le 16$
Reflection collected	34911	19108	20092
Independent reflections (Rint)	11720 (0.0373)	5716 (0.0237)	13496 (0.0668)
Completeness to θ = 66.38º (%)	99.5	95.9	100
Data/restraints/Parameters	11720/2/614	5716/0/279	13496/3/358
Goodness-of-fit on F^2	1.154	1.069	1.082
Final *R* indices [$I > 2\sigma(I)$]	$R_1 = 0.0619$, $wR_2 = 0.1487$	$R_1 = 0.0432$, $wR_2 = 0.1350$	$R_1 = 0.0877$, $wR_2 = 0.1852$
R indices (all data)	$R_1 = 0.0701$, $wR_2 = 0.1532$	$R_1 = 0.0453$, $wR_2 = 0.1368$	$R_1 = 0.1300$, $wR_2 = 0.2079$
Largest difference in peak and hole (e $Å^{-3}$)	1.112 and –2.227	2.196 and –0.512	1.223 and –1.916

Table 3.3: Selected bond distances (Å) and angles (°) for $C_{49}H_{38}C_lF_6N_2OP_3Ru_1$ (5).

Distances (Å)			
N(1)-Ru(1)	2.110(3)	C(1T)-O(1T)	1.222(8)
N(2)-Ru(1)	2.127(3)	C(1T)-Ru(1)	1.866(9)
P(1)-Ru(1)	2.3732(9)	C(2T)-O(2T)	1.193(8)
P(2)-Ru(1)	2.3782(9)	C(2T)-Ru(1)	1.891(11)
Cl(2)-Ru(1)	2.480(5)	Cl(1)-Ru(1)	2.475(3)
Angles (°)			
C(1T)-Ru(1)-C(2T)	93.3(6)	C(1T)-Ru(1)-N(1)	177.1(4)
C(2T)-Ru(1)-N(1)	89.5(3)	C(1T)-Ru(1)-N(2)	99.0(4)
C(2T)-Ru(1)-N(2)	167.7(3)	N(1)-Ru(1)-N(2)	78.19(13)
C(1T)-Ru(1)-P(1)	88.7(3)	C(2T)-Ru(1)-P(1)	90.7(3)
N(1)-Ru(1)-P(1)	90.89(8)	N(2)-Ru(1)-P(1)	88.99(8)
C(1T)-Ru(1)-P(2)	90.3(3)	C(2T)-Ru(1)-P(2)	87.5(3)
N(1)-Ru(1)-P(2)	90.28(8)	N(2)-Ru(1)-P(2)	92.98(8)
P(1)-Ru(1)-P(2)	177.88(3)	C(1T)-Ru(1)-Cl(1)	97.5(4)
C(2T)-Ru(1)-Cl(1)	4.9(4)	N(1)-Ru(1)-Cl(1)	85.32(15)
N(2)-Ru(1)-Cl(1)	163.22(15)	P(1)-Ru(1)-Cl(1)	88.20(9)
P(2)-Ru(1)-Cl(1)	90.14(9)	C(1T)-Ru(1)-Cl(2)	1.6(5)
C(2T)-Ru(1)-Cl(2)	94.6(3)	N(1)-Ru(1)-Cl(2)	175.81(12)
N(2)-Ru(1)-Cl(2)	97.66(12)	P(1)-Ru(1)-Cl(2)	89.61(8)
P(2)-Ru(1)-Cl(2)	89.36(8)	Cl(1)-Ru(1)-Cl(2)	98.86(16)

Table 3.4: Selected bond distances (Å) and angles (°) for $C_{35}H_{23}F_6N_2O_5P_1Ru_1$ (6).

Distances (Å)			
N(1)-Ru(1)	2.062(3)	C(31)-O(1)	1.145(5)
N(2)-Ru(1)	2.133(3)	C(31)-Ru(1)	1.864(4)
O(2)-Ru(1)	2.086(3)	P(1)-Ru(1)	2.3020(10)
O(4)-Ru(1)	2.148(3)		
Angles (°)			
C(31)-Ru(1)-N(1)	93.95(16)	C(31)-Ru(1)-O(4)	95.47(15)
C(31)-Ru(1)-O(2)	99.28(15)	N(1)-Ru(1)-O(4)	88.54(12)
N(1)-Ru(1)-O(2)	165.79(12)	O(2)-Ru(1)-O(4)	85.08(11)
C(31)-Ru(1)-N(2)	173.27(15)	N(2)-Ru(1)-O(4)	83.44(11)
N(1)-Ru(1)-N(2)	79.40(13)	C(31)-Ru(1)-P(1)	88.53(13)
O(2)-Ru(1)-N(2)	87.25(12)		

Table 3.5: Selected bond distances (Å) and angles (°) for $C_{47}H_{39}F_6N_2O_1P_3Ru_1$ (10).

Distances (Å)			
N(1)-Ru(1)	2.102(6)	C(47)-O(1)	1.151(18)
N(2)-Ru(1)	2.163(6)	C(47)-Ru(1)	1.816(15)
P(1)-Ru(1)	2.347(5)	P(2)-Ru(1)	2.349(5)
Ru(1)-H(1)	2.040(5)		
Angles (°)			
O(1)-C(47)-Ru(1)	174.5(14)	C(47)-Ru(1)-N(1)	179.2(5)
C(47)-Ru(1)-N(2)	105.1(5)	N(1)-Ru(1)-N(2)	74.20(17)
C(47)-Ru(1)-P(1)	88.9(5)	N(1)-Ru(1)-P(1)	91.0(2)
N(2)-Ru(1)-P(1)	94.7(2)	C(47)-Ru(1)-P(2)	90.7(5)
N(1)-Ru(1)-P(2)	89.5(2)	N(2)-Ru(1)-P(2)	90.4(2)
P(1)-Ru(1)-P(2)	174.8(2)	C(47)-Ru(1)-H(1)	99.8
N(1)-Ru(1)-H(1)	81.0	N(2)-Ru(1)-H(1)	155.0
P(1)-Ru(1)-H(1)	82.5	P(2)-Ru(1)-H(1)	92.4

3.3.4 Spectroscopic characterization

Infrared spectral analysis

The infrared spectra of the metal bound carbonyl stretching region (ν_{CO}) provided important information about the stepwise ligand substitutions performed on the precursor **1**. All of the complexes synthesized contain metal-coordinated carbonyl ligands. M–CO shows CO stretching modes around 2150–1750 cm^{-1}, which are easily distinguishable from organic CO frequencies. The M–CO signals are very sensitive to the electronic properties of the other ligands present on the metal. The observed changes in the carbonyl stretching region are due to the replacement of CO ligands by phosphines and diimine ligands, respectively. Introduction of electron rich ligands such as Ph_3P, dppe and dppene decreased the energy of the M–CO bands. Phosphine compounds **2**–**4** showed two strong M–CO stretches at 2066 and 2002 cm^{-1}, confirming that they are di-carbonyl complexes; the strong ν_{CO} at 1696 cm^{-1} is due to the two CF_3COO^- ligands. The complexes **5**–**16** have only one M–CO ligand, and usually the strong M–CO stretch appears at 1995–1985 cm^{-1} for the non-hydride complexes. Replacement of CF_3COO^- by the more electron-donating hydride ligand shifts ν_{CO} to lower energy in complexes **9**, **10** and **16**. A strong absorption at 1734 cm^{-1} was also observed for the carboxyl groups of 4,4′-dicarboxy-2,2-bipyridyl of **8** and **9**. Raman spectra of the metal hydrides show characteristic $\nu_{M–H}$ stretches at 1800–2000 cm^{-1} [39]. Raman spectra of complexes **9** and **10** have $\nu_{M–H}$ at 1920 and 1950 cm^{-1}, respectively.

NMR spectral analysis

The ^1H and ^{31}P NMR spectra of these complexes obtained in acetone d^6 are consistent with the predicted structures. NMR spectral analysis was an important tool to

assign the presence of the terminal hydride ligand in the complexes **9**, **10** and **15**. The aromatic region of the ^{1}H spectra is complex due to presence of phenyl protons of phosphine ligands and the aromatic protons of diimine ligands. The chemical shifts and coupling constants are listed in Table 3.1. The phenyl protons of PPh_3 (complexes **2** and **5**–**10**) and chelating phosphines (complexes **3**, **4** and **11**–**16**) appear as multiplets at δ 7.2–7.6 ppm. The CH═CH protons of diphenylphosphinoethylene are observed around δ 6.4–6.9 ppm and the alkyl protons of diphenylphosphinoethane are observed around δ 2.03–3.6 ppm. The M–H resonance appears as a triplet at δ −11.09 (J = 20 Hz) and −11.07 (J = 20 Hz) for complexes **9** and **10**, respectively. In the case of complex **16**, the pentaplet is observed at δ −7.8 ppm (J = 20 Hz).

The ^{31}P NMR spectra greatly facilitated structural characterization of these complexes. The chemical shift of the metal bound phosphines ligands are in good agreement with the similar Ru(II) phosphine complexes. Complexes **2**, **5**, **6** and **7** show singlet resonances at 26–30 ppm, relative to external H_3PO_4, due to the PPh_3 ligands. The sharp singlet observed for these complexes (**2**, **5** and **7**) indicated that the two phosphorous nuclei are magnetically equivalent, and therefore are *trans* to each other. In the chelating phosphine complexes, the two phosphorous nuclei must be *cis* to each other and therefore two singlets at 45.8 and 45.07 ppm for complex **3** and at 53.9 and 53.4 ppm for complex **4** are observed. The ^{31}P–^{31}P coupling is apparently small in these complexes. The observation of two resonances in the ^{31}P NMR for **3** and **4** requires that one of the two remaining CO ligands and one of the two remaining TFA ligands are trans to each phosphorous. Otherwise the molecule would have a plane of symmetry and one ^{31}P NMR resonance would be observed. However, when the diimine ligand is introduced, only one

sharp signal for the chelating phosphine ligand is observed. This indicates that complexes **11**–**16** have a symmetry component that makes the two phosphorous nuclei equivalent (Scheme 3.2–3.5). With the exception of complex **6**, complexes **5**–**16** all contain [PF_6] as a counter ion, which appeared in the ^{31}P NMR as a septet at −155 ppm with an integrated relative intensity of 1:2 when compared with the phosphine ligand resonances.

3.3.5. Electrochemistry

The redox properties of the series of Ru carbonyl complexes (**7**, **9**, **10**, **13**, **14** and **15**) were determined by cyclic voltammetry. The cyclic voltammetric (CV) responses are, generally speaking, not well resolved and have as many as four ill-defined peaks. In the bipyridyl-based complexes (**7**, **9** and **10**), a series of four redox steps are observed. It is likely that both metal- and ligand-centered reductions occur, but it is not possible to discriminate them on the basis of the obtained CVs. As an example, we show in Figure 3.2 the cyclic voltammetric (CV) response on a glassy carbon electrode (GC) of a CH_2Cl_2/0.1 M [NBu_4]PF_6 solution of **7** at a 0.2 V s^{-1} scan rate (v). Apparently, only the first peak couple ($E°'$ (A/A') = −1.02 V vs. SCE) is chemically reversible (dashed line in Figure 3.2), although the second and the third ($E_{p,c}$ (B) = −1.76 V, and $E_{p,c}$ (C) = −2.06 V vs. Fc/Fc^+, respectively) show a hint of a return peak in the reverse scan, in particular when the fourth peak ($E_{p,c}$ = (D) −2.30 V vs. Fc/Fc^+) is not traversed. The other complexes of the series show similar behavior and

number of peaks. Changing the scan rates to 0.5 and 1.0 V s^{-1} did not significantly change the appearance of the voltammograms.

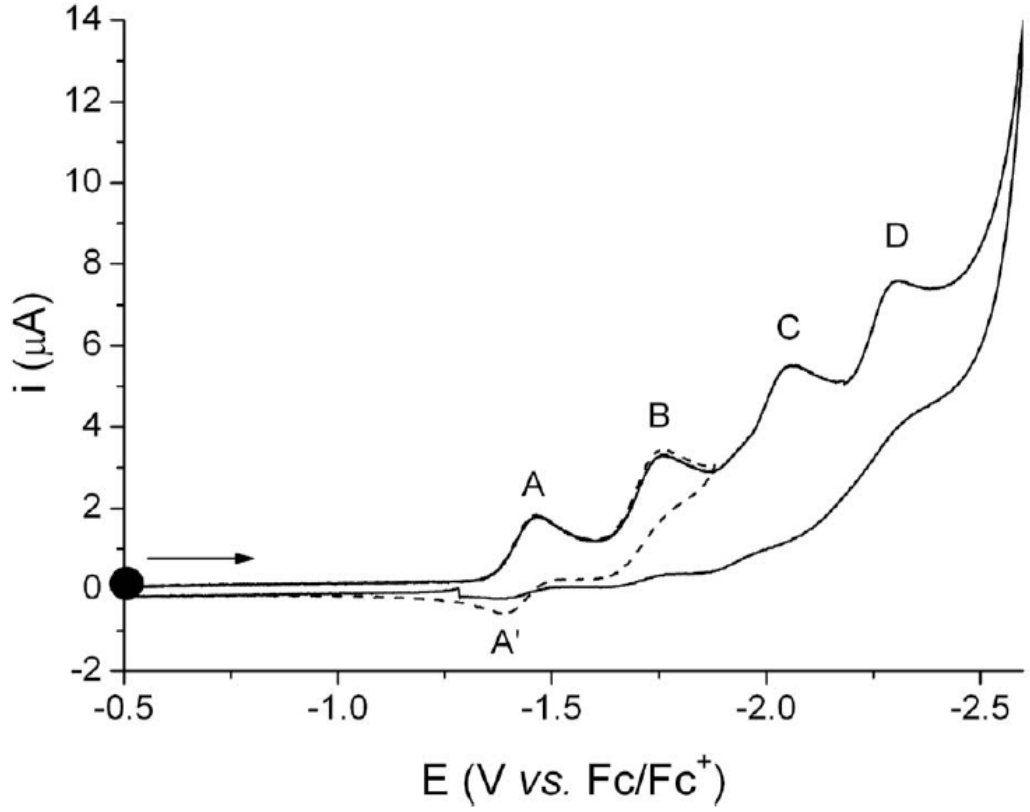

Figure 3.2: CV of a 1.0 mM solution of [Ru{P(C_6H_5)$_3$}$_2$(2,2′-bipyridyl)(CO)TFA][PF_6] (7) in CH_2Cl_2 containing 0.10 M [NBu_4][PF_6], at a GC working electrode; v = 0.2 V s^{-1} (• starting potential).

The phenanthroline-based series of complexes exhibit considerable overlap of the observed redox wave CVs. Only complex **5** shows three well-resolved, chemically and electrochemically reversible redox steps: two reductions ($E^{\circ\prime}$ (E/E') = −1.70, and $E^{\circ\prime}$ (F/F') = −1.93 V vs. Fc/Fc^+, respectively), accompanied by an oxidation in the positive scan ($E^{\circ\prime}$ (G/G') = +1.04 V vs. Fc/Fc^+) (Fig. 3). The closely related **7** does not show this

reversible oxidation, probably owing to the differences between the electronic properties between the phenanthroline and bipyridyl ligands.

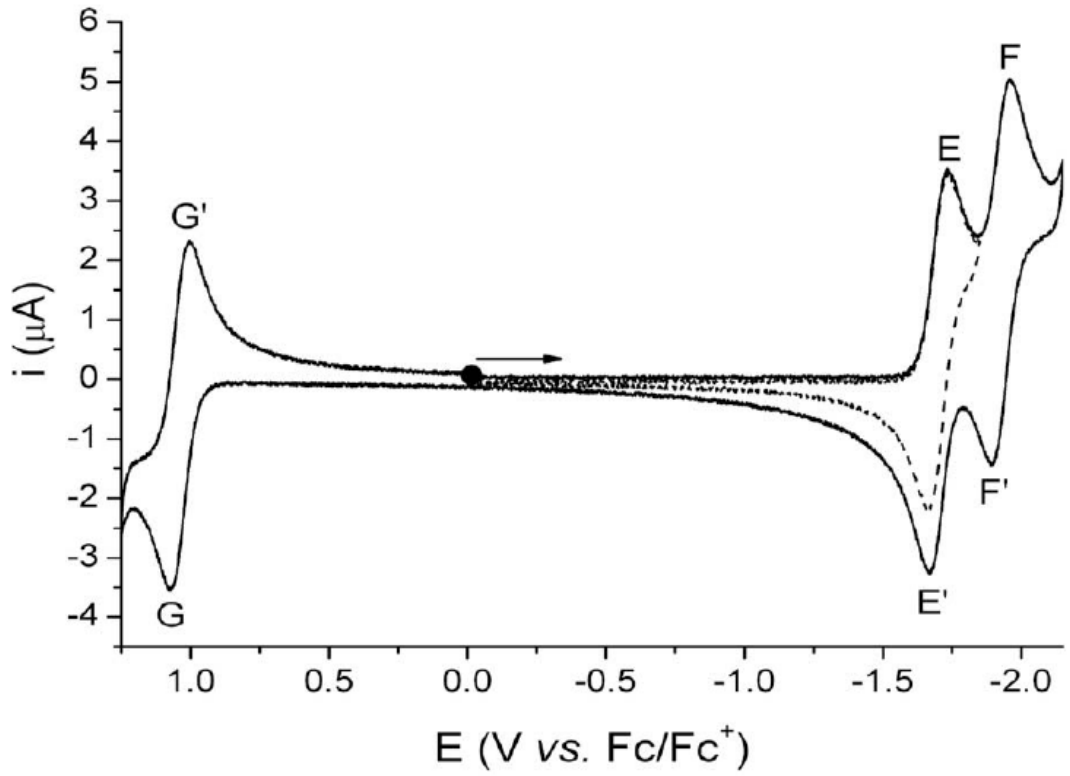

Figure 3.3: CV of a 1.0 mM solution of $[Ru\{P(C_6H_5)_3\}_2(1,10\text{-phenanthroline})(CO)Cl][PF_6]$ (5) in CH_2Cl_2 containing 0.10 M $[NBu_4][PF_6]$, at a GC working electrode; v = 0.2 V s^{-1} (• starting potential).

A reasonable interpretation of the multiple redox couples observed for complexes **5** and **7** is that the first reduction is the Ru(II) to Ru(I) couple, while the complex and more negative potentials are the result of electron donation to the diimine ligand and/or the phenyl rings on the phosphine ligands [40]. There is considerable

precedent for such multiple electron transfers to diimine ligands in related Ru(II) complexes [40]. However, we cannot differentiate at this time whether the CO and phosphine ligands are also participating as electron acceptors. The different reduction potentials and the different degrees of redox-wave-overlap are consistent with this interpretation. The observation of a reversible oxidation wave for complex **5** makes this complex a good candidate for electrochemiluminescence studies. The other compounds in the series also show complex electrochemical behavior, preventing meaningful tabulation of the electrochemical parameters.

3.3.6 Photophysical properties of 5–16

Absorption spectra

The UV–Vis absorption spectra of the synthesized complexes **5–15** were measured at room temperature in ethanol and/or acetonitrile solution (Table 3.6). The absorption spectra were also recorded in water for complexes **10** and **15**, as both of these complexes have bio-conjugable functional groups. The ruthenium complexes [(CO)LRu(diimine) (L_2)][PF_6] have six *d* electrons in the three t_2 orbitals, and the diimine ligand provides low-energy π^* orbitals that upon excitation can accept an electron from the electron-rich metal center. Consequently, these complexes display weak absorption bands around 400–500 nm due to the singlet metal-to-ligand charge-transfer (^{1}MLCT) [5]. The strong absorption bands below 390 nm are assigned to intra-ligand charge-transfer (π–π and *n*–π).

Table 3.6 UV–Vis absorption and emission data for 5–7 and 9–15.

Compound	λ_{abs} MLCT(nm)	$\lambda_{Excitation}$ (nm)	λ_{E}m (nm)	φ[a]	τ(ns)
5	420[b]	425	595[b]	0.08	110 (330)[b,c]
6	410[b]	410	-----	-----	-----
7	420[b]	425	611[b]	0.12	185 (680)[b,c]
9	450	450	647	0.30	720 (2630)[c]
10	445	450	607	0.11	847
11	445[b]	450	590[b]	0.12	106 (325)[c]
12	450[b]	450	610[b]	0.08	180
13	440[b]	450	590[b]	0.09	126
14	445	450	610	0.07	190
15	450	470	607	0.25	250 (570)[c]

The photophysical studies were done making solutions in acetonitrile and ethanol.

[a] Referenced to 0.73 Quinine disulfate in H_2SO_4 (dilute) (31). Estimated error in relative yields is nearly 15%. Rhodamine emission is in the same region as the MLCT transition.

[b] Solvent was acetonitrile.

[c] The lifetime was recorded after exclusion of oxygen by purging Ar for 30 min in ethanol solution. The MLCT absorptions are broad.

The room temperature emission spectra of the complexes **5–16** (except compound **6**) showed red-shifted emission spectra, similar to those of other known Ru–MLCT complexes (Table 3.6). Compound **6**, containing only one PPh_3 ligand, did not have detectable emission at room temperature. It is significant that for this series of ligands that it is necessary to have two phosphine ligands in order to observe emission. This is most likely due to the more electron rich and more symmetrical structures of the

bis-phosphine complexes, which could reduce distortion in the excited-state. The quantum yields (φ) for the luminescent complexes in the presence of oxygen, listed in Table 6, were calculated relative to a Rhodamine B standard using Eq. (1). In general, these newly synthesized complexes showed higher quantum yields than [$Ru(bpy)_3^{2+}$] (i.e. $\varphi > 0.06$).

Time-resolved luminescence decay measurements were performed by time-correlated single-photon counting (TCSPC). The data were analyzed by non-linear least-squares as described in the experimental section (3.2.4). The excited-state lifetimes of the luminescent complexes containing phenanthroline ligands (**5**, **11** and **13**) are in the range of 110–126 ns. However, complex **15**, which contains amino-phenanthroline ligand, has a lifetime of 250 ns.

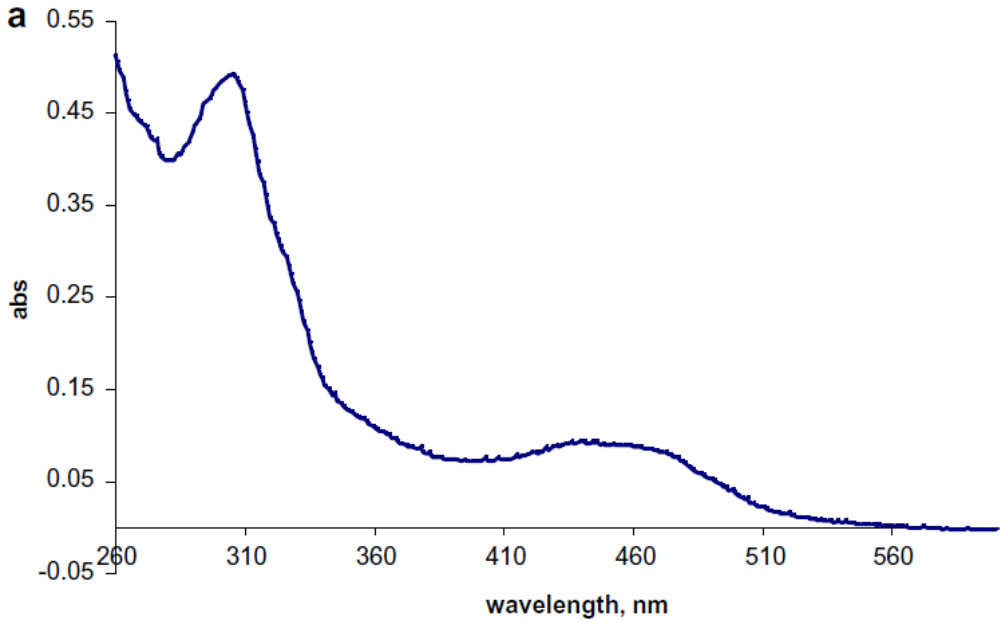

Figure 3.4: (a) Absorption spectrum of [$HRu\{P(C_6H_5)_3\}_2$(4,4′-dicarboxy-bipyridyl)(CO)][PF_6] (9) in ethanol.

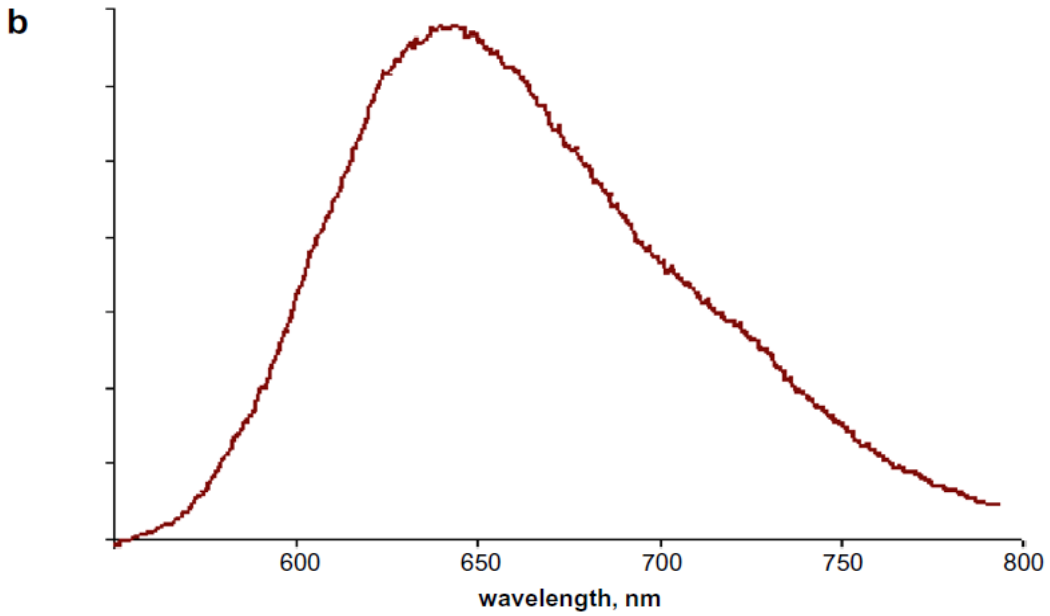

Figure 3.4: (b) emission spectra of [HRu{P(C_6H_5)$_3$}$_2$(4,4′-dicarboxy-bipyridyl)(CO)][PF_6] (9) in ethanol.

The bipyridyl complexes, when lacking the hydride ligand, have lifetimes of 180–200 ns. The hydride complexes **9** and **10**, at room temperature and in the presence of oxygen, had much longer lifetimes of 720 and 847 ns, respectively. Comparatively shorter lifetime observed for the TFA complexes could be resulted from the labiality of the TFA ligand in solutions [42]. The effect of oxygen on the photophysical properties of complexes **5**, **7**, **9**, **11** and **15** was also studied by measuring the lifetimes in both air-equilibrated and deoxygenated solutions in ethanol. The deoxygenated samples had longer excited-state lifetimes of 330, 680, 2630, 325 and 570 ns, for complexes **5**, **7**, **9**, **11** and **15,** respectively. The anisotropy decay of complex **10** and **15** were studied in glycerol at 0 °C. The fundamental anisotropy, which reflects the angle between the absorption and emission transition dipole moments, was

0.124 and 0.07, respectively, for complexes **10** and **15**. These values are higher than that (<0.001) observed for $Ru(bpy)_3^{2+}$ [5].

3.4 Conclusions

Several important conclusions can be drawn from these results. First, our original hypothesis that Ru(II) complexes with one diimine ligand and ancillary π-acceptor ligands will have longer excited-state lifetimes and higher quantum yields than previously reported for Os(II) complexes has been verified [24]. Furthermore, this series of complexes exhibit a wide range of excited-state lifetimes (110–850 ns), indicating that they will be useful for studying a wide range of dynamical biomacromolecular processes. The observed Stokes shifts and the emission wavelengths are similar to those obtained for Ru(II) complexes with two or three diimine ligands. The associated higher quantum yields relative to those previously reported for Ru(II) diimine complexes, also increases their usefulness. To help develop an understanding of the fundamental reasons for the observed variations in the photophysical properties we are now pursuing computational studies. Finally, the synthesis work reported here demonstrates the usefulness of the starting material **1** for making diverse ligand substitutions at the Ru(II) center. Although the low solubility of these complexes is an obstacle for using them in aqueous medium, their lipophilicity makes them promising for applications in lipid/membrane systems.

References

1. L. Li, H. Szmacinski and J.R. Lakowicz, *Anal. Biochem.* **244** (1997), p. 80.
2. L. Li, H. Szmacinski and J.R. Lakowicz, *Biospectroscopy* **3** (1997), p. 155.
3. L. Li, H. Szmacinski and J.R. Lakowicz, *Anal. Biochem.* **247** (1997), p. 465.
4. L. Li, *Chem. Phys. Lipids* **99** (1999), p. 991.
5. J.R. Lakowicz, Principles of Fluorescence Spectroscopy (3rd ed.), (2006). Springer, New York.
6. G. Piszczek, *Arch. Biochem. Biophys.* **453** (2006), p. 54.
7. J.V. Caspar, E.M. Kober, B.P. Sullivan and T.J. Meyer, *J. Am. Chem. Soc.* **104** (1982), p. 630.
8. E.M. Kober, J.L. Marshall, W.J. Dressick, B. Sullivan, J.V. Caspar and T.J. Meyer, *Chem. Phys. Lett.* **91** (1982), p. 91.
9. E.M. Kober, J.L. Marshall, W.J. Dressick, B.P. Sullivan, J.V. Caspar and T.J. Meyer, *Inorg. Chem.* **24** (1985), p. 755.
10. C.V. Caspar and T.J. Meyer, *J. Phys. Chem.* **87** (1983), p. 952.
11. C. Garino, S. Ghiani, R. Gobetto, C. Nervi, L. Salassa, V. Ancarani, P. Neyroz, L. Franklin, J.B.A. Ross and E. Seibert, *Inorg. Chem.* **44** (2005), p. 3875.
12. E. Terpetschnig, H. Szmacinski, H. Malak and J.R. Lakowicz, *Biophys. J.* **68** (1995), p. 342.
13. E. Terpetschnig, H. Szmacinski and J.R. Lakowicz, *Anal. Biochem.* **227** (1995), p. 140.
14. H. Szmacinski, E. Terpetschnig and J.R. Lakowicz, *Biophys. Chem.* **62** (1996), p. 109.

15. X.Q. Guo, F.N. Castellano, L. Li and J.R. Lakowicz, *Anal. Chem.* **70** (1998), p. 632.

16. E.M. Kober, J.V. Caspar, B.P. Sullivan and T.J. Meyer, *Inorg. Chem.* **27** (1988), p. 4587.

17. Felix N. Castellano, Xiang-Qun Guo, L. Li, Henryk Szmacinski, Jeffrey Sipior and Joseph R. Lakowicz, *Proc. SPIE-Int. Soc. Opt. Eng.* **3256** (1998), p. 223.

18. B.P. Sullivan, J.V. Caspar and T.J. Meyer, *Organometallics* **3** (1984), p. 1241.

19. T.A. Treadway, G.F. Strouse, R.R. Ruminski and T.J. Meyer, *Inorg. Chem.* **40** (2001), p. 4508.

20. T. Tuyen and J.C.M. Nguyen, *J. Am. Chem. Soc.* **102** (1980), p. 7383.

21. C. Garino, S. Ghiani, I. Bottero, R. Gobetto, C. Nervi, L. Salassa, E. Rosenberg, G. Caputo, G. Viscardi, I. Miletto and M. Milanesio, *Eur. Inorg. Chem.* **14** (2006), p. 2839.

22. A. Albertino, C. Garino, S. Ghiani, R. Gobetto, C. Nervi, L. Salassa, E. Rosenberg, G. Viscardi, R. Buscaino, G. Croce, M. Milanesio and A. Sharmin, *J. Organometal. Chem.* **692** (2007), p. 1377.

23. C. Garino, S. Ghiani, R. Gobetto, C. Nervi, L. Salassa, E. Rosenberg, J.B.A. Ross Xi Chu, K.I. Hardcastle and C. Sabatini, *Inorg. Chem.* **46** (2007), p. 8752.

24. E.M. Kober, B.P. Sullivan, W.J. Dressick, J.V. Caspar and T.J. Meyer, *J. Am. Chem. Soc.* **102** (1980), p. 7383.

25. SMART Version 5.628, Bruker AXS Inc., Analytical X-ray Systems, 5465 East Cheryl Parkway, Madison WI 53711-5373, 2003.

26. SAINT Version 6.36A, Bruker AXS Inc., Analytical X-ray Systems, 5465 East Cheryl Parkway, Madison WI 53711-5373, 2002.

27. SADABS Version 2.10, George Sheldrick, University of Göttingen, 2003.

28. SHELXTL V6.12, Bruker AXS Inc., Analytical X-ray Systems, 5465 East Cheryl Parkway, Madison WI 53711-5373, 2002.

29. A.A.J.C. Wilson (Ed.), International Tables for X-ray Crystallography, vol. C. Kynoch, Academic Publishers, Dordrecht, Tables 6.1.1.4 (pp. 500–502) and 4.2.6.8 (pp. 219–222), 1992.

30. D. Collini, C. Femoni, M.C. Iapalucci, G. Longoni and P. Zanello, *Special Publ. – R Soc. Chem. (Perspect. Organomet. Chem.)* **287** (2003), p. 183.

31. C.A. Parker, Photoluminescence of Solutions with Applications to Photochemistry and Analytical Chemistry, Elsevier, Amsterdam (1968) p 262.

32. M.D. Barkley, A.A. Kowalczyk and L. Brand, *J. Chem. Phys.* **75** (1981), p. 3581.

33. R.E. Dale, L.A. Chen and L. Brand, *J. Biol. Chem.* **252** (1981), p. 7500.

34. M.G. Badea and L. Brand, *Methods Enzymol.* **61** (1979), p. 378.

35. J. Paoletti and J.B. Le Pecq, *Anal. Biochem.* **31** (1969), pp. 33–41.

36. B. Carlson, *Inorg. Chim. Acta* **357** (2004), p. 3967.

37. G. Croce, M. Milanesio, D. Viterbo, C. Garino, R. Gobetto, C. Nervi and L. Salassa, *CR Chim.* **8** (2005), p. 1676.

38. C. Garino, T. Ruiu, L. Salassa, A. Albertino, G. Volpi, C. Nervi, R. Gobetto and H.I. Hardcastle, *Eur. J. Inorg. Chem.* **23** (2008), p. 3587.

39. H. Jacobsen, *Helv. Chim. Acta* **82** (1999), p. 297.

40. S. Zalis, M. Krejcik, V. Drchal and A.A. Vlcek, *Inorg. Chem.* **34** (1995), p. 6008.

41. T.J. Meyer, *Pure Appl. Chem.* **62** (1990), p. 1003.

42. C. Garino, R. Gobetto, C. Nervi, L. Salassa, *Inorg. Chim. Act.* **358** (2005), p. 196.

CHAPTER 4: PHOTOPHYSICAL STUDIES OF RUTHENIUM METAL-LIGAND COMPLEXES (MLC) INCORPORATED IN LIPID MEMBRANE BILAYER

4.1 Introduction

The dynamics of proteins and protein assemblies that associate with membrane surfaces are slow compared to the dynamics of proteins in solution [1]. For example, the correlation times of the rotational motions of membrane-bound proteins can be more than 200 ns [2-5]. The difference in timescales of the dynamics—microseconds versus tens of nanoseconds—results from interactions between the proteins and membrane lipids. Fluorescence probes most useful for studying protein dynamics in solution have excited-state lifetimes in the range of 5–30 ns. Longer excited-state lifetimes are needed to measure dynamics of biomacromolecules on or in membranes. Microsecond and millisecond timescale dynamics are often studied by using phosphorescent probes [6-8]. The transition-metal complexes containing one or more diimine ligands, referred as metal-ligand complexes (MLC), exhibit tunable long luminescence lifetimes (100 ns ~ 10 μs), polarized emission, high photostability, large stokes shifts and sensitivity to the probe environment [9-11]; the lifetimes of these probes can be tuned by varying the ligands attached to the metal center [11, 12]. Typically, phosphorescence studies of organic fluorophores at room temperature require complete removal of oxygen although some Ru-MLCs exhibit excited-state lifetimes > 100 ns in the presence of oxygen at

room temperature [11]. Therefore these phosphorescent MLC probes can be used without exclusion of oxygen. Long excited-state lifetimes and polarized emissions make them useful probes for studying slow dynamics on membranes. $Ru^{II}(bpy)_3^{2+}$ and other similar MLCs are now extensively used to understand the nature of the charge-transfer excited state [2, 3, 13-17]. Typically these complexes contain diimine ligands such as 2,2-bipyridyl (bpy), 1,10-phenanthroline and their derivatives 4,4-dicarbxy-2,2-bipyridyl (dcbpy) and 5-amine-1,10-phenanthroline (5-amin-1,10-phen), which provides lower energy anti-bonding π^* orbitals. Other ligands such as phosphines, carbonyl and halides can also be introduced along with the diimine ligands to tune the luminescence properties (excited state lifetime, quantum yield, polarized emission), solubility and overall photo-stability of the complexes. The presence of the heavy-metal atom at the center of the complex has a significant effect on the excited states. The heavy metal facilitates excited singlet (^{1}MLCT) to excited triplet (^{3}MLCT) intersystem crossing through spin-orbit coupling [11, 18-19]. Because the transition from triplet-excited state to singlet-ground state is spin forbidden, the lifetime of emission from the ^{3}MLCT is expected to be long compared to ^{1}MLCT relaxation, which is spin allowed. However, ^{1}MLCT emission is not generally observed because the intersystem crossing greatly facilitated by the strong spin-orbit coupling, with a quantum yield close to unity. The radiative lifetime of the ^{3}MLCT state reflects the degree of singlet-triplet mixing in the excited state due to spin-orbit coupling. Because the quantum yield for intersystem crossing is essentially unity, the luminescent lifetime and overall quantum yield of these complexes, depends only on the (k_r) and non-radiative (k_{nr}) decay rates of the triplet state. The quantum yield (φ) and the

excited-state lifetime (τ) are related to the radiative rate (k_r) and non-radiative rate (k_{nr}) by the following expressions.

$$\varphi = k_r/(k_r+k_{nr}) \quad (1a)$$

$$\tau = 1/(k_r+k_{nr}) \quad (1b)$$

According to the energy gap law, k_{nr} increases exponentially as the energy gap (emission energy) decreases [20-23]. Other factors such as Jahn-Teller distortion of the excited ^{1}MLCT state also increase non-radiative decay (k_{nr}) [24-26]. Therefore, in order to obtain luminescence from MLCs, a delicate combination of the metal's and ligand's energy levels has to be established.

Because the emission of the metal-ligand complex is dominated by the MLCT transition, the MLCs behave like a single chromophoric unit, and they usually have high chemical and photochemical stabilities under physiological conditions. Highly polarized emission from some of these complexes stimulated the interest in using them as anisotropy probes for biophysical studies [9]. Luminescence anisotropy is an important observable that can serve as a useful tool to study molecular dynamics. The anisotropy is defined as the ratio of the difference between the emission intensity parallel to the polarization of the electric vector of the exciting light ($I_{\|}$) and that perpendicular to that vector ($I_{\perp}$) divided by the total intensity ($I_T = I_{\|} + 2\, I_{\perp}$),

$$r = (I_{\|} - I_{\perp})/(I_{\|} + 2I_{\perp}) \quad (2)$$

The depolarization can occur by a number of pathways. The anisotropy contains information about average angular displacement between absorption and emission transition dipoles that occurs during the lifetime of the excited state. Rotational diffusion is the most common pathway for depolarization as the direction of the emission transition

moment changes due to rotation. The anisotropy of emission (*r*) is related to the rotational correlation time (ϕ) of the fluorophore through the Perrin equation,

$$r = r_0 /(1+\tau/\phi) \quad (3)$$

where, r_0, also called the fundamental or time-zero anisotropy, is the anisotropy in the absence of any rotational diffusion and τ is the luminescence lifetime. The value of r_0 depends on the angle between the absorption and emission transition dipoles. The value of ϕ reflects the rate of rotational correlation time, which depends on the viscosity of the solvent and the size and shape of the rotating molecule. The mathematical relationship between rotational correlation and solvent viscosity can be used to obtain hydrodynamic information about size and shape of macromolecules and macromolecular complexes in solution. Luminophores covalently attached to macromolecules exhibit local rotational motion in addition to depolarization through global Brownian tumbling of the macromolecule. This results in complex anisotropy decays. Whereas the interpretation of steady-state measurements depends on a simple, assumed form (model) for the anisotropy decay, the time-resolved anisotropy measurement can be used to resolve additional information about segmental motion, global motion, size and shape of the macromolecule, and flexibility of the system [5].

From the practical point of view, for MLCs to show measurable anisotropy, the fundamental anisotropy should be at least or greater than 0.05. Anisotropy is related to the symmetry of the luminescent molecule. For example, $Ru(II)(bpy)_2(dcbpy)$ and $Ru(II)(bpy)_2(aphen)$ which contain more than one type of diimine ligand, (i.e., less symmetric) show higher fundamental anisotropies (0.26 and 0.15, respectively) than the more symmetric $[Ru(bpy)_3]^{2+}$ (0.001) [2-3,5]. Introducing electron withdrawing groups

on the diimine ligand results in red-shifted emission and an increase in anisotropy, which suggests that one ligand accepts an electron preferentially over other diimine ligands [5]. The possibility of increasing the fundamental anisotropy with a single chromophoric ligand in metal-ligand complexes was observed for Re(I) and Ru(II) complexes (e.g. $[Re(4,7\text{-}Me_2phen)(CO)_3(4\text{-}COOHPy)]PF_6$ [27] and $[Ru^{II}H(dcbpy)(PPh_3)_2(CO)]$ [11]).

MLCs containing diimine ligands with functional groups such as -COOH, and $-NH_2$ are suitable for covalent conjugation to lipids, cholesterols and proteins [5, 9]. The carboxyl or amine groups on the diimine ring need further modification to facilitate efficient covalent attachment to these bio-molecules. Most phospholipids are esters of glycerol comprising two fatty acyl residues (non-polar tails), a single phosphate ester substituent (polar head group) and an amine group. The primary amine group of a lipid, for example, phosphatidyl ethanolamine (PE), can be covalently bonded to a carboxyl group on a diimine ring via an activated ester. The MLC-lipid conjugate can then be incorporated into a lipid bilayer vesicles or biological cell membranes. Also, cholesterol is an important component of lipid membranes and is known to affect membrane fluidity. We therefore made an MLC-cholesterol conjugate and characterize its dynamics in a model lipid vesicle. Synthesis of this conjugate was accomplished via reaction of an amine-substituted diimine ligand with cholesterol chloroformate. We report here these two types of MLC-conjugates for the complexes $[HRu(CO)(PPh_3)_2(dcbpy)]PF_6$ **1** and $[(TFA)Ru(CO)(dppene)(5\text{-}amin\text{-}1,10phen)]PF_6$ **2** along with a detailed analysis of their polarized emissions on incorporation in different types of lipid vesicles.

4.2 Experimental

4.2.1 General Methods and Materials

Reactions were carried out under a nitrogen atmosphere. Purification was carried out in air by using preparative thin-layer chromatography (10x20 cm plates coated with 1 mm silica gel PF 60254-EM Science). Activated neutral alumina (150 mesh, 58 A) was also used to purify compounds by column chromatography. Reagent grade solvents were purchased from J.T. Baker. Methylene chloride (CH_2Cl_2) and acetonitrile (MeCN) were distilled from calcium hydride. Ruthenium carbonyl was purchased from Strem Chemicals. 2,2′-bipyridine, 1,10-phenantroline, 4,4′dicarboxy-2,2′-bipyridyl, 5-amine-1,10 phenanthroline and thiophosgene were purchased from Sigma-Aldrich and used as received. 1,2-dihexadecanoyl-*sn*-glycero-3-phosphoethanolamine (DPPE), 1,2-dihexadecanoyl-*sn*-glycero-3-phosphocholine (DPPC), L-α-phosphatidylcholine from chicken egg (egg-PC), cholesterol, cholesterol-chloro-formate were purchased from Avanti Inc. and used as received. The complexes $[HRu(CO)(PPh_3)_2(dcbpy)]PF_6$ **1** and $[(TFA)Ru(CO)(dppene)(5\text{-amin-}1,10\text{-phen})]PF_6$ **2** were synthesized according to the published procedures [11].

^1H NMR and $^{31}P\{^1H\}$ NMR spectra were obtained on a Varian 400 MHz Unity Plus or a Varian NMR Systems 500 MHz spectrometer. Infrared spectra were obtained on a Thermo-Nicolet 633 FT-IR spectrometer. ESI-MS spectrum was obtained on Watts/Micromass LCT using 80% MeCN as carrier solvent.

4.2.2 Luminescence spectroscopy

Steady-state UV-visible absorption spectra and emission spectra were recorded on a Molecular Device Spectra Max M2. The quantum yields (φ) for the luminescent

complexes in the presence of oxygen were calculated using equation 4, relative to a Rhodamine B standard (φ= 0.73, in ethanol) [11].

$$\varphi = \frac{\text{abs Rhodamine}}{\text{area Rhodamine}} \text{ X } \frac{\text{area Ru}}{\text{abs Ru}} \text{ X } 0.73 \qquad (4)$$

Here abs refers to the absorbance of the luminophores at the excitation wavelength and area refers to the total area under the emission spectral curve.

Time-resolved luminescence decay and anisotropy decay measurements were performed by time-correlated single-photon counting (TCSPC), using the Quantum Northwest FLASC 1000 sample chamber (Spokane, WA). In the FLASC 1000, the vertical (V or 0° to vertically polarized excitation) and horizontal (H or 90°) emission components are separated on one side of the sample cuvette, orthogonal to the excitation path, by a beam-splitting Glan-Thompson polarizer (Karl Lambrecht, Chicago, IL). This allows simultaneous detection of the V and H anisotropy decay components by separate detectors, which assures data collection under identical excitation conditions. A variable-angle polarizer, in the emission path on the opposite side of the sample cuvette, was set at the magic angle (54.7° to vertically polarized excitation) for determination of the luminescence lifetime. Pulsed excitation at 470 nm and a repetition rate of either 250 KHz or 5.0 MHz from a LDH-P-C 470 laser diode (PicoQuant, Berlin, Germany) was used for the time-dependent studies. The H and V emission components were isolated through matched bandpass filters, using 590/25 nm (Andover, Salem NH) for complex **1**, **2**, **3** and **7** or 530/25 nm (Andover, Salem NH) for complexes **4** and **6**. The V and H decay curves were collected for equal lengths of time using the TimeHarp 200 PCI board (PicoQuant, Berlin) until 4×10^4 counts were obtained at the maximum of the V curve.

The timing resolution was either 1120 ps/channel or 35 ps/channel. The luminescence intensity decays for the probes in solution were calculated by fitting the data to a single exponential decay model, where I(t) is the time dependent intensity, I_0 is intensity at time 0 and τ is the excited-state lifetime.

$$I(t)=I_0\exp(-t/\tau) \qquad (5)$$

A single exponential decay model was used in excited-state lifetime analyses for the probes in organic solvent. A multi-exponential decay model was required for fitting the lifetime data of these probes in model membrane environments.

In the time-resolved anisotropy experiment, the depolarization of the emitted light that results from molecular rotation is given by

$$r(t) = \frac{I_{VV}(t) - I_{VH}(t)}{I_{VV}(t) + 2I_{VH}(t)} = \sum_{j=1}^{5}\beta_j e^{-t/\phi_j} \qquad (6)$$

where $I_{VV}(t)$ and $I_{VH}(t)$ represent the vertical and horizontal decays, respectively, obtained using vertical excitation. The pre-exponential factors, β_j, are trigonometric functions of the angles between the excitation and emission transition dipole moments of the probe and the symmetry axes of the ellipsoid of revolution [29], and the sum of β_j is the fundamental anisotropy at zero time, r_0, when no motion has occurred. The rotational correlation times, ϕj, depend on the size and shape of the probe and also on the temperature and viscosity of the surrounding medium. The denominator of Equation 6 is the total intensity decay, $I(t)$.

$$I_{VV}(t) + 2I_{VH}(t) = I(t) = \sum_{i=1}^{n}\alpha_i e^{-t/\tau_i} \qquad (7)$$

Here, τ_i is the lifetime and α_i is the amplitude of the ith component; the magic angle decay is $I(t)$.

The anisotropy decay data were analyzed using the software package FluoFit Pro (PicoQuant, Berlin). For anisotropy analysis, the individual vertical and horizontal decays, $I_{VV}(t)$ and $I_{VH}(t)$, respectively, were fit simultaneously according to the following relationships:

$$I_{VV}(t) = G\,\frac{1}{3}\sum_{i=1}^{n}\alpha_i e^{-t/\tau_i}\left[1 + 2\left(r_\infty + \sum_{j=1}^{n}\beta_j e^{-t/\phi_j}\right)\right] \quad (8a)$$

$$I_{VH}(t) = \frac{1}{3}\sum_{i=1}^{n}\alpha_i e^{-t/\tau_i}\left[1 - \left(r_\infty + \sum_{j=1}^{n}\beta_j e^{-t/\phi_j}\right)\right] \quad (8b)$$

where r_∞ is the anisotropy at infinite time [30], and $G = \int I_{HV}dt \Big/ \int I_{HH}\,dt$ is a factor, obtained using horizontal excitation, that corrects for the difference in the efficiencies of the V and H detection channels; under ideal conditions $G \sim 1$ [31, 32].

Synthesis

4.2.3 Synthesis of $HRu(CO)(PPh_3)_2$(dcbpy-succinimide) [3]

A mixture of $[HRu(CO)(PPh_3)_2(dcbpy)]$ (**1**) (155 mg, 0.16 mol) and *N*-hydroxysuccinimide (34 mg, 0.32 mmol) was stirred in 4 mL dry MeCN (distilled from CaH_2) under N_2 at room temperature in a 10 mL round bottom flask until all the reactants dissolved. *N,N'*-dicyclohexylcarbodiimide (DCC) (103 mg, 0.48 mmol) was added to the mixture and the reaction was stirred for three hours. The solid precipitate (urea) was removed by filtering through a 0.2 μm syringe filter. The filtrate was added to stirring

iso-propanol and the mixture was kept at -4°C for complete precipitation. The orange ppt was filtered and washed three times with 2mL aliquots of dry ethyl ether. Compound $[HRu(CO)(PPh_3)_2(dcbpy\text{-}succinimide)]PF_6$ **3** was obtained in 32% yield (60 mg). IR (KBr) (υ cm^{-1}): CO stretching frequency at 1956vs, 1775m, 1742s, 1650m and CH aliphatic 2980. ^1H NMR ($CDCl_3$) δ = 9.6-7.2(m, 36H), -11.1(t, 1H), 2.8 (4H). $^{31}P\{^1H\}$ NMR ($CDCl_3$) δ = 49.2 (s, 2P), -155(m, 1).

4.2.4 Synthesis of $[HRu(CO)(PPh_3)_2(dcbpy\text{-}DPPE)_2]$ [4] (DPPE = 1,2-dihexadecanoyl-*sn*-glycero-3-phosphoethanolamine)

30 mg of DPPE (0.043 mmole) was dissolved in $CHCl_3$ and 3.5 mL of triethylamine was added to the lipid solution under N_2. The mixture was stirred for 15 min and then a solution of complex **3** (60 mg, 0.021 mmol) in 2 mL dry MeCN was added drop-wise under N_2. The reaction was stirred overnight and the solvent was then removed by rotary evaporation. The residue was purified by thin layer chromatography on silica gel. Two elutions with the solvent mixture hexane/methylene chloride/ethanol {6.5:3.5:0.5 (v/v)} yielded two bands. The baseline contained un-reacted complex **3**. The faster moving UV-absorbing band was identified as the un-reacted DPPE and the slower moving deep yellow band gave $[(CO)HRu(PPh_3)_2(dcbpy\text{-}DPPE_2)]PF_6$ **4** in 15% yield (22 mg). IR (KBr) (υ cm^{-1}): CO stretching frequency at 1956vs, 1734s, 1684vs and CH aliphatic 2963s, 2924s, 2851m. ^1H NMR ($CDCl_3$) δ = 9.5-7.0 (m, 36H), 5.2(2H), 5.1-2.2 (35H), 1.9-0.78(107H), -11.19 (broad, 1H); $^{31}P\{^1H\}$ NMR ($CDCl_3$) δ = 49.6 (s, 2P),

25.04 (2P), -155(m, 1P). ESI-MS: *m/z* 2034 [M^+- ($C_{15}H_{31}$ + PF_6)] (Calc. M^+- ($C_{15}H_{31}$ + PF_6) = 2034).

4.2.5 Synthesis of [(TFA)Ru(CO)(dppene)(1,10-phen-5-NCS] PF_6 [5]

122 mg (0.13 mmol) of [(TFA)Ru(CO)(dppene)(5-amin-1,10-phen)]PF_6 (**2**) was dissolved in 3 mL of dry acetone. Finely crushed $CaCO_3$ (45 mg, 0.45 mmol) was added to the probe solution followed by addition of thiophosgene (11 μL, 0.07 mmol) under N_2. The reaction mixture was stirred at room temperature for 1 hour and then refluxed for 2.5 hour. After cooling to room temperature, $CaCO_3$ was removed by using a 0.45μm filter and acetone was removed by rotary evaporation. Compound [(TFA)Ru(CO)(dppene)(1,10-phen-5-NCS]PF_6 **(5)** was obtained in 94% yield (50 mg). IR (KBr) (υ cm^{-1}): CO stretching frequency at 1993vs and 1691vs, N=C=S at 2102m and 2050m. ESI-MS: *m/z* 860 [M^+-PF_6] (Calc. M^+-PF6 = 860).

4.2.6 Synthesis of [(TFA)Ru(CO)(dppene)(1,10-phen-DPPE] PF_6 [6]

A solution of compound **5** (50 mg, 0.049 mmol in 3mL dry CH_2Cl_2) was added drop-wise into a stirring solution of DPPE (35 mg, 0.048 mmol in 5 mL dry CH_2Cl_2) over 1 hourr at room temperature and the reaction proceeded overnight under N_2. Solvent was removed by rotary evaporation and the residue was purified by thin-layer chromatography on silica plate. Three bands were resolved by elution with the solvent mixture, hexane/methylene chloride/ethanol {5:4:1 (v/v)}. The fastest moving UV-

absorbing band was identified as the unreacted DPPE and the second moving yellow band was too small for further characterization. The slowest moving deep yellow band yielded [(TFA)Ru(CO)(dppene)(1,10-phen-DPPE]PF_6 (**6**) in 10% yield (15 mg). IR (KBr) (υ cm^{-1}): CO stretching frequency at 1997vs, 1736vs, 1684; NH stretching at 3438 and aliphatic C-H stretching at 2940s, 2919vs, 2851s. ^{1}HNMR ($CDCl_3$) δ = 8.8-6.2(m, 29H), 5.1(1H), 4.3-3.1(9H), 2.4-0.9(63 H), $^{31}P\{^1H\}$ NMR ($CDCl_3$) δ = 71.1(s, 2P), 58 (br, 1P), -155 (m,1P). ESI-MS: *m/z* 1454 [M-(PF_6+TFA)] (Calc. M^+-(PF6+TFA) = 1453).

4.2.7 Synthesis of [(TFA)Ru(CO)(dppene)(1,10phen-Chol)] PF_6 (7)

100 mg (0.10 mmol) [(TFA)Ru(CO)(dppene)(5-amin-1,10phen)]PF_6 (**2**) was dissolved in 15 mL dry CH_2Cl_2 and 1 mL dry MeCN, and then 1 mL triethylamine was added to the deoxygenated solution. A 10 mL CH_2Cl_2 solution of cholesterol-chloroformate (chol) (45 mg, 0.10 mmol) was added to the probe solution drop-wise over 20 minutes under N_2. The reaction mixture was refluxed for 5 hours. Progress of the reaction was monitored by the disappearance of the peak at 1776 cm^{-1} in the IR spectrum, corresponding to the chloroformate, and by the appearance of a new peak at 1730 cm^{-1}. Solvent was removed by rotary evaporation. The residue was purified by thin layer chromatography on silica gel. Elution with the solvent mixture hexane/methylene chloride/methanol {1:1:1 (v/v)} yielded two bands. The [(TFA)Ru(CO)(dppene)(1,10-chol)] PF_6 (**7**) was recovered in 20% yield (30 mg) from the orange band that was moving slower on the TLC plate than the UV-absorbing un-reacted cholesterol-chloroformate. IR (KBr) (υ cm^{-1}): CO stretching frequency at 1993vs, 1730s, 1690vs, and CH aliphatic

3139w, 2950vs, 2868s. ^{1}H NMR ($CDCl_3$) δ = 8.8-6.2(m, 29H), 5.4(1H), 4(1H), 2.5-0.9(44 H); $^{31}P\{^{1}H\}$ NMR ($CDCl_3$) δ = 52.2 (s, 2P), -155(m, 1P). ES-MS (m/Z) = 1232 (M^+). ESI-MS: *m/z* 1232 [M^+-PF_6] (Calc. M^+-PF_6 = 1232).

4.2.8 Synthesis of dcbpy-$(DPPE)_2$ (8)

The succinimidal ester of 4,4'-dicarboxylic-2,2'-bipyridyl (dcbpy) was synthesized by reacting 50 mg (0.204 mmol) of dcbpy with 46 mg (0.408 mmol) of *N*-hydroxysuccinimide in the presence of *N,N'*-dicyclohexylcarbodiimide (126 mg, 0.61 mmol) for 3 hr at room temperature under N_2. Precipitate was removed by filtering on 0.45 μm filter and the filtrate was added to a large excess of stirring isopropanol. Recrystallization was completed maintaining the isopropanol solution at 4 ^{o}C. After filtering and washing with dry ethylether, 40 mg of dcbpy-N-Succinimide (dcbpy-NS) crystals were obtained in 35% yield (31 mg). 70 mg (0.10 mM) DPPE in 7 mL chloroform was added to the dimethylfomamide (DMF) solution of dcbpy-NS (20 mg, 0.05 mM) in the presence of a catalytic amount of triethylamine. The reaction proceeded for 24 hrs at room temperature under N_2. Solvent was removed by rotary evaporation and the residue was purified by thin-layer chromatography on silica plate. Two elutions with the solvent mixture hexane/ methylene chloride/ ethanol (6.5: 3.5: 0.5) yielded three bands. The fastest moving UV-absorbing band was identified as un-reacted dcbpy-NS, the second UV-absorbing band was the un-reacted DPPE and the slowest moving pale-yellow band gave dcbpy-$DPPE_2$ (**7**) in 10% yield (8 mg). IR (KBr) (υ cm^{-1}): CO

stretching frequency at 1732s, 1687s and CH aliphatic 2963s, 2924s, 2851m. ^{1}H NMR ($CDCl_3$) δ = 9.3-7.6 (6H), 4.8-2.3 (18H), 2.1-0.81 (124H).

4.2.9 Synthesis of [Ru(bpy)$_2$(1,10-phen-Chol)] [2PF$_6^-$] (9)

Complex [Ru(bpy)$_2$(5-amino-1,10-phen)][2PF$_6^-$] was prepared according to the published method [33] according to published method. 100 mg (0.11 mmol) [Ru(bpy)$_2$(5-amino-1,10-phen)][2PF$_6^-$] was dissolved in 10 mL dry CH_2Cl_2 and then 1 mL triethylamine was added to the deoxygenated solution. A 5 mL CH_2Cl_2 solution of cholesterol-chloroformate (chol) (50 mg, 0.11 mmol) was added to the probe solution drop-wise over 20 minutes under N_2. The reaction mixture was refluxed for 4 hours. Progress of the reaction was monitored by the disappearance of the peak at 1776 cm^{-1} in the IR spectrum, corresponding to the chloroformate, and by the appearance of a new peak at 1731 cm^{-1}. Solvent was removed by rotary evaporation. The residue was chromatographed by silica thin layer chromatography. Elutions with the solvent mixture hexane/methylene chloride/methanol {1:2:1 (v/v)} yielded two bands. The [Ru(bpy)$_2$(1,10 phen-Chol)] [2PF$_6^-$] (**9**) was recovered in 14 % yield (23 mg) from the orange band that was moving slower on the TLC plate than the UV-absorbing un-reacted cholesterol-chloroformate. IR (KBr) (υ cm^{-1}): CO stretching frequency at 1731s and CH aliphatic 3139w, 2950vs, 2868s. ^{1}H NMR ($CDCl_3$) δ = 8.8-6.7(24H), 5.37(1H), 3.99(1H), 2.5-0.9(43 H).

4.2.10 Vesicle preparation

A chloroform mixture of conjugated probe (**4**, **6** or **7**) and phospholipids containing a choline head group (egg-PC or dipalmitoylphosphatidylcholine) was prepared in a molar ratio of 1:99. The organic solvent was removed by using a gentle stream of argon gas for 1 hr and the lipid was further dried under vacuum overnight. Then 0.52 mL HBS buffer (20 mM HEPES, 100 mM NaCl, pH 7.5) was added to the dried lipid and the solution was maintained above the phase-transition temperature of the corresponding PC (room temperature for egg-PC and 45ºC for DPPC) to obtain a final lipid concentration of 1 mM. Addition of buffer to the lipid mixture produced cloudy suspensions. The suspensions were incubated above the phase-transition temperature for 1 hr with occasional vortexing. A freeze/thaw cycle was carried out 5 times. Clear solutions of 100-nm-diameter vesicles were prepared by extruding the suspension through a 100-nm sizing membrane [34].

4.3 Results and Discussions

4.3.1 Synthesis

Schemes 4.1 & 4.2 describe the ligand modification and conjugation of the ruthenium probes with lipids and cholesterol. For the phospholipid conjugations, we used diimine ligands containing either activated ester or highly reactive isothiocyanate functional groups. The complex **1** has emission maximum at 647 nm (excited at 470 nm), a quantum yield of 0.3, a lifetime of 720 ns (air equilibrated) in ethanol and a

fundamental anisotropy of 0.124 in glycerol at 0 ºC [11]. This complex contains a 2,2′-bipyridyl ligand with two carboxylic acid groups which for bioconjugation were converted to the activated ester groups in complex **3**. The activated ester groups were used to form peptide bonds with the primary amine of phosphatidylethanolamine (PE). Complex **4** conjugated to two di-palmitoyl-phosphatidylethanolamine (DPPE) molecules was synthesized and purified by standard chromatographic methods. Complex **5** was obtained by converting the amine group on the 5-amino-1,10-phenanthroline ligand of the complex **2** into 5-isothiocyanato-1,10 phenanthroline (NCS-phen). Complex **2** has its emission maximum at 607 nm (excited at 470 nm), a quantum yield of 0.25, and a lifetime of 230 ns (air equilibrated) in ethanol and a limiting anisotropy of 0.07 in glycerol at 0ºC [11]. Complex **6** was obtained by conjugating one molecule of DPPE with the ruthenium probe through a thiourea bond formation between NCS-phen-Ru and the primary amine group of PE lipid. Because cholesterol is an important component of biological membranes, we synthesized cholesterol conjugate of ruthenium MLCT complex **2**. The amino group of the 5-amino-1,10-phenanthroline was used to form a carboxy-amide bond in complex **7** by reacting complex **2** with the highly reactive cholesterol-chloroformate.

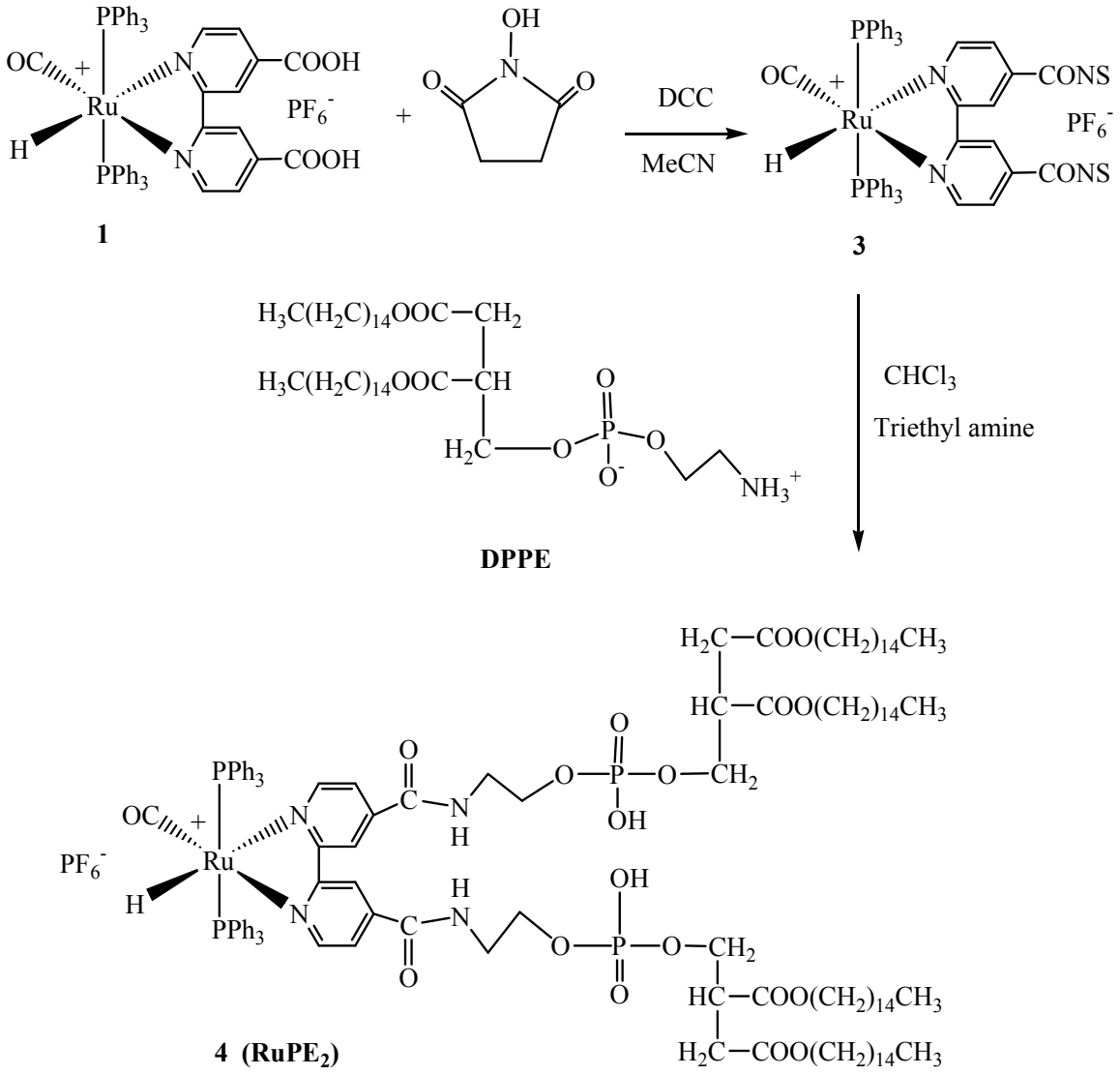

Scheme 4.1 Synthesis of complex 4.

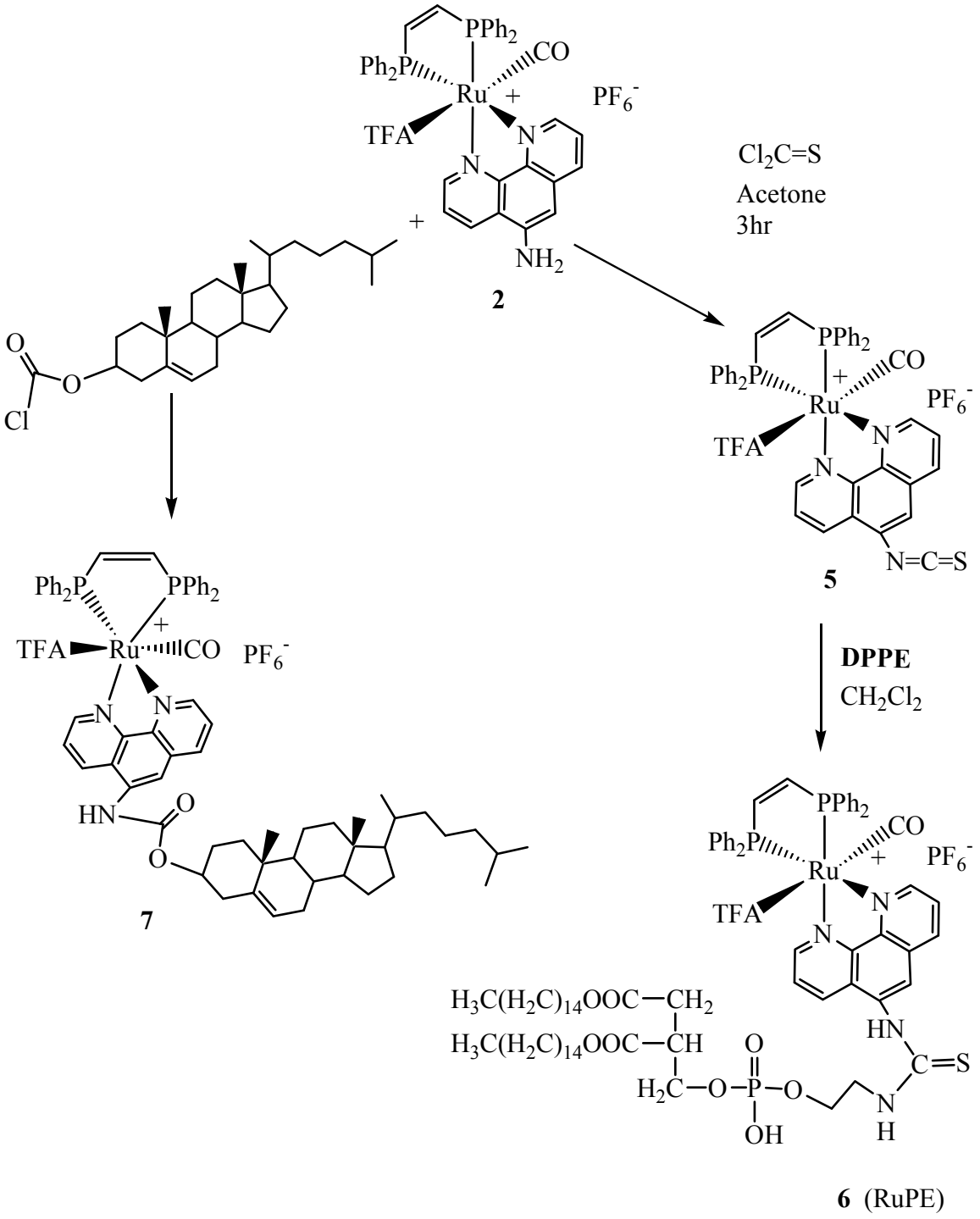

Scheme 4.2 Synthesis of complex 6 & complex 7

All the bioconjugated MLC complexes reported here contain metal-coordinated carbonyl ligands. The terminal M–CO shows CO stretching modes around 2150–1850 cm^{-1}, which are easily distinguishable from organic CO frequencies. The M–CO signals are very sensitive to the electronic properties of the other ligands present on the metal. These complexes (**1**–**7**) have only one M–CO ligand. The strong M–CO stretch appears at 1949 and 1956 cm^{-1} for the hydride complexes **1** and **3** respectively, and the TFA complexes showed strong M-CO stretch at 1990-1997 for the complex **5**, **6** and **7**. The more electron-donating hydride ligand shifts ν_{CO} to lower energy in the complexes **1, 3** and **4**. Strong absorptions in the organic carbonyl region were also observed due to the presence of activated ester group on complex **3**, for the amide functional groups in complex **4**, for the carboxy-amide functional group in complex **7** and for the glycero-ester groups of lipids in complex **4** and **6**. The strong ν_{CO} at 1690-1680 cm^{-1} was also observed due to the CF_3COO^- ligand in complex **5-7.** Moderate absorption at 2102-2050 cm^{-1} was observed in complex **5** because of the iso-thiocyanate (N=C=S) stretch. The ^1H and $^{31}P\{^1H\}$ NMR spectra of these complexes were obtained in chloroform[d]. NMR spectral analysis was an important tool for assigning the presence of the terminal hydride ligand in the complexes **3** and **4**. The M–H resonance appeared as a triplet at δ −11.07 (J = 20 Hz) for complexes **3** and a broad multiplet at -11.19 upon conjugation with lipids in complex **4**. The aromatic region of the ^1H spectra is complex due to presence of phenyl protons of phosphines ligands and the aromatic protons of diimine ligands. The CH═CH protons of diphenylphosphinoethylene are observed around δ 6.2–6.9 ppm for complex **5-7**. The conjugates showed chemical shifts in the aliphatic regions characteristic of the corresponding lipid and cholesterol. The ^1H NMR spectra is broadened for the lipid and

cholesterol conjugates (complex **4**,**6** and **7**) compared to the un-conjugated complexes (complex **1**- **3** and **5**). The chemical shift of the metal-bound phosphines ligands in ^{31}P NMR spectra are in good agreement with similar Ru(II)phosphine complexes (11). Complexes **2**-**4**, and **7** show singlet resonances at 49.6–52 ppm relative to external H_3PO_4, which is due to the triphenyl and diphenylphosphinoethylene ligands. The singlet observed for these complexes (**2**, **3** and **7**) indicated that these complexes have a symmetry component that makes the two phosphorous nuclei magnetically equivalent. The multiplet observed at 25.04 ppm (2p) was due to the covalent conjugation of phospholipids in complex **4**. The down-field shift might result from the interaction of the phospholipids with the Ru^{2+} metal center of the complex. Signals at 73 ppm (br, 2P) and 54 ppm (br, 1P) were observed in ^{31}P NMR spectra of complex **6**. The shifts observed in this complex could also be a result of the phospholipid's interaction with the metal center. The counter anion [PF_6] appeared as a septet at −155 ppm in all the ^{31}P NMR with an integrated relative intensity of 1:2 when compared with the phosphine ligand resonances.

4.3.2 Photophysical characterization of complex 3-7

Table 4.1 lists the absorption and emission maxima and the intensity-averaged excited-state lifetimes for the membrane probes. The intense higher energy absorption at 270-295 nm observed for these complexes is due to the spin-allowed intra-ligand (π-π^*) transitions. The absorption at 365 nm observed for complexes **2**, **6** and **7** is due to the presence of the double bond in the chelating phosphine ligand in these complexes. The less intense absorption bands ($\varepsilon_{450} \sim 2 \times 10^3$ $M^{-1}cm^{-1}$) of all probes and their conjugates in

the visible region (410-490nm) are attributed to spin-allowed metal-to-ligand charge transfer ^{1}MLCT (d - π^*) transitions. The ^{1}MLCT absorption bands of the complexes containing dcbpy and the activated ester of dcbpy, **1** and **3,** were at slightly lower energy than the lipid derivative (complex **3**) (Figure 4.1).

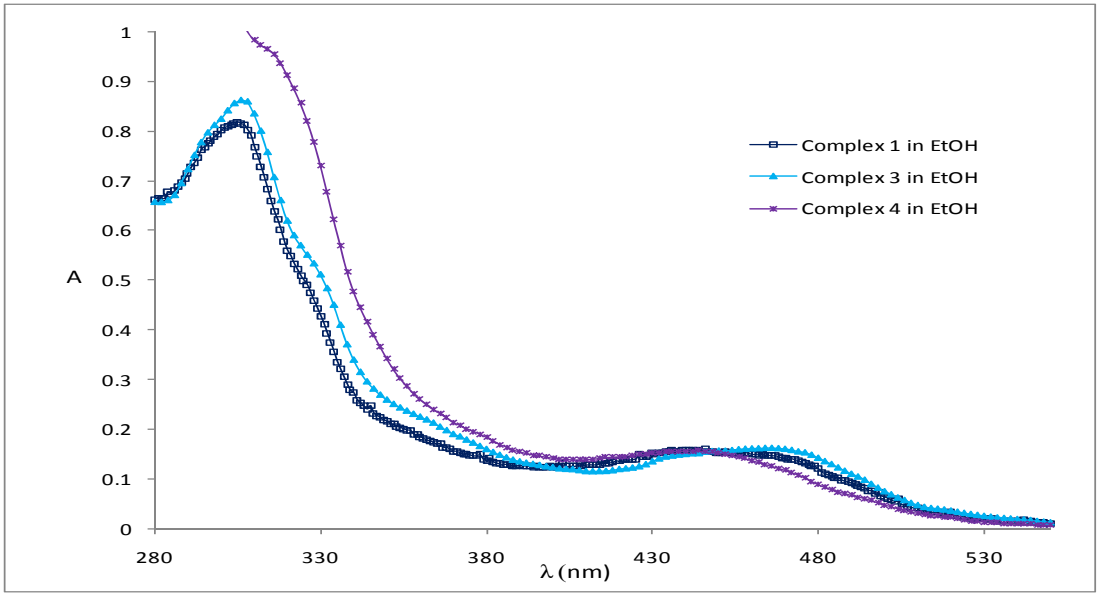

Figure 4.1: Absorption spectra of complex [HRu(CO)(PPh$_3$)$_2$(dcbpy)] (1), [HRu(CO)(PPh$_3$)$_2$(dcbpy-succinimide)]PF$_6$ (3) and [(CO)HRu(PPh$_3$)$_2$(dcbpy-DPPE$_2$)]PF$_6$ (4) in ethanol

All the complexes containing chelating phosphine and the phenanthroline ligands displayed ^{1}MLCT absorption bands at similar wavelengths (Figure 4.2). Complexes **1, 3, 4** and **7** displayed long-lived orange-red luminescence in solutions under ambient conditions (Figure 4.3). These emissions are characteristic of a ^{3}MLCT excited state.

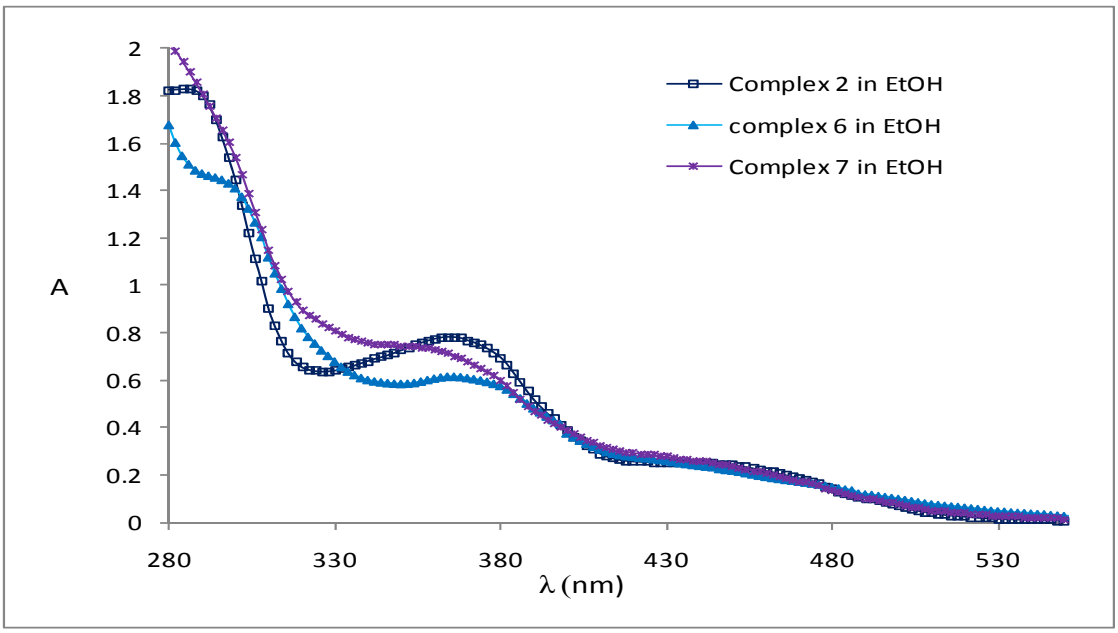

Figure 4.2: Absorption spectra of complex [(TFA)Ru(CO)(dppene)(5-amonio-1,10 phen)] PF_6 (2), [(TFA)Ru(CO)(dppene)(1,10 phen-DPPE] PF_6 (6) and [(TFA)Ru(CO)(dppene)(1,10 phen-Chol)] PF_6 (7) in ethanol.

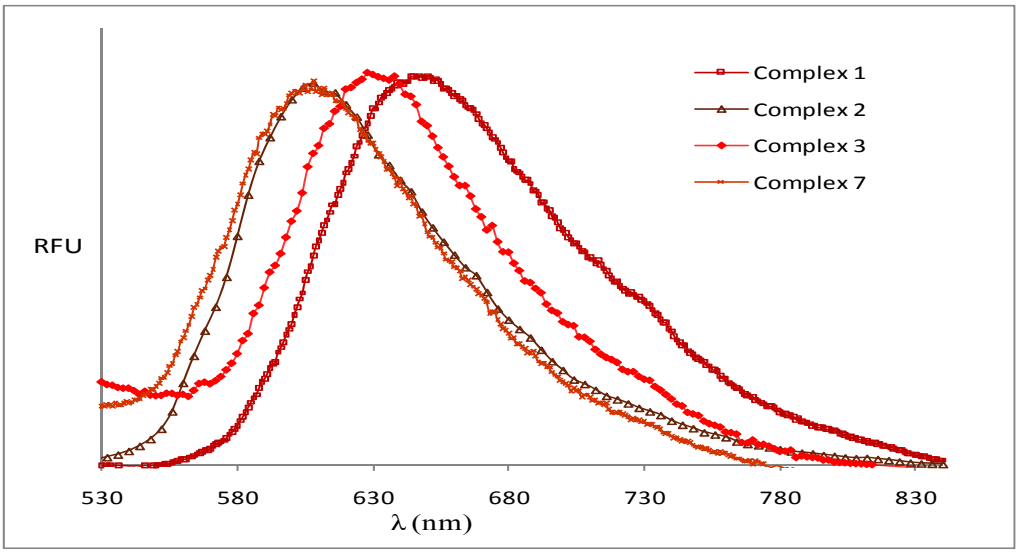

Figure 4.3: Emission spectra of complex [$HRu(CO)(PPh_3)_2$(dcbpy)] (1), [(TFA)Ru(CO)(dppene)(5-amonio-1,10 phen)] PF_6 (2) [$HRu(CO)(PPh_3)_2$(dcbpy-succinimide)] PF_6 (3) and [(TFA)Ru(CO)(dppene)(1,10 phen-Chol)] PF_6 (7) in ethanol.

The conjugation with cholesterol resulted in a two-fold increase of excited-state lifetime, which was observed from the time-resolved intensity decay of complex **7**. No emission was observed from complex **4** and a very weak emission at 618 nm was observed from complex **6**. The emission was too weak for accurate lifetime measurements. Complex **4** and **6** are the lipid conjugates of probes **1** and **2**, respectively. The limiting anisotropy (r_0) reflects the angle between the absorption and emission transition dipole moments. Because high viscosity reduces rotational freedom, glycerol was used as the solvent to measure fundamental anisotropy for the probes. The time-resolved anisotropy decay study of complexes **1**, **2** and **7** in neat glycerol at 0 ^{0}C had r_0 values 0.124, 0.077 and 0.121 respectively. These values are higher than the value (<0.01) observed for $Ru(bpy)_3^{2+}$ [5]. Lipid conjugates (complexes **4** and **6**), had very weak emission and the polarization was not measured.

Table 4.1 Absorption, emission, and excited-state lifetimes of ruthenium MLC probes in ethanol.

Compound	$\lambda_{Absorption}$ (nm)	λ_{em} (nm)	$\langle\tau\rangle$ (ns)
1 [$HRu(PPh_3)_2(CO)$ (4,4'dicarboxybpy)]PF_6	303, 468	647	720
2 [(TFA)Ru(CO) (dppene)(5-amino-1,10 phen)] PF_6	289, 364, 442	610	250
4 [$HRu(PPh_3)_2(CO)$(bpy-$DPPE_2$)]PF_6	316, 442	----	----
6 [(TFA)Ru(CO)(dppene)(1,10 phen-DPPE)] PF_6	289, 366, 440	618 (very weak)	----
7 [(TFA)Ru (CO)(dppene)(1,10 phen-chol)] PF_6	356, 440	605	470

4.3.3 Photophysical studies of complex 4, 6 and 7 incorporated in lipid membrane Bilayers

The lipid conjugates **4**, **6** and the cholesterol conjugate **7** were incorporated in model membrane bilayers to study the photophysical properties of these probes in a membrane-like environment. The motion of these probes incorporated in the model membrane systems (100-nm diameter liposomes) was determined by analyzing the anisotropy decay of the polarized emission. The maximum of the low-energy absorption band near 442 nm is the characteristic metal-to-ligand charge transfer transition of a Ru-bpy MLC. No emission was observed from the lipid (phosphatidylcholine, PC) vesicles in the absence of ruthenium probes. Although the absorption spectrum for complex **4** was identical in $CHCl_3$, ethanol and lipid vesicles (Figure 4.4), emission was only observed when the probe was incorporated in the lipid vesicle.

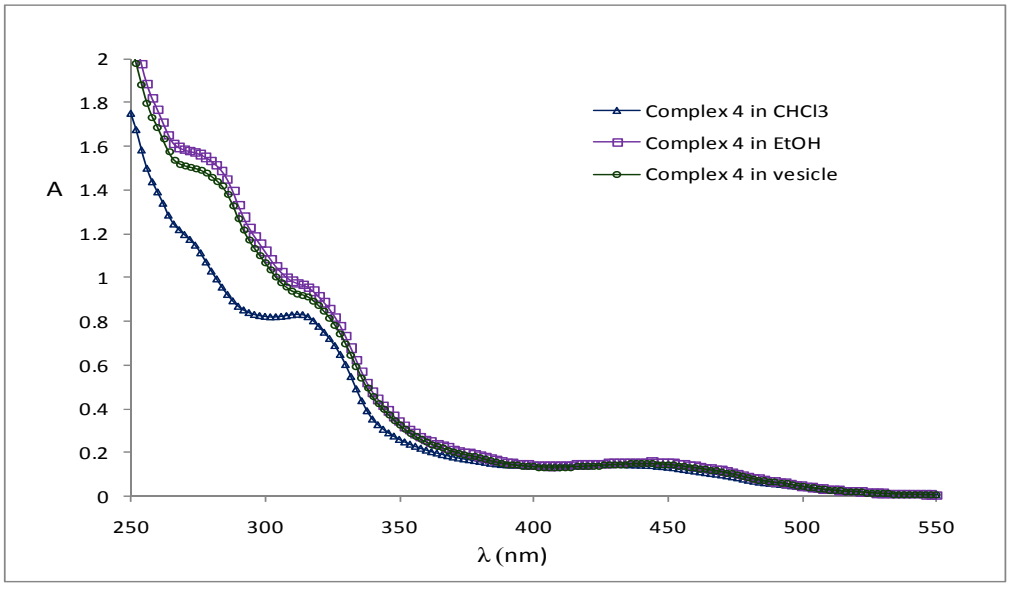

Figure 4.4: Absorption spectra of complex $[(CO)HRu(PPh_3)_2(dcbpy\text{-}DPPE_2)]PF_6$ (4) in chloroform, ethanol and egg-PC vesicles

The emission spectrum of bis-lipid-Ru complex **4** in the model membrane-like environment was blue-shifted (λ_{max} = 534 nm) with respect to the precursor probe (λ_{max} = 628 nm in chloroform). This complex also exhibited a very short excited-state lifetime (11 ns at 5ºC, air equilibriated) in PC vesicles. The mono-lipid conjugate complex **6** showed weak emission at 618 nm in chloroform solution. Like the bis-lipid conjugate **4**, this complex in PC vesicles also had a blue-shifted emission (545 nm) with a short lifetime (8 ns). Both complexes showed more intense emission in vesicles compared to the red-shifted emission of the unconjugated precursor probes (**1**, **2**) in chloroform solution. The emission of the bis-lipid-Ru complex **4** was brighter than the mono-lipid-Ru conjugate **6** (Figure 4.5).

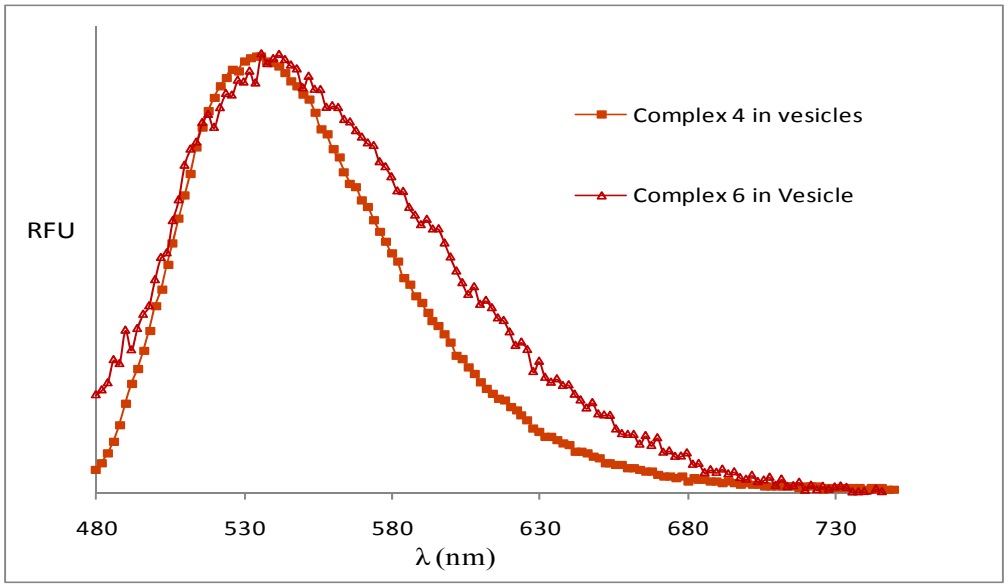

Figure 4.5: Peak normalized emission spectra of complex [(CO)HRu(PPh$_3$)$_2$(dcbpy-DPPE$_2$)]PF$_6$ (4), and [(TFA)Ru(CO)(dppene)(1,10 phen-DPPE]PF$_6$ (6) in egg-PC vesicles

A progressive decrease in luminescence intensity with increasing temperature was observed over the range of temperature 5 to 50 ºC. We also studied the change in excited-state lifetime and the anisotropy decay for the complexes **4** and **6** incorporated in PC vesicles over a range of temperatures to determine the sensitivity of these probes toward changes in the micro-viscosity of the bilayer environment. The excited-state lifetime decreased progressively with increasing temperature, consistent with the decrease in luminescence as expected for thermally activated motions. An increase in the probes local motions was also observed with increasing temperature. Lipid-conjugated probes (**4** and **6)** showed high fundamental anisotropy values (r_0 = 0.24 and 0.35 respectively) in vesicles compared to complex **1**, **2** and **7** in glycerol. The results of analyses of the time-resolved anisotropy data in terms of a double exponential decay for complexes **4** and **6** at variable temperature are summarized in Table 4.2. The anisotropy decay analysis revealed a significant contribution from the limiting anisotropy (r_∞) at lower temperatures. Restricted motions of the probe in the membrane are suggested by the r_∞ values recovered in these analyses. The probes were incorporated in natural egg-PC liposomes, which has a phase transition temperature (T_m) below 0 ºC (T_m = -9 ºC). Therefore, it was not possible to study the change in rotational correlation time at or below the phase-transition temperature. The rotational correlation times observed for complexes **4** and **6** above the phase-transition temperature are probably due to the local motion of the probes in the lipid environment. The corresponding correlation time decreases progressively with increasing temperature as expected for a probe undergoing thermal motion.

Table 4.2 Average lifetime, limiting anisotropy and rotational correlation times for complex 4 and 6 at a range of temperature in egg-PC vesicles (100 nm).

Compound	Temperatre (ºC)	$<\tau>^a$ (ns)	r_∞	ϕ_1 (ns)	ϕ_2 (ns)	χ^2
	5	11	0.09	10.8	2.6	1.18
	10	9.4	0.08	7.9	1.95	1.10
4	20	7.9	0.05	5.5	1.2	1.13
	30	6.7	0.04	3.23	0.97	1.19
	40	5.5	0.02	1.97	0.6	1.15
	50	4.5	0.013	1.4	0.2	1.14
	5	---	---	---	---	---
	10	7.4	0.07	7.6	0.7	1.1
6	20	6.3	0.05	5.2	0.6	0.99
	30	5.3	0.03	3.5	0.6	1.08
	40	4.3	0.02	1.7	0.5	1.0
	50	3.1	0.01	1.1	0.1	1.1

[a.] Intensity average lifetime

The cholesterol probe **7** showed an increase in excited-state lifetime and fundamental anisotropy in PC vesicles. Egg-PC has a low phase-transition temperature (-9 ºC) because it contains mixed saturated and unsaturated acyl chains of different lengths. Therefore, the lipids of egg-PC vesicles were in disordered phase during the photophysical studies.

To understand the effect of a more ordered membrane, we measured the photophysical properties of **7** incorporated in 1,2-dipalmitoyl-*sn*-glycero-3-phosphatidylcholine (DPPC) vesicles, which has 15–carbon saturated acyl chains. The

phase-transition temperature for DPPC is 41ºC, hence the lipids remain in ordered phase below this temperature. The absorption and emission spectra of complex **7** incorporated in the egg-PC vesicle are shown in Figure 4.6. Although the emission maximum of complex **7** is identical in ethanol solution and in PC vesicles, the excited-state lifetime increased from 470 ns in ethanol to 886 ns in vesicles at 25 ºC (air equilibrated).

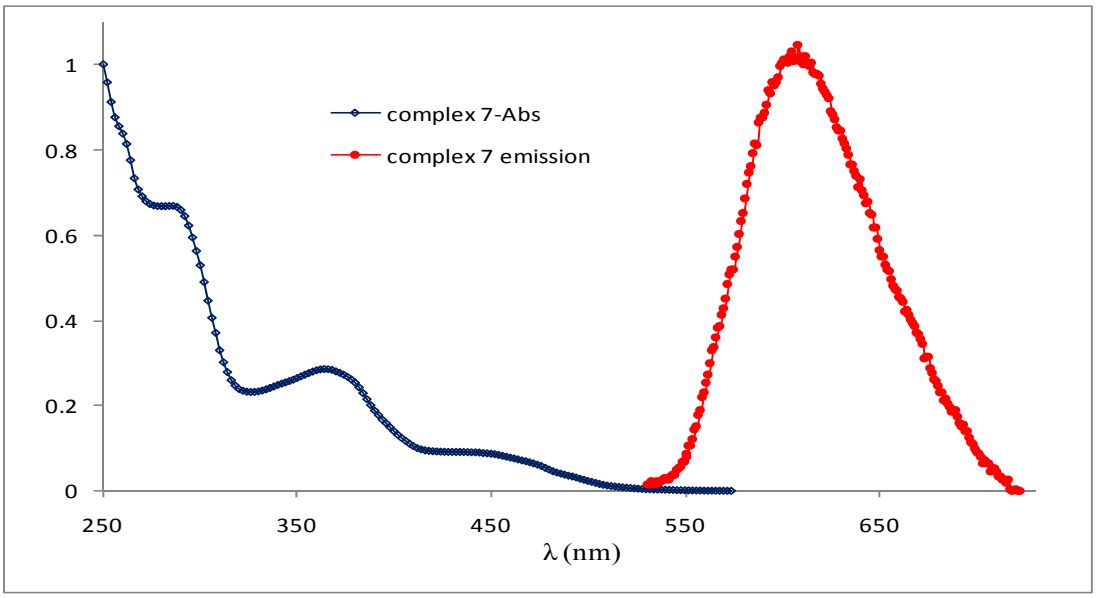

Figure 4.6 Absorption and emission spectra of complex [(TFA)Ru(CO)(dppene) (1,10-phen-Chol)] PF_6 (7) in vesicles

A fundamental anisotropy value ~ 0.1 was recovered from analysis of the time-dependent anisotropy decay of complex **7** incorporated in egg-PC and DPPC vesicles. The long excited-state lifetime and the anisotropy value for complex **7** are adequate for studying "slow" dynamics in a membrane environment. The time-resolved intensity decay of complex **7** was analyzed using a single exponential decay law. The decay time of complex **7** ranges from 1099 ns at 10 ºC to 428 ns at 50 ºC in the DPPC vesicles. This

temperature range spans the phase-transition temperature of DPPC (41ºC). In the egg-PC vesicles the lifetime is 956 ns at 10 ºC and 448 ns at 50 ºC (Figure 4.7). The excited-state lifetime of complex **7** incorporated in DPPC vesicles was longer at low temperatures than when incorporated in egg-PC vesicles. A progressive decrease in lifetime with increasing temperature was observed for both kinds of vesicles from 10 ºC to 30 ºC; a more rapid decrease was observed from 35ºC to 45ºC for DPPC vesicles. These long decay times suggest that these probes can be used to measure rotational motions in membranes as long as 3 μs (three times the mean decay time) [4].

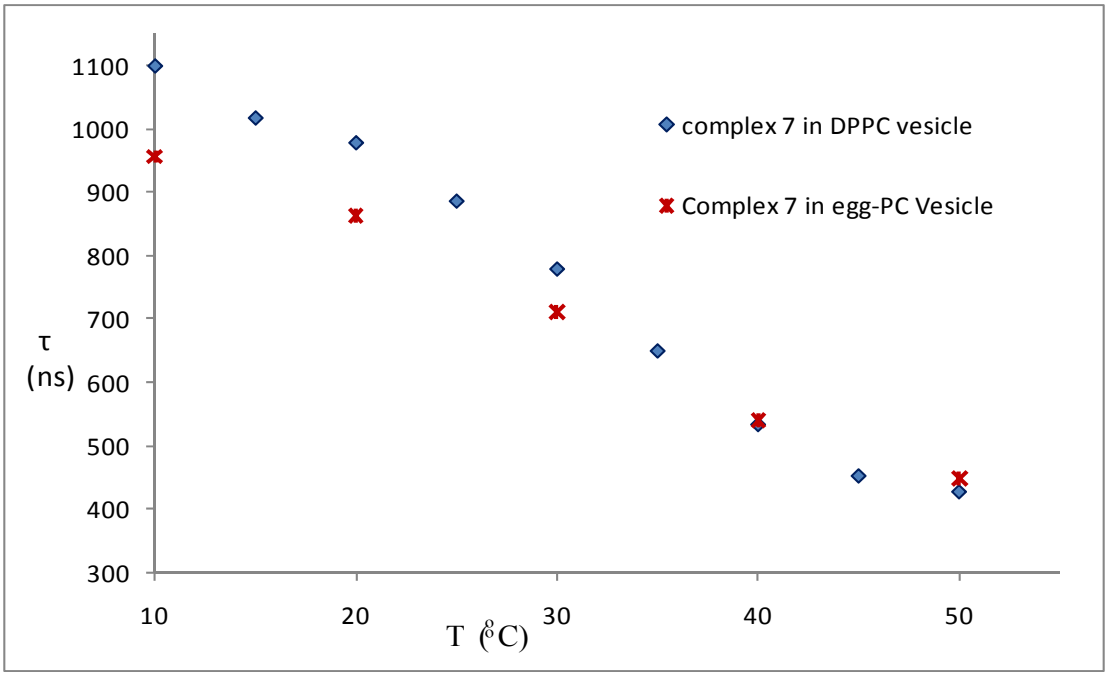

Figure 4.7 Average lifetime of complex [(TFA)Ru(CO)(dppene)(1,10-phen-Chol)] PF_6 (7) in vesicles over a range of temperatures

The rotational motions of complex **7** in egg-PC vesicles were also analyzed over a range of temperatures. The rotational correlation time decreased from 112 ns to 14 ns as

the temperature increased from 10 ºC to 50 ºC (Table 4.3). The recovered rotational correlation times were not due to the overall rotation of the liposomes of 100-nm diameter. The global rotational correlation time of vesicles with diameter of 100 nm would be much slower (ϕ ~ sub-millisecond). There is considerable uncertainty in measuring longer correlation times of the prepared vesicles because of the difficulty of measuring a correlation time above 3 μs with a probe of 1 μs lifetime. Considering its luminescence lifetime, probe **7** would be more appropriate for studying the overall rotational motion corresponding vesicles of size less than 25-nm diameter, which would be in the sub-μs range. The time-dependent anisotropy decays at variable temperature were analyzed using a single correlation time and a non zero baseline limiting anisotropy (r_∞), reflecting restricted motion of the probe during the lifetime of the excited-state [35-37].

Table 4.3 Average lifetime, limiting anisotropy and rotational correlation times for complex 7 at a range of temperature in egg-PC vesicles (100 nm)

Compound	Temperatre (ºC)	$<\tau>^a$ (ns)	r_∞	ϕ (ns)	χ^2
7 in egg-PC vesicles	10	956	0.031	112	1.06
	20	862	0.030	75	1.02
	30	710	0.019	40	1.08
	40	540	0.013	19	1.08
	50	448	0.009	14	1.18

[a.] Intensity average lifetime

To determine whether having only one diimine ligand in complex **7** has any significant effect on or advantage for the photophysical properties of this complex in membrane-like environment, we synthesized a cholesterol derivative of $[Ru(bpy)_2(5\text{-aminophen})]^{2+}$ $[2PF_6^-]$ (**9**), that contains three diimine ligands. The cholesterol conjugated $[Ru(bpy)_2(5\text{-amino-1,10 phen})]$ had an MLCT absorption and emission maximum similar to complex **7** and a similar average lifetime of 610 ns at 20ºC when incorporated in egg-PC vesicles. This complex showed $r_o = 0.023$ in 100 nm diameter egg-PC vesicle at 10ºC. This suggests that having only one diimine in [(TFA)Ru(CO)(dppene)(5-aminphen-Chol)] (**7**) results in a substantially higher fundamental anisotropy ($r_o = 0.098$).

4.3.4 Discussion

The ruthenium MLC probes reported in this paper synthesized with only one diimine ligand, showed long excited-state lifetimes and fundamental anisotropies sufficient to study sub-microsecond dynamics. It is of interest that the lipid conjugates showed almost no emission in alcohol/chloroform solution but showed bright blue-shifted emission in the PC vesicles. They also have short excited-state lifetime and high fundamental anisotropy (Table 4.2). These photophysical properties observed for complexes **4** and **6** in lipid vesicles are characteristics of a singlet emission. It might be possible that the emission of these complexes is from a singlet excited-state.

We synthesized a bis-lipid derivative of the 4,4′dicarboxy-2,2′bipyridyl (dcbpy) and studied the photophysical behavior of this compound in egg-PC vesicles. This lipid conjugate, lacking the metal center, showed a less intense absorption band at 327 nm

along with the intense absorption band at 295 characteristic of the un-conjugated dcbpy ligand. Further, the emission maximum was at 405 nm when excited at 327 nm. Finally, a complex time-dependent intensity decay was observed with a 4.9 ns intensity averaged lifetime for the dcbpy-PE_2 complex in 100-nm-diameter PC vesicles. In another experiment, we prepared the PC-vesicle without any probe incorporated. As expected, the PC vesicle showed no emission when excited at 327 or 450 nm. These vesicles were then incubated at 35ºC with complex **4** in THF solution (THF was less than 5% by final volume) to adsorb the probe on the vesicles. The emission spectrum of the bis-lipid-conjugate adsorbed into preformed vesicles gave an emission at 620 nm but when it was extruded through the sizing membrane a blue-shifted emission was observed again with a maximum at 530 nm. These results indicate that the blue-shifted emission and short excited-state lifetime observed for complex **4** is not due to decomposition of the complex to a free bpy-PE moiety. This conclusion is also supported by the observation that the MLCT absorption of complex **4** is the same in alcohol solution and in PC-vesicles.

Complex **4** contains two very hydrophobic and bulky phosphine ligands and also a hydrophobic carbonyl ligand. Therefore, unlike the derivatives of hydrophilic $[Ru(bpy)_3]^{2+}$, which are assumed to be situated at the lipid water interface [4], there is a possibility of the hydrophobic groups being situated deeper inside the hydrophobic interior of the bilayer and not exposed to the water interface. Another possible explanation could be a mixing of LC and MLCT excited states in the lipid conjugates. The short lifetime of probes **5** and **6** observed may be the result of large distortions in the excited state which can lead to increases in the non-radiative decay and a shortening of the observed lifetime [23]. In addition, if the singlet MLCT state is close in energy to the

singlet intra-ligand state there can be energy transfer between Ru dπ-π* and π-π* states [24]. Accompanying the short excited-state lifetime (11ns and 8 ns), the lipid conjugates have high fundamental anisotropy and temperature sensitive rotational correlation times, which are helpful for studying faster, local motions (up to 33 ns) in the vesicles. Interestingly, complexes **4** and **6**, which have two and one lipid conjugates respectively, showed almost the same longer rotational correlation times (7-8 ns at 10 ºC, Table 4.2) in egg-PC vesicles [37]. This timescale and its insensitivity to the number of lipid anchors suggests that this motion could reflect restricted diffusion, commonly referred as 'wobble in a cone' [34-37], and not be due to axial rotation. The axial rotation involves rotation of the entire lipid about its long axis. 'Wobble in a cone' can be described as the restricted diffusive reorientation of the lipid long axis with respect to the bilayer normal [35, 38].

Kinosita et al. [36-37], have developed two ways for analyzing fluorescence anisotropy decay data to model restricted diffusion of lipid probes in membranes. In one, a fluorophore wobbles uniformly within a cone (square-well potential). In the other, the probe rotational distribution is Gaussian. The wobbling-cone model provides a simple but useful way to assess the impact of interactions of the lipid probe with the neighboring lipids. In the wobbling-cone model, it is assumed that the major axis of the probe wobbles uniformly within a cone of semiangle θ_c (i.e., probe's major axis is confined within a cone of angle θ_c). The angle θ_c with respect to the symmetry axis of the cone can be estimated using the following relationship

$$r_\infty / r_0 = [1/2 \cos \theta_c (1 + \cos \theta_c)]^2 \qquad (9)$$

The motion of the lipid probes in egg-PC vesicles were analyzed using this model. The cone angle θ_c varied from 44–72º for complex **4** and from 55–74º for complex **6** over the

temperature range from 10–50 ºC. The shorter correlation times are significantly different for complex **4** and **6** being 1.9 and 0.7 ns, respectively. This timescale and dependence on the numbers of anchoring lipids indicate that these shorter rotational correlation times are due to the axial motion of the lipid incorporated in the vesicle [38]. Thus, these probes could be useful for studying the lipid head-group motions.

To our knowledge, the cholesterol-conjugated probe is the first example of a cholesterol-labeled MLC membrane probe. The long excited-state lifetime and high anisotropy values observed for probe **7** in glycerol and PC-vesicles make this probe a good candidate for studying membrane dynamics on the microsecond timescale. The temperature dependent changes in lifetime and rotational diffusion times observed for this probe in egg-PC and DPPC liposomes show that this probe is sensitive to changes in micro-viscosity in model-membrane systems. The vesicles we reported in this article were prepared by extruding the lipid suspension through 100-nm diameter membrane. Therefore, it was not possible to study the global rotational motion (sub-ms) of the vesicles with this probe. Because of the sensitivity of this probe to membrane environment, this probe could be useful for studying the changes in rotational correlation time within a membrane as a function of cholesterol composition and temperature. For example, cholesterol is an important membrane component in formation of lipid rafts. It should be possible to study the formation of lipid rafts using this probe at different compositions of lipid and probe-free cholesterol [39]. We tried using a 30-nm-diameter sizing membrane to make smaller DPPC vesicles, but the vesicle yield was very low, and most of the lipid suspension was adsorbed on the sizing membrane.

4.4 Conclusion

Three MLC probes have been designed and synthesized as luminescent membrane probes. Steady-state and time-dependent photophysical properties of these probes were studied in solution and in a model membrane environment. Despite their short luminescent lifetimes in liposomes, the lipid conjugates **4** and **6** showed sensitivity to changes in membrane viscosity. Complex **2**, which is the precursor of complex **6** and **7**, could also be conjugated with thiols by converting the amine group on the phenanthroline ring into an iodo-acetamide, making a probe useful for specific labeling of sulfhydryl groups on the proteins. Designing these probes included incorporation of phosphine ligands, which improved their quantum yields. The phosphine ligands used to synthesize these probes could be replaced by bio-conjugable phosphine ligands (diphenyl-phosphino-benzoic acid or diphenyl-phosphino-propionic acid). Conjugation with lipids through the phosphine ligands could reduce the distortion of the excited state of the bipyridyl ligand and result in different photophysical properties. This work is being continued in our laboratories.

The cholesterol conjugate incorporated in phosphotidylcholine liposomes had lifetime and anisotropy decays that were sensitive to temperature-dependent motions in vesicles. Studies of cholesterol conjugated [$Ru(bpy)_2$(5-aminophen)] revealed that having only one diimine as in complex **7** resulted in a higher anisotropy value. In summary, the MLC-cholesterol probe complex **7** has advantages of a broad absorption band (410-500 nm), which allows excitation over a broad range of wavelengths and a red-shifted

emission (> 600 nm) with a long lifetime (470 ns) and high anisotropy (0.098), enabling studies of membrane dynamics in the μs time range.

Reference

1. H. Szmacinski, E. Terpetschnig, and J. R. Lakowicz, *Biophys Chem,* **62** (1996), p.109.
2. L. Li, H. Szmacinski, and J. R. Lakowicz, *Anal Biochem,* **244** (1997), p.80.
3. L. Li, H. Szmacinski, and J. R. Lakowicz, *Biospectroscopy,* **3** (1997), p.155.
4. L. Li, H. Szmacinski, and J. R. Lakowicz, *Anal. Biochem.* **247** (1997), p.465.
5. J. R. Lakowicz, *Principles of Fluorescence Spectroscopy*, 3rd ed. (2006) Springer, New York.
6. V. Dadak, J. M. Vanderkooi, and W. W. Wright, *Biochim Biophys Acta,* **1100** (1992), p.33.
7. M. Bartholdi, F. J. Barrantes, and T. M. Jovin, *Eur J Biochem,* **120** (1981), p.389.
8. A. Che, and R. J. Cherry, *Biophys J,* **68** (1995), p.1881.
9. G. Piszczek, *Biochem. Biophys.,* **453**(2006), p.54.
10. Y. Chi, and P.-T. Chou, *Chem. Soc. Rev.,* **36** (2007), p.1421.
11. A. Sharmin, R. C. Darlington, K. I. Hardcastle, M. Ravera, E. Rosenberg, and J. B. A. Ross, *J. of Organomet. chem*., **694** (2009), p.988.
12. E. M. Kober, B. P. Sullivan, W. J. Dressick, J. V. Caspar and T. J. Meyer, *J. Am. Chem. Soc.,* **102** (1980), p.7383.
13. P. Chen, and T. J. Meyer, *Chem. Rev.,* **98** (1998), p.1439.
14. B-Z. Shan, Q. Zhao, N. Goswami, D. M. Eichorn, and D. P. Rillema, *Coord. Chem. Rev.,* **211**(2001), p.117.
15. D. J. Stufkens, and Jr. A. Vleek, *Coord. Chem. Rev.,* **177** (1998), p.127.

16. E. Terpetschnig, H. Szmacinski, H. Malak, and Lakowicz, J. R., *Biophys. J.,* **68** (1995), p.342.

17. X. Guo, L. Li, F. N. Castellano, H. Szmacinski, and J. R. Lakowicz, *Anal. Biochem.,* **254** (1997), p.179.

18. E. M. Kober, and T. J. Meyer, *Inorg. Chem.,* **22** (1983), p.1614.

19. E. M. Kober, and T. J. Meyer, *Inorg. Chem.,* **23** (1984), p. 3877.

20. J. V. Casper, and T. J. Meyer, *J. Phys. Chem.,* **87** (1983), p.952.

21. K. F. Freed, *Acc. Chem. Res.,* **11** (1978), p. 74.

22. E. M. Kober, J. L. Marshall, W. J. Dressick, B. P. Sullivan, J. V. Casper and T. J. Meyer, *Inorg. Chem.,* **24** (1985), p. 2755.

23. E. M. Kober, J. V. Casper, R. S. Lumpkin, and Meyer, T. J., *J. Phys. Chem.,* **90** (1986), p.3722.

24. S. Boyde, G. F. Strouse, W. E. Jones, and T. J. Meyer, *J. Am. Chem. Soc.,* **112** (1990), p.7395.

25. G. C. Balaz, A. Gurezo, and R. H. Schmehl, *Photochem. Photobiol. Scii.,* **4** (2005), p.89.

26. J. A. Treadway, B. Loeb, R. Lopez, P. A. Anderson, F. R. Keene, and T. J. Meyer, *Inorg. chem.,* **35** (1996), p.2242.

27. L. Li, F. N. Castellano, I. Gryczynski, and J. R. Lakowicz, *Chem. and phys. of lipids,* **99** (1999), p.1.

28. C. A. Parker, Photoluminescence of Solutions with Applications to Photochemistry and Analytical Chemistry, (1968), Elsevier, Amsterdam, p.262.

29. M. D. Barkley, A. A. Kowalczyk, and L. Brand, *J. Chem. Phys.* **75** (1981), p.3581.

30. R. E. Dale, L. A. Chen, and L. Brand, *J. Biol. Chem.*, **252** (1981), p.7500.

31. M. G. Badea, and L. Brand, *Methods Enzymol.,* **61** (1979), p.378.

32. Paoletti and Le Pecq, J. B. *Anal. Biochem.,* **31** (1969), p.33.

33. Youn, H. J., Terpetschnig, E., Szmacinski, H., and Lakowicz, J. R., *Anal. Biochem.* **232** (1995), p.24.

34. Preparing Large, Unilamellar Vesicles by Extrusion http://avantilipids.com/index.

35. K. Jr. Kinosita, S. Kawato and A. Ikegami, *Biophys. J.,* **20** (1977), p.289.

36. K. Jr. Kinosita, A. Ikegami and S. Kawato, *Biophys. J.,* **37** (1982), p.461.

37. A. S. Minazzo, R. C. Darlington, and J. B. A. Ross, *Biophysical Journal,* **96(2)** (2009), p.681.

38. J. B. Klauda, M. F. Roberts, A. G. Redfield, B. R. Brooks and R. W. Pastor, *Biophys. J.,* **94** (2008), p.3074.

39. A. Gidwani, D. Holowka B. Baird, *Biochemistry,* **40** (2001), p.12422.

CHAPTER 5: FUTURE DIRECTIONS

5.1.1 Covalent conjugation of luminescent Ru-MLC probes through a phosphine ligand

In Chapter 3, we discussed efficient phosphine substitution of complex $[Ru(CO)_3(TFA)_3]^-K^+$ under moderate reaction conditions. The phosphine ligands used to synthesize these probes could be replaced by bio-conjugable phosphine ligands (diphenyl-phosphino-benzoic acid or diphenyl-phosphino-propionic acid). We expect that conjugation with lipids through the phosphine ligand would reduce the distortion of the excited state of the bipyridyl ligand and thus result in different photophysical properties. We have synthesized an Ru-MLC containing a bioconjugable phosphine (the succinimidal ester of diphenyl-phosphino-propionic acid) (Scheme 5.1) and have studied its photophysical properties.

The three strong absorption bands in the M-CO stretching region and two signals in the ^{31}P {H} NMR observed for complex $[Ru(PPh_2C_2H_4CONS)_2(CO)_2(TFA)_2]$ **1** together indicate the presence of two isomers. Reaction of complex **1** with 2,2′-bipyridyl in refluxing THF gave the complex $[Ru(PPh_2C_2H_4CONS)($ 2,2′-bipy$)(CO)(TFA)][PF_6]$ (**2**). The single strong absorption bands in the M-CO stretching region and a sharp singlet signal in the ^{31}P {H} NMR together indicate a single complex with two phosphines *trans* to each other. No evidence of hydride formation was fond in the ^1H NMR spectrum.

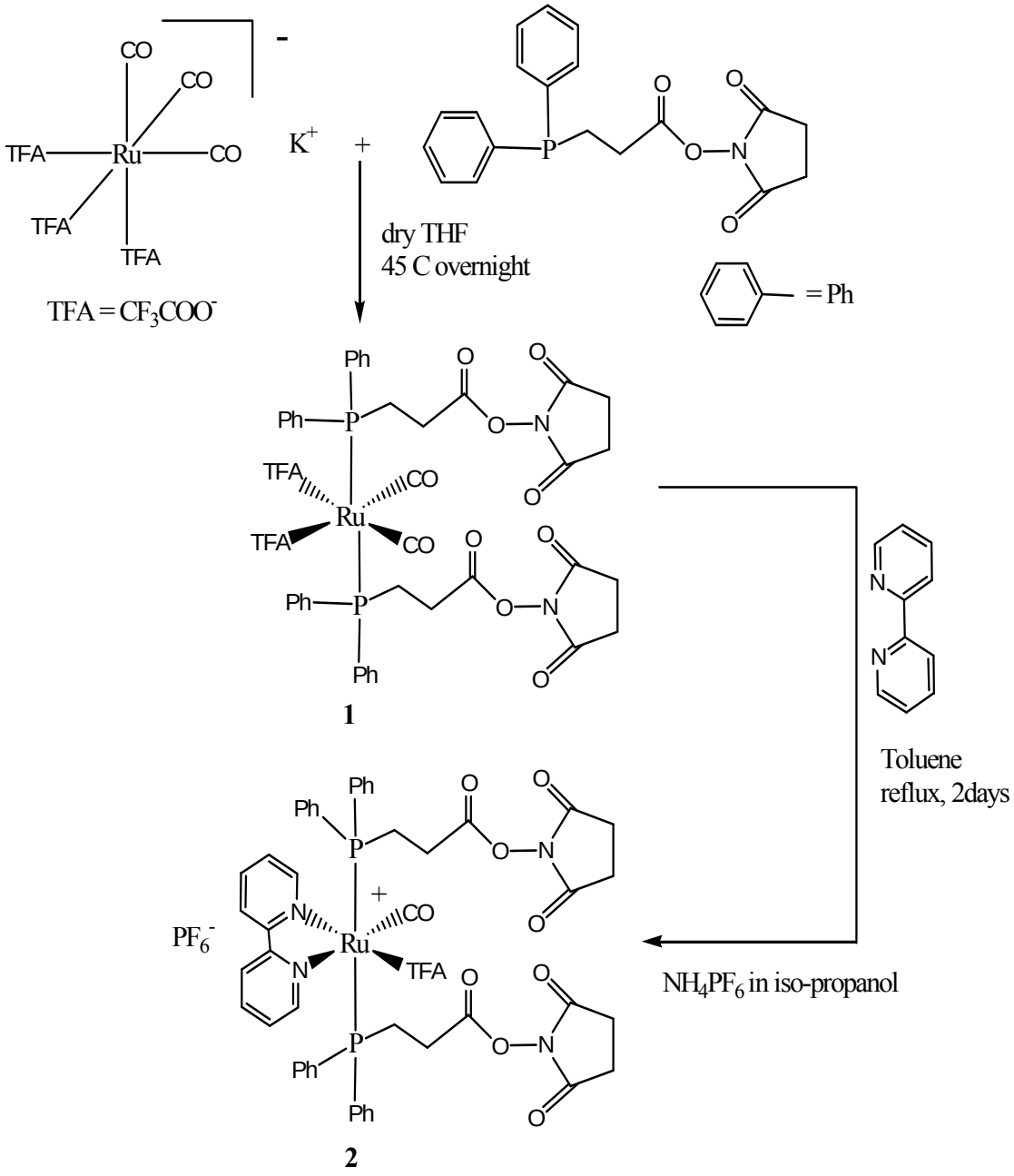
CO
CO
TFA
Ru
CO
TFA
TFA
-
K+
+
dry THF
45 C overnight
= Ph
TFA = CF3COO-
Ph
P
O
N
TFA
CO
Ru
1
Toluene
reflux, 2days
PF6-
NH4PF6 in iso-propanol
2

Scheme 5.1

5.1.2 Photophysical characterization of [Ru($PPh_2C_2H_4CONS$)(2,2′-bipy)(CO)(TFA)][PF_6] (2)

The UV–Vis absorption and emission spectra (Figure 5.1) of complex **2** in ethanol solution was recorded at room tem-erature. The intense higher energy absorption at 270-295 nm, observed for this complex is due to the spin-allowed intra ligand (π-π^*) transitions. The less intense absorption band ($\varepsilon_{450} \sim 2 \times 10^3$ $M^{-1}cm^{-1}$) in the visible region (410-500 nm) is attributed to spin-allowed metal-to-ligand charge-transfer ^{1}MLCT (d-π^*) transitions. Complex **2** has its emission maximum at 606 nm, a quantum yield of 0.2, a lifetime of 237 ns (air equilibrated) in ethanol and a limiting anisotropy of 0.08 in neat glycerol at 10ºC.

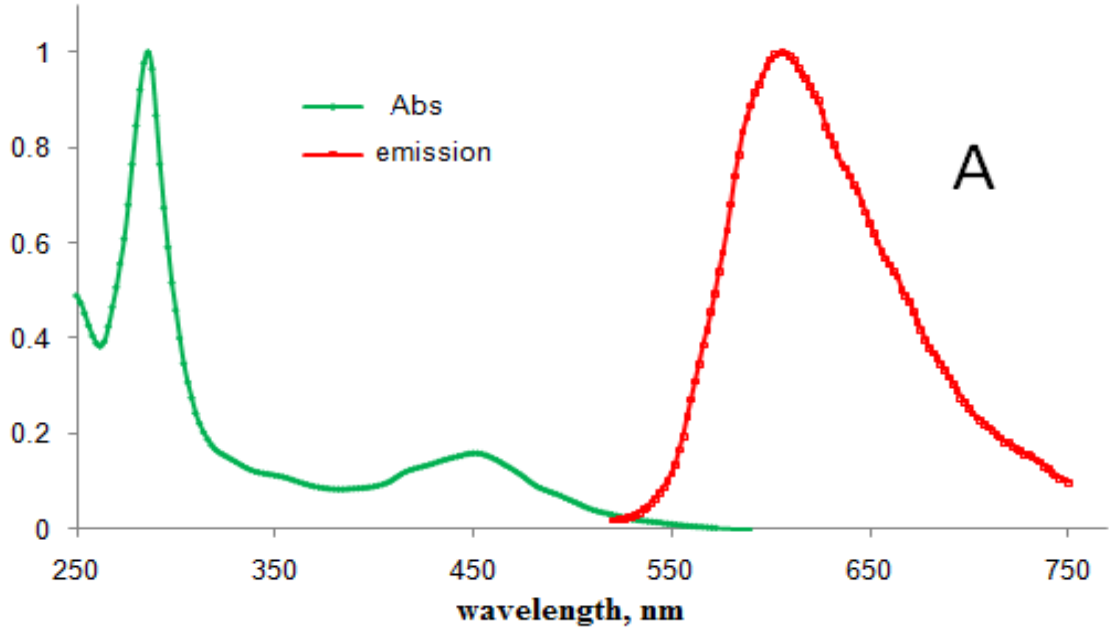

Figure 5.1 (a) Steady state UV-Vis spectra of [Ru($PPh_2C_2H_4CONS$)(2,2′-bipy)(CO)(TFA)][PF_6] (2)

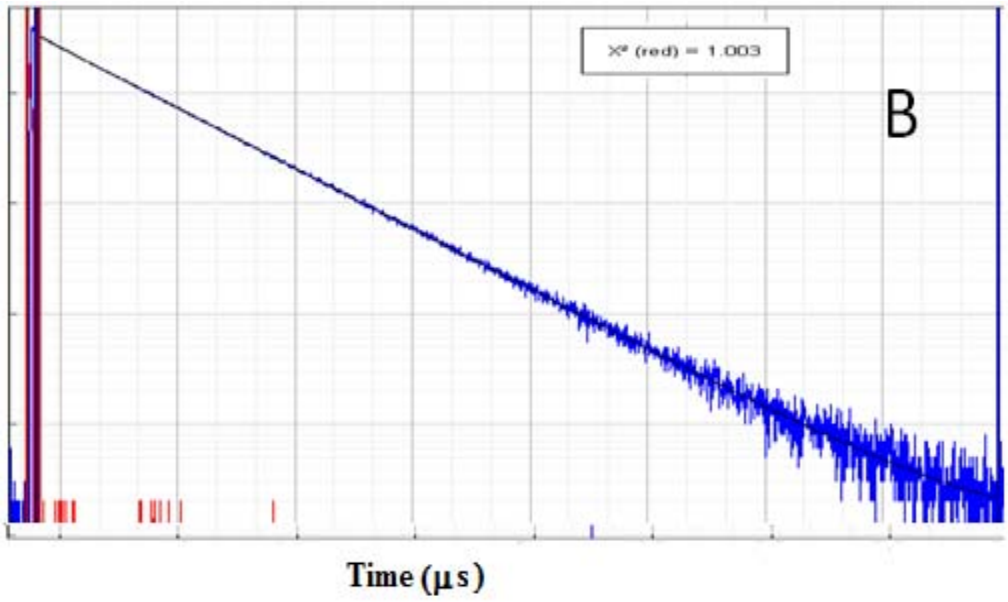

Figure 5.1 (b). Time dependent excited state decay of complex [Ru($PPh_2C_2H_4CONS$) (2,2′-bipy)(CO)(TFA)][PF_6] 2.

The photophysical properties of complex **2** are similar to that of the complex [(TFA)Ru(CO)(2,2′-bpy)(PPh_3)$_2$][PF_6^-] [1]. The favorable photophysical properties and the presence of a bio-conjugable functional group on the phosphine make this complex a potential probe to study slow dynamics in biological systems (> 100 ns). Small-scale reaction of the complex **2** with lipid di-myristoylphosphatidylethanolamine (DMPE) has demonstrated that complex **2** forms covalent conjugates with lipid molecules. The yields were very low; therefore a larger scale reaction needs to be performed to obtain enough material for complete characterization of the new compounds. Experiments to complete this study are currently undergoing in the Ross-Rosenberg groups.

5.2 Nanodiscs as model lipid Bilayers

Several model membrane systems such as detergent micelles, liposomes, bicelles and mixes lipid/detergent micelles have been used to facilitate studies of membrane proteins structure and dynamics. Although all these established systems have advantages for specific applications, they also have certain limitations. Over the past decade Sligar *et al.* [2-6] have developed a method to make homogeneous nanoscale phospholipid bilayer structures referring them as 'Nanodiscs'. Nanodiscs are of interest as an improved mimic of bio-membrane. Nanodiscs are derived from the naturally occurring high-density lipoprotein (HDL) particles, whose function is to transport cholesterol in aqueous-soluble form [6]. HDL, which is formed by wrapping of two apolipoprotein A-I monomers (243 residues) to a segment of phospholipid bilayer, has been studied for its role in reverse cholesterol transport [2,6]. The apolipoprotein A-I (apoA-I) is largely helical and amphipathic in nature, i.e., the protein helix is lipophilic on one flank and hydrophilic on the other. The lipophilic flank of the protein remains in direct contact with the phospholipid molecules and the hydrophilic flank orients toward the aqueous medium. Nanodiscs are derived based on the architecture of HDL particles using a recombinant modified version of ApoA-I (termed as membrane scaffolding proteins [3]. These constructs are soluble model membrane systems useful for studying membrane-bound proteins in the absence of detergents. Nanodiscs consist of a phospholipid bilayer surrounded by a belt of protein. The Nanodiscs have diameters of ~9 to 13 nm and thicknesses of ~4.5 to 6 nm, depending on protein sequence and ratio of lipid to protein (Figure 5.2) [5, 9].

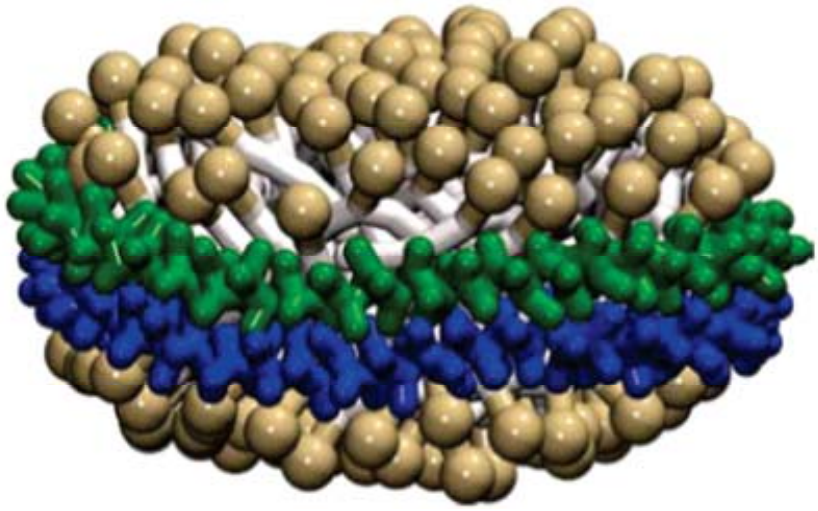

Figure 5.2 Model Nanodisc structure

(The protein-lipid particle is formed by two identical apolipoproteins in a double-belt configuration (shown in blue and green) wrapped around a lipid bilayer [10].)

Nanodiscs have certain advantages over other model membrane systems. For example, (1) because the membrane scaffolding proteins determine the size of Nanodisc formation, particles of consistent and monodispersed size are obtained [3]; (2) Shaw *et al.* has demonstrated that Nanodisc's complex phase transition behavior more closely resembles that of biological membranes than that of liposomes [8,9]. Because Nanodiscs have consistent size and are monodisperse, they are candidates for single-molecule experiments. The smaller size (10 nm) of nanodiscs compared to vesicles (100 nm) prepared by extrusion, have provided us with an opportunity to utilize the cholesterol-conjugated-ruthenium probe to study the hydrodynamics of the Nanodiscs. The probe's motion when incorporated in the Nanodiscs is important to determine. Using 4~20 ns excited-state lifetime probes and ~ 1000 ns excited-state lifetime luminescent probes

(MLC-cholesterol conjugate), we will be able to study local and global rotational motions in the ns–μs timescale.

We have prepared 10 nm diameter nanodiscs contains the lipid di-myristoylphosphocholine (DMPC) according to the procedures published by Sligar *et. al.* [3]. We used membrane scaffold protein MSP1D1 developed by the Sligar group [5] as the scaffold protein and 1,2-dimyristoyl-*sn*-glycero-3-phosphoethanolamine-N-(7-nitro-2-1,3-benzoxadiazol-4-yl)(ammonium salt) (DMPE-NBD) (5% of total lipid concentration) was used as the fluorescent membrane probe. We studied the changes in lifetime and local motions of the probe DMPE-NBD incorporated in Nanodiscs over a range of temperature and the results are summarized in Table 5.1.

Table 5.1 Average lifetime $<\tau>$, rotational correlation time ϕ, limiting anisotropy r_∞ and fundamental anisotropy value r_0 for DMPE-NBD in Nanodiscs

Temperature (°C)	$<\tau>$ (ns)	r_0	ϕ_1 (ns)	ϕ_2 (ns)	r_∞	χ^2
10	9.2	0.29	22.3	2.27	0.035	1.13
15	8.9	0.29	16.4	1.89	0.031	1.18
20	8.6	0.29	16.2	1.87	0.022	1.15
25	8.1	0.29	14.2	1.67	0.010	1.11
30	7.5	0.29	13.0	1.46	0.009	1.10

The preliminary time-dependent fluorescence decay studies of the Nanodisc over the temperature range from 10–30 ºC revealed that the changes in excited-state lifetime

(<τ>) and rotational correlation times (ϕ_1, ϕ_2) are small. The slower correlation time (ϕ_1) and small changes in lifetime could result from additional interaction of the lipid molecules with the scaffolding proteins. Therefore, the packing of lipids in Nanodiscs appears to be different than the packing of lipids in liposomes. To understand the extent of differences in lipid packing in Nanodiscs and in 100-nm-liposomes, experiments of changes in excited state lifetime and rotational correlation times (ϕ_1 and ϕ_2) of the probe DMPE-NBD in 100-nm-diameter DMPC vesicles have to be conducted at the same condition. Vesicle experiments are currently underway in the Ross group.

Future studies of the Nanodisc's hydrodynamics including the global rotational correlation time will be carried out by incorporating the cholesterol conjugate [(TFA)Ru(CO)(dppene)(5-aminphen-cholesterol)] [PF_6] in Nanodiscs. Optimization of conditions to make Nanodiscs with a range of cholesterol composition and using the MLC-cholesterol probe is currently underway in the Ross group.

5.4 Experimental

5.4.1 Synthesis of [$Ru(PPh_2C_2H_4CONS)_2(CO)_2(TFA)_2$] (3)

A THF solution of $K[Ru(CF_3CO_2)_3(CO)_3]$ (100 mg, 0.18 mmol) and the succinimidal ester of diphenyl-phosphino-propionic acid (126 mg, 0.36 mmol) was heated overnight at 45 ºC under N_2. The solvent was removed on a rotary evaporator and the residue was purified by thin layer chromatographed on silica. Elution with hexane/acetone (1:1 v/v) gave three bands. The slower moving, pale yellow band

afforded [Ru($PPh_2C_2H_4CONS)_2$ $(CO)_2(TFA)_2$] (**3**) (97 mg, 37%) as a pale yellow solid. IR in KBr: 2066 (vs), 2002 (vs), 1963 (s), 1783 (m), 1739 (vs), 1700 (vs), 1685 (vs) cm^{-1}; ^1H NMR in $CDCl_3$: 7.9-7.3 (m, 20 H), 2.95-2.5 (m, 16 H); ^{31}P {H} NMR: 30 (s, br), 20 (s) ppm.

5.4.2 Synthesis of [Ru($PPh_2C_2H_4CONS$)(2,2′-bipy)(CO)(TFA)][PF_6] (4)

The reaction of **3** (97 mg, 0.088 mmole) with 2,2′-bipyridyl (15.2 mg, 0.097 mmole) in toluene (10 mL) refluxing at 110 ^oC for 48 h produced an orange solution. A deep orange precipitate was obtained by the addition of NH_4PF_6 in cold isopropanol (1.0 g/10 mL). The residue was filtered and washed three times with cold isopropanol, three times with diethyl ether and then dried under vacuum. Complex [Ru($PPh_2C_2H_4CONS$)(2,2′-bipy)(CO)(TFA)][PF_6] (**4**) was obtained in 46% yield (50 mg). IR in KBr: 1975 (s), 1776 (m), 1740 (vs), 1670 (m) cm^{-1}; ^1H NMR in $CDCl_3$: 8.38-6.95 (m, 28 H), 2.9-2.7 (m, 16 H); ^{31}P {H} NMR: 31.4 (s, 2P), -155(m, 1P) ppm.

5.4.3. Reaction of [Ru($PPh_2C_2H_4CONS$)(2,2′-bipy)(CO)(TFA)][PF_6] (4) with DMPE

An acetonitrile solution of complex **4** (5 mg, 0.004 mmol) was added drop-wise into a stirring methylene chloride solution of DMPE (5.2 mg, 0.008 mmol) under N_2 in the presence of triethylamine (100 μL). The reaction was carried out overnight. The solvent was removed on a rotary evaporator and the residue was purified by thin layer chromatography on silica. Elusion with hexane/ methylene chloride/ methanol (6:3:1) on

silica gave two yellow band and a faster moving UV band with a heavy yellow baseline. The yellow compound on the baseline and the UV absorbing band were identified as unreacted complex **4** and DMPE, respectively. The two new yellow bands on the TLC plate indicated formation of new compounds. The yields were very low; therefore a larger scale reaction needs to be performed to obtain enough samples for complete characterization of these new compounds.

References

1. A. Sharmin, R. C. Darlington, K. I. Hardcastle, M. Ravera, E. Rosenberg, and J. B. A. Ross, *J. of Organomet. chem*., **694** (2009), p.988.
2. T.H. Bayburt, and S.G. Sligar, *Protein Sci*, **12** (2003), p. 2476.
3. A. Nath, W.M. Atkins, and S.G. Sligar, *Biochemistry,* **46** (2007), p. 2059.
4. T.H. Bayburt, Y.V. Grinkova, and S.G. Sligar, *Arch Biochem Biophys,* **450** (2006), p. 215.
5. I. G. Denisov, Y. V. Grinkova, A. A. Lazarides, S. G. Sligar, *J. Am. Chem. Soc.* **126** (2004), p.3477-3487.
6. D. Atkinson, D. M. Small, *Annu. Rev. biophys. Biophys. Chem*., **15** (1986), p. 403.
7. T.H. Bayburt, Y.V. Grinkova, and S.G. Sligar, *Nano Letters,* **2** (2002), p. 853-856.
8. A.W. Shaw, M.A. McLean, and S.G. Sligar, *FEBS Lett*, **556** (2004), p. 260.
9. I.G. Denisov, M.A. McLean, A.W. Shaw, Y.V. Grinkova, and S.G. Sligar, *J Phys Chem B*, **109**(2005), p. 15580.
10. A. Y. Shih, A Arkhipov, P. L. Freddolino, S. G. Sligar, K. Schulten, *J. Phys. Chem. B, **111*** (2007)**,** p**.**11095.